Identification of a non-linear model for fluidelastic instability in a normal triangular tube array.

Craig Meskell

Department of Mechanical and Manufacturing Engineering,

Trinity College,

Dublin 2,

Ireland.

May, 1999.

A thesis submitted to the University of Dublin for the degree of Ph.D.

Fluidelastic instability of a single flexible cylinder subject to fluid cross flow has been investigated in arrays of rigid tubes arranged in a normal triangular configuration with pitch ratios of 1.58 and 1.32. The test facility designed and built for this purpose has two novel features: (i) the flexible tube is supported by a linear structure which allows only pure translation of the tube in a direction perpendicular to the flow; (ii) the linear damping of the structure can be modified passively using a specially designed electromagnetic shaker (EMS) without affecting the modal stiffness or mass. This device can also be used to provide a measurable excitation force, either random or deterministic. For the two tube bundles considered, the parameters of a linearized model of the fluid force acting on the tube have been identified using both a time domain and frequency domain technique. The linear fluid damping and stiffness appear to vary with dynamic head for a pitch ratio of 1.58, but this was not observed for the other array. The parameters from the linearized models have been used to produce estimates of the stability boundaries. For pitch ratio 1.58 the predictions agree reasonably well with experimentally determined thresholds. However, for the pitch ratio of 1.32, the linearized model is inadequate as the predicted critical velocities overestimate the experimental values by as much as 100%. Using a force state mapping technique, a non-linear model of the fluid force has been identified for this array. The fluid stiffness is modelled as the sum of a linear and a cubic spring and two models for the fluid damping are considered. The predictions for stability thresholds from the non-linear model are in much better agreement with experiment. The limit cycle amplitudes are overestimated, but they agree qualitatively with the trends found experimentally. The results suggest that none of the available theoretical models for single degree of freedom fluidelastic instability are universally applicable.

"If it happens that a question which we wish to examine is too complicated to permit all its elements to enter into the analytical relation which we wish to set up, we separate the more inconvenient elements, we substitute for them other elements less troublesome, but also less real, and then we are surprised to arrive, notwithstanding our painful labor, at a result contradicted by nature; as if after having disguised it, cut it short, or mutilated it, a purely mechanical combination would give it back to us."

Jean le Rond d'Alembert (1752)

Declaration

I declare that I am the author of this thesis and that all the work described herein is my own, unless otherwise referenced. Furthermore this work has not been submitted in whole or part, to any other university or college for any degree or qualification.

I authorise the library of Trinity College, Dublin to lend this thesis.

Craig Meskell, May 1999

Acknowledgements

I would like to thank my supervisor, John Fitzpatrick, for all his help and guidance. Thanks are also due to Frank Waters, of UCD, for fabricating the inlet of the windtunnel, and the technicians from the workshop in Dept. Mechanical Engineering, TCD, who made most of the other components. I would also like to thank José Antunes for his help with the electro-magnetic shaker.

Finally, thanks to all the guys who have worked in the fluids lab during the past few years for the tremendous fun I have had with them.

A	Amplitude of tube response
$\underline{B}$	Vector of non-linear parameters β_i
$\vec{B}$	Magnetic field vector
$\underline{D}$	Augmented measurement matrix
E	Fluidelastic force
$F(\omega)$	Fourier transfoirm of input excitation force
$F(t)$	Restoring force
$E(t)$	Fluidelastic force
$H(\omega)$	System transfer function
$\vec{I}$	Induced electrical current
N_1	Non-linear function in y
N_2	Non-linear function in y and $\dot{y}$
N_3	Non-linear function in $\dot{y}$
P	Array pitch
R	EMS circuit resistance
S_{XY}	Cross-spectrum between X and Y
S_t	Strouhal number
S_X	Auto-spectrum of X
T	Turbulent excitation
U	Freestream flow velocity
U_c	Critical flow velocity
U_r	Gap velocity
V_r	Reduced gap flow velocity
W	Work done per cycle
$Y(\omega)$	Fourier transform of tube response
$\underline{Z}$	Matrix of non-linear functionals

c	Linear damping coefficient
d	Tube diameter
f	Frequency of vibration
$\jmath$	$\sqrt{-1}$
k	Linear stiffness
m	Tube mass
$\vec{v}$	Velocity vector of EMS coil
y	Tube displacement
z_i	Non-linear functional
α_i	Parameters obtained from DHS method.
$\beta_{1,2}$	Non-linear damping parameters from FSM method
γ^2_{FT}	Coherence between excitation force and turbulent excitation
δ	logarithmic decrement
δ_r	Mass damping parameter=$\frac{\mu\delta}{\rho d^2}$
$\vec{\epsilon}$	Induced emf vector
ε	Total unsigned error
ζ	Damping ratio
$\eta_{1,2}$	Non-linear stiffness parameters from FSM method
θ	Phase angle between tube displacement and velocity
λ	Signed error
Λ	Matrix of signed errors
μ	Tube mass per unit length
ρ	Fluid denisty
τ	Lag angle
ϕ	Phase of tube response
ω	Angular frequency of vibration
ω	Angular natural frequency
ω_f	Fluidelastic angular frequency

Subscripts

EX	Associated with the excitation
RMS	Root mean square value
FIT	Fitted curve
d	Damping
em	Electromagnetic
f	Parameter associated with fluid loading
s	Parameter associated with structural loading

Abbreviations

DHS	Downhill simplex method
EMS	Electromagnetic shaker
FEA	Finite element analysis
FRF	Frequency response function
FSM	Force state mapping
TLS	Total least squares
ncdt	Non contact displacement transducer

Contents

List of Figures

List of Tables

Chapter 1

Introduction

Cylinder arrays are common in many engineering structures. For example, tube bundles can be found in heat exchangers, boilers or steam generators, clusters of fuel rods in nuclear reactors, underwater piping and naval architecture. Each of these applications involve a fluid flowing across the array and it is the vibration induced by this flow which is often responsible for the failure of the plant. Such failures may necessitate very expensive repairs and in the case of the nuclear industry they represent a health hazard. For these two reasons, flow induced vibration (FIV) in tube bundles is a major concern for designers.

Although some fatigue and fretting wear at the tube supports due to turbulent buffeting is inevitable, the time taken for a component to fail in this way is literally years. However, under certain conditions the coupled fluid-structure force system can cause the cylinders to vibrate at large amplitudes, causing a dramatic increase in the fretting wear at supports, impact damage due to adjacent tubes clashing or even divergerence and hence catastrophic failure of the structure. This phenomenon, known as *fluidelastic instability* (FEI), was recognized as a problem in industrial heat exchanger installatioins over 30 years ago (Roberts 1966).

As an illustration of the destructive potential of the fluidelastic instability mechanism, Yu (1986) reported the total failure of a U-tube heat exchanger with 749 $18mm$ tubes arranged in a normal triangular array (pitch ratio 1.5). Before the unit was installed

in the PWR power plant for which it was intended, it was tested under operational conditions. Yu recorded the first tube failure after just 60 hours of operation. The damage was repaired and the unit brought online again. After a further 290 hours, an inspection of the heat exchanger revealed that 60 tube pairs had failed, 7 of these had been completely severed. In addition, substantial wear was discovered at the tube supports and baffles, some of which disintegrated during disassembly. This is not an isolated incident of catastrophic failure due to flow induced vibration. For example, Paidoussis (1979) describes 50 such cases, of which 10 were definitely due to fluidelastic instability.

The potentially disastrous effect of fluidelastic instability has led to a large research effort being expended on this phenomenon in the past three decades. Even in the commonly studied idealization of a 2D array, the flow is separated and turbulent and the flow domain is multiply connected with moving boundaries. In a real installation the situation may be even more complex since the flow will be three dimensional, the fluid may be two phase and subject to thermal gradients, and the structure itself may exhibit non-linearities such as impacting or dry friction. Hence, it is not surpirising that much of the effort has been devoted to determining empirically based design guidelines which will be sufficiently conservative to ensure that FEI is avoided.

Notwithstanding this, there has been significant progress in developing theoretical models which describe fluidelastic behaviour in tube arrays. These have enjoyed much success, particularly for high levels of structural damping where the fluid dynamic mechanism dominating the system depends on multiple cylinders vibrating. In this situation dynamic instability is impossible for an array with only a single flexible cylinder. At lower levels of structural damping (or when water is used as the working fluid), a different mechanism appears to be responsible for the dynamic fluid forces causing vibration since a single flexible cylinder in an otherwise rigid array may exhibit fluidelastic instability. Several models have been proposed to account for this type of behaviour, based on various physical assumptions and requiring different levels of empirical input.

Validation of a proposed model usually depends on comparing the predicted stabil-

ity thresholds with those obtained experimentally. Indeed, some models which require empirically determined data, use the same results to identify the model as to validate it. For this reason there are several contradictory models of single degree of freedom fluidelastic forces which all purport to be definitive, implying that a fundamental understanding of the physical fluid dynamics involved is still lacking. In their review of FIV in tube arrays, Weaver & Fitzpatrick (1988) note the deficit in understanding the fundamental mechnisms at work. They also point out that an improved theoretical basis would facilitate the examination of the effects of novel designs and strategies for avoiding FEI. One of the aims of this study is to investigate the applicability of the theoretical models which are currently available by comparing the trends in fluid force parameters predicted by these models with those measured measured directly.

Once instability has been established it is the non-linear nature of the fluid structure interactions as well as the structural mechanics which will determine the severity of the increased fretting wear and fatigue which ultimately will be the cause of structural failure (Price 1995). Despite this, there has been almost no advance in modelling the non-linear nature of the fluid structure interactions for predicting tube behaviour in a post-stable regime.

The complexity of even an idealized system means that a purely theoretical analysis seems to be some way off. The variability of results reported by different researchers suggests that an experimental programme is problematic. In light of this, it might seem that the obvious way forward is to employ computational fluid dynamics and indeed such an approach has been successful for simple systems, such as a single cyclinder is cross flow. However, at the time this work commenced, computational power was such that a numerical simulation of a fully coupled fluidelastic tube array was not feasible. Indeed, the hardware and software still may not be sufficiently developed. Furthermore, even if this approach was practicable, some experimental tests would be necessary for validation purposes. For these reasons, it was decided that an experimental study was the best way to achieve the goals of the work.

1.1 Objectives & Overview

Although there remains much work to be done in the area of fluidelastic instability to determine the underlying mechanisms, this work will concentrate on three objectives:

1. Design and built a test facility to investigate fluidelastic instability in tube arrays with just one degree of freedom. From the outset, it was intended to eliminate some of the possible sources of experimental variability by design. The test rig was designed to facilitate completion of objectives two and three below.

2. To investigate the limitations of linearized relationships between the tube motion and the fluid force. This is achieved by quantifying effective linear fluid force coefficents and comparing the dependency of these coefficients on fluid flow velocity with that predicted by available models.

3. To identify an empirical non-linear model which describes the behaviour of the vibrating tube at different flow velocities.

The documentation of the attempts to meet these objectives has been organized into seven parts.

The experimental facility which was designed and built for this project will be described in chapter three, along with the attendant instrumentation. The results of the validation tests are also presented.

Chapter four describes three system identification techniques. Two of these assume a linear system while the third provides parameter estimates for a non-linear model. The sensitivity of the techniques to noise and calibration errors is also considered.

The results of preliminary tests of two tube arrays subject to cross flow are presented in chapter five. This chapter also documents the linearized models which have been identified to describe the coupled fluid-structure system and compares the predictions obtained with experimental data.

Chapter six presents direct evidence of the non-linear dependence of the fluid force on the tube motion. The nature of this non-linearity is examined by a qualitative dis-

cussion of these results. A non-linear model is proposed, the parameters of which are quantified. The identified model is used to estimate the system behaviour and these predictions are again compared to the real system.

Chapter seven and eight serve to summarize the main achievements of the study and presents the conclusions which may be drawn. Possible avenues of research which might be explored in the future are also discussed.

Before the body of work is discussed, a review of the salient studies, selected from the wealth of work previously reported in the open literature, is presented in chapter two. The discussion will concentrate on flow induced vibration in tube arrays similar to the type of system under investigation here. It will perhaps become clearer at this stage why there is a need for yet another experimental study.

Chapter 2

Literature review

Paidoussis (1981), having reviewed the research into flow induced vibration in tube bundles observes that the field was in considerable disarray due to "researchers' rivalling and often insufficiently substantiated claims of doubtful generality". He concluded that, although empirically determined designed guidelines did exist, fundamental understanding of the phenomena involved was sparse. In an effort to clarify the area, he proposed a classification of flow induced flow (FIV) mechanisms in tube bundles:

- TURBULENT BUFFETING
- FLOW PERIODICITY (e.g. vortex shedding)
- FLUIDELASTIC INSTABILITY

This taxonomy has been widely adopted. Weaver (1987) even extended it to flow induced vibration problems involving other structures, renaming the mechanisms *forced vibration*, *self-controlled vibration* and *self-excited vibration*, respectively.

Weaver & Fitzpatrick (1988) present a detailed review of current (1980s) research in the area of FIV in tube arrays. In their introduction, they note that four standard tube configurations have been widely tested and the naming scheme which the authors employ has been adopted generally. These geometries are shown schematically in fig 2.1 (page 19). The normal square and rotated (parallel) triangular arrangements are often

referred to as *inline* arrays, while the rotated square and the normal triangular are called *staggered* arrays. This thesis will be primarily concerned with vibration in normal triangular tube bundles.

Table 2.1 (see page 20) summarizes the salient experimental studies in the area of FIV in tube bundles published in the last 20 years. This list is confined to single phase flow studies and excludes those which are dominated by non-linear structural dynamics (such as impacting). As can be seen, many of these examine all three excitation mechanisms. This is indicative of the fact that, although fluidelastic instability is potentially the most destructive source of vibration, all tube bundles subject to cross flow will experience both turbulent buffeting and vortex shedding. All three mechanism may interact, so consideration of fluidelastic instability in isolation is unrealistic.

2.1 Turbulence in tube arrays

High levels of broadband turbulence are inevitable in tube arrays and from the point of view of heat transfer, this is desirable. The turbulent flow field generates a pressure on the tube surface which varies randomly both in space and time. Hence each tube experiences a random buffeting. Weaver (1987), classifies turbulent buffeting in tube arrays as a forced vibration, since the fluid force does not depend on the tube motion.

Weaver & Fitzpatrick (1988) point out that, since some industrial heat exchangers (e.g. steam generators) have a projected service life of 20-40 years, turbulent excitation is an important consideration when designing against fatigue or fretting wear at tube supports. However, achieving a reliable design guideline for this mechanism is complicated by the difficulty in predicting excitation levels and specifying safe response levels (Weaver 1987).

Grover & Weaver (1978a) conducted an experimental study into turbulent buffeting on a rotated triangular array ($\frac{P}{d} = 1.375$) in air crossflow. Their turbulence spectra, for a range of flow velocities, show a strong peak at a Strouhal number (non-dimensional frequency) of about 0.2 . This would suggest that they observed some form of vortex

shedding, rather than broadband turbulent buffeting. The authors also point out that the turbulence levels had settled into a fixed pattern after four rows of tubes. This result is supported by Weaver & El-Kashlan (1981). Chen & Jendrzejzcyk (1987), examined turbulent buffeting on a normal (inline) square array ($\frac{P}{d} = 1.5$) in water flow. They suggest that by the fifth row, the local turbulence levels are independent of upstream turbulence conditions. However, Fitzpatrick et al. (1986), using hotwire anemometry, report that the turbulence structures are still evolving as deep as the fifteenth row of a normal square array. Furthermore they report strong peaks in the turbulence spectra. The spectra have been shown to strongly depend on measurement location and Reynolds number as well as the array geometry.

Pettigrew & Gorman (1978) have employed a procedure in which the fluid force per unit length acting on the tube over a range of flow velocities is characterized by a single parameter. This non-dimensional force coefficient per unit length was inferred from measured tube response spectra by assuming that:

1. the power spectral density of excitation force per unit length is proportional to dynamic head. (This was contradicted byPrice et al. 1987)

2. turbulence is isotropic and perfectly correlated along tube length.

3. there is no significant off-resonant tube response i.e. no peak in turbulence spectrum away from structural natural frequency.

Axisa et al. (1990) measured the spectra of fluid force caused by turbulent buffeting directly, rather than deriving them from tube response spectra. They go on to generalize the formulation of a non-dimensionalized excitation spectrum to take account of the spanwise turbulence correlation length and a more realistic turbulence spectrum. They proved that for the purposes of tube excitation, the correlation length is largely irrelevant as long as it is much smaller than tube span. The authors use their representation of the broadband turbulent buffeting to predict tube response RMS. It was found that Pettigrew & Gorman's model of the excitation systematically overestimates (by an order of magnitude!) the tube response to turbulent buffeting. Axisa et al. attributed this discrepancy

to the assumption of perfect spatial correlation and a flat turbulence spectrum. They conclude by describing a method of comparing turbulence data from different array geometries. They report that preliminary work suggests that "scaled" turbulence spectra are independent of array geometry, but concede that more work is needed.

The condition assumed by Axisa et al. was shown to be generally applicable by Zukauskas & Katinas (1991). Using a hotwire probe they measured the spanwise turbulence correlation length in a five row array and found that it was the same order of magnitude as the tube diameter, starting at about 3 diameters in leading rows and dropping to 0.9 diameters deeper in the array.

Price et al. (1987), reported the results of a study on FIV of a single flexible cylinder in a rotated square array ($\frac{P}{d} = 2.12$). They noted that the tube suffers significant vibration from turbulent buffeting. In the absence of any other excitation (e.g. Strouhal periodicity), they report a linear relationship between tube response RMS and gap velocity, rather than with dynamic head as had been previously assumed by Pettigrew & Gorman (1978).

2.2 Vortex shedding in tube arrays.

Weaver (1987) notes that if periodicity exists in the flow in the absence of structural motion then "self-controlled vibrations" may occur. This flow periodicity may be generated by acoustic resonance or by another mechanism referred to as Strouhal periodicity. Both mechanisms will produce similar tube responses, a fact that led Weaver & Fitzpatrick (1988) to dismiss as unreliable much earlier (pre1980) Strouhal data for tube arrays, since it was obtained from heat exchangers prone to acoustic resonance.

Prior to the 1960s, vortex shedding within heat exchangers (which was thought to be identical to that from a single cylinder) was accepted as the major cause of FIV in tube bundles. But Owen (1965) disputed the possiblity that discrete vortex shedding could occur in closely packed tube arrays. He attributed the widely observed resonant phenomenon to a peak in the turbulence spectrum, the frequency of which was dependent

on flow velocity and array geometry. He derived a semi-empirical formula to predict the frequency of this peak. Paidoussis (1981) pointed out that other predictive formulae, which were based on the vortex shedding concept, agreed well with Owen's model. He argued that, since the various semi-empirical formulae were based on the same experimental data, it was hardly surprising that the predictions were comparable.

However, Owen's ideas highlight the fact that even at the time of Paidoussis' review (1981), there was no definitive proof of the exact nature of Strouhal periodicity, as the phenomenon had come to be known. For example, Grover & Weaver (1978b), despite setting out to clarify the issue, succeeded only in observing a strong resonant peak in tube response, the existance of which was not in doubt. It was not until 1985, that Weaver & Abd-Rabbo published a flow visualization study of water flow in a fully flexible, normal square (inline) array ($\frac{P}{d} = 1.5$), which shows periodic vortex shedding, although not very clearly. Several other visualization studuies followed for various array geometries. Price et al. (1992) show pictures of vortex shedding in a parallel triangular array ($\frac{P}{d} = 1.375$); Weaver et al. (1992) present photographs of vortex shedding in rotated square arrays ($\frac{P}{d} = 1.21$ to 1.83) with air as the working fluid. Perhaps the clearest images of vortex shedding have been produced by Oengören & Ziada (1995) who investigated both inline and staggered array configurations subject to water cross flow including several normal triangular arrays.

Before the acceptance of vortex shedding as the mechanism of Strouhal periodicity, much was known about the phenomenon. Weaver & Yeung (1984) having studied all four array geometries, produced a general expression which relates the RMS tube response, normalized against tube diameter, to the mass damping parameter (including "fluid added mass"). The authors suggest that vortex shedding will not produce significant tube response for mass damping parameters greater than about unity, although they caution that the experimental data is quite sparse.

Savkar (1984) reported that upstream turbulence generators (grids) in air flow eliminated the problem of Strouhal periodicity altogether. This result suggests that, since turbulence levels by the fifth row are very high (Weaver & El-Kashlan 1981), the prob-

lem of Strouhal periodicity is only a problem in the first few rows. However, Fitzpatrick et al. (1986) report a substantial peak in the turbulence spectra as deep as the fifteenth row of inline arrays. They also reported multiple Strouhal numbers. This result has been found by other researchers. Paidoussis et al. (1988) found 2 Strouhal numbers for a rotated square array, $\frac{P}{d} = 1.5$. Price et al. (1987) report three Strouhal numbers, but note that only one Strouhal number persists beyond the fourth row.

Previously, Zukauskas & Katinas (1980) attempted to collapse all the Strouhal data on to a single curve, however, the presence of mulitple vortex shedding frequencies renders their curve obsolete. Oengören & Ziada (1995) collated all the available data, including new data from their own study, to provide two empirical curves which predict the Strouhal number as a function of pitch ratio. Furthermore, they go on to show experimentally, that the higher value is dominant at small pitch ratios ($\frac{P}{d} < 1.6$), while the lower Strouhal number dominates in arrays with large pitch ratios ($\frac{P}{d} > 3.4$). At intermediate spacing, both Strouhal numbers are apparent, but which is strongest depends on which row is being examined, and in some cases, how many tubes are in a row. The presence of a third shedding frequency can be attributed to a non-linear interaction between the other two frequencies. This explains the behaviour reported by Price et al. (1987).

2.3 Fluidelastic instability

Prior to the mid 1960s, rapid catastrophic failure in heat exchanger tube bundles was attributed solely to vortex shedding (Paidoussis 1981). However, in 1962, Roberts described a mechanism of self-excited oscillations (fluidelastic instability) in his PhD thesis which was published as a monograph (Roberts 1966). He considered the vibration of a single and a double row of cylinders. He observed that the motion was predominantly in the in-flow direction with adjacent tubes moving out-of-phase. He assumed that the wake downstream of any pair of tubes could be considered as two separated regions, of different sizes but with a constant pressure in each, with an inviscid jet

between them. The effect which he descirbed involved a Coanda-like "jet-switching" phenomenon, where the jet between adjacent tubes switched direction in phase with the tube motions. The resulting drag force depends on the tube displacement, but exhibits a hysteretic effect around zero displacement which can be attributed to the neccessity for a finite pressure difference between the two wake regions to cause the jet switching to occur. The hysteresis means that the drag force is greater as the tube moves downstream than when its moving upstream, which implies that if the cylinder vibrates at constant amplitude, the fluid imparts net energy to the structure during one cycle. If the amount of energy extracted from the flow in this way is larger than that dissipated by the structure, the vibration amplitude will increase. By ignoring the effect of positive fluid damping Roberts extended his analysis to predict the flow velocity necessary to initiate fluidelatsic instability. He combines the tube mass and structural damping into one parameter (sometimes referred to as the Scruton number). This mass-damping parameter is defined as:

$$\delta_r = \frac{\mu\delta}{\rho d^2} \tag{2.1}$$

The expression for critical velocity obtained by Roberts is:

$$\frac{U_c}{f\,d} = G{\delta_r}^{0.5} \tag{2.2}$$

where G is a constant. Although this analysis is limited to predicting in-flow motion of tubes with no obstruction downstream, it does illustrate how a fluid flow can overcome structural damping to amplify small perturbations in the position of cylinders and so lead to fluidelastic instability.

In an attempt to predict the instability in the transverse flow direction, Connors (1970) considered the fluid force as a function of tube displacements only and produced a stability threshold with the same functional form as eq 2.2. When the analysis is applied to tube arrays, the parameter G depends on the particular array geometry. This relationship has been found to be approriate for high values of mass damping parameter. At lower values the viscous drag of the fluid, which effectively provides a positive

damping, becomes significant. The assumption that the fluid force depends only on the instantaneous displacement of the tubes means that the analysis cannot account for the dynamic instability in the cross flow direction which has been widely obsereved in tests when a single flexible cylinder is placed in an otherwise rigid array. The fluidelastic instability predicted depends on all (or at least several) cylinders being flexible. This suggests that two distinct mechanisms are at work. The mechanism which is accounted for by Connors' approach is referred to as "stiffness controlled", while the single degree of freedom FEI is governed by the "damping controlled" mechanism. Both of these phenomena will be discussed below.

The relationship of eq 2.2 has formed the basis for design guidelines (Chen 1984; Weaver & Fitzpatrick 1988) which define the lower bound of the critical velocity as a function of mass-damping parameter. This has been achieved by collating all available experimental data for stability thresholds. In both cases the parameter G and the exponent of δ_r depend on the value of δ_r. This takes account of the effect of the damping controlled mechanism and positive fluid damping at low value of mass-damping. Weaver & Fitzpatrick (1988) propose four different design limits, one for each standard array geometry. Data from arrays with different tube spacing, tube diameter and natural frequency, but with similar configurations (e.g. normal triangular) are combined using the "gap velocity" which is defined as:

$$U_r = \left(\frac{P}{P-d}\right)\left(\frac{U}{fd}\right) \tag{2.3}$$

where P is the centre-to-centre tube pitch.

Chen (1984), on the other hand, attempts to collapse all the data from different array geometries using a "reduced gap velocity" defined as:

$$V_r = \left(\frac{P}{P-d}\right)\left(\frac{U}{fd}\right)\left(\frac{1}{2.105\left(\frac{P}{d}-0.9\right)}\right) \tag{2.4}$$

Austermann & Popp (1995) reported critical velocities for two different pitch ratios, in an otherwise identical experiemental facility. They present the data in a non-dimensional reduced form using eq 2.4 but the points do not collapse onto a single curve

highlighting the fact that Chen's gap velocity is not perfect. However, it is a common format for presenting such data. It was also noted that the mass damping parameter may also be inappropriate as a non-dimensionalizing parameter. This assertion is supported by the data from Price & Zahn (1991), who obtained desired values of δ_r, by varying both tube mass and damping, and by the theoretical analysis of Rzentkowski & Lever (1992).

Tanaka & Takahara (1981) proposed an analysis framework which was applicable to fully flexible arrays and took account of the unsteady nature of the fluid force. Their expression, which is linear in the tube displacements and velocities, relates the fluid force experienced by a tube to the motion of its neighbours and itself through non-dimensional coefficients which must be determined experimentally. In effect, the authors considered the fluid force as a multi-degree of freedom second order system. The authors have shown that the framework is equally applicable to an array with a single flexible cylinder (Tanaka et al. 1982). When applied to this case their formulation reduces to:

$$E = \frac{1}{2}\rho d^2 m_f \ddot{y} + \frac{1}{2}\rho d U c_f \dot{y} + \frac{1}{2}\rho U^2 k_f y \tag{2.5}$$

where m_f, c_f, k_f are the fluid mass, damping and stiffness respectively. Chen (1983) used the experimental data provided by Tanaka et al. (1981, 1982) to analyse of a number of simple cases. He proved that there were in fact two mechanisms. For a single flexible cylinder in a rigid array the fluidelastic instability is due to a negative fluid damping. This is the "damping controlled" mechanism. An array with multiple flexible cylinders may be prone to the damping controlled mechanism at low values of mass-damping, but in general the fluidelastic instability will be dominated by fluid stiffness terms and will occur even if the fluid damping is positive. This mechanism, referred to as "stiffness controlled" FEI, is similar in behaviour to coupled mode aerofoil flutter.

The stiffness controlled mechanism is reasonably well understood and there are several approaches available to analyse the behaviour of a tube bundle under this type of excitation (Granger 1990a; Price et al. 1990). The same is not true for the damping controlled mechanism. However, there are several models available, in addition to that

of Tanaka et al., which attempt to describe the damping controlled mechanism.

Lever & Weaver (1982, 1986) assume that the stability of an array of cylinders could be analysed by considering the flow around a single flexible cylinder. Their approach was similar to Roberts', in that the flow around this cylinder is represented as an inviscid, one dimensional jet on either side of the tube. The outside shape of these streamtubes and the wake region behind the tube is determined from experimental observation and is fixed for each array geometry. This is sometimes referred to as the "wavy-wall" model. The unsteady fluid force is caused by the change in the width of the streamtubes as the flexible cylinder vibrates. It is argued that, because of fluid inertia, the redistribution of flow downstream lags behind the motion of the cylinder. An approximate expression for this phase lag is assumed. The fluid force predicted by this model is:

$$E = (c_{f1})U\dot{y} - (c_{f2}\sin\theta_0)\dot{y} - k_f\cos\theta_0 y \tag{2.6}$$

where c_{f1},c_{f2}, k_f are force coefficients dependent on the flow velocity and θ_0 is the phase lag between the calculated force and the tube motion. The variation of this lag with flow velocity is not easily obtainable, however, it is based on the phase lag between streamtube area and vibration which is assumed to be inversely proportional to flow velocity. The model predicts multiple stability regions at low mass-damping. This was initially rejected by the authors on the basis that once instability had established itself, non-linearities in the fluid force would prevent the system from stabilizing at a higher flow velocity. Andjelic & Popp (1988) have measured the upper and lower boundaries of one such region, lending weight to the validity of the model. Unfortunately, the values of the stability thresholds are overestimated by as much as 100%. Lever & Weaver (1986) have shown that their model is very sensitive to the value of phase lag chosen, which may account for the discrepancy.

Price & Paidoussis (1986) make a quasi-steady assumption to represent the fluide-lastic system. In other words they assume that the only effect of the cylinder motion is to modify the flow velocity vector relative to the tube. The values of the lift and drag coefficients are assumed to be identical to those measured with the tube at rest

in the same location. The authors linearize the variation of the lift and drag forces with position. They also assume that the fluid force lags the tube motion by a time lag. The justification for this is based on the paper by Simpson & Flower (1977), in which the retardation of the flow as it approaches a cylinder is considered. The time lag is found to be inversely proportional to flow velocity. However, Simpson & Flower chose an arbitrary deviation from the stagnation streamline to obtain a time lag which is not infinite, but this means that any value of time lag can be obtained. To remedy this Price & Paidoussis (1986) assumed a constant of proportionality. Once the model is developed, the fluid force obtained has a functional form very similar to eq 2.6. The quasi-steady model also predicted multiple stability thresholds, which the authors also rejected as physically improbable. There have been several attempts to improve this model (e.g. Granger & Paidoussis 1995), but these have usually involved chosing an alternative value for the time lag based.

The final model for the fluidelastic force is more akin to the model of Tanaka et al. (1981, 1982), in that it is really just an assumed framework into which a large number of experimentally determined parameters must be introduced. Chen (1987) proposed a generalized framework relating the fluid force on a tube to the motion of itself and the tubes around it. It was demonstrated that this model could be reduced to any of the others, with the application of the appropriate assumptions. For a single flexible cylinder, the model becomes:

$$E = m_f \rho U^2 \ddot{y} + c_f \rho U^2 \dot{y} + k_f \rho U^2 y \tag{2.7}$$

It was noted that the parameters, m_f, c_f, k_f, are in general functions of U, but in a later paper (Chen et al. 1994) he claims that they can be considered constant except at very low flow velocities. In a subsequent paper (Chen et al. 1997) which deals specifically with damping controlled fluidelastic instability of a single flexible cylinder in a rigid array, this claim is repeated. This is in direct conflict with the other models.

The effects of non-linearities in the coupled fluid-structure system have been considered by several researchers (e.g. Paidoussis et al. 1992, 1993), but in these studies the

non-linearities were due to impacting or friction or some other structural non-linearity. There have been two attempts to develop a non-linear model for the fluid force. The first of these (Price & Valerio 1990) extends the quasi-steady model of Price & Paidoussis (1986) by considering the non-linear dependence of the steady lift and drag coefficients on tube displacement. The predicted stability thresholds are almost identical to those from the linear model. However, since the post-stable behaviour has not been compared to any experimental observations, it is impossible to assess the merit of the approach.

The second non-linear model proposed by Rzentkowski & Lever (1992) uses the same starting point as the Lever & Weaver (1982) model, but the non-linear terms are not neglected as the model is developed. The authors have used this non-linear model to investigate the interaction of turbulent buffeting with fluidelastic instability (Rzentkowski & Lever 1998). The model compares favourably with experiment in a qualitative sense, but not quantitatively.

2.4 Summary

It has been seen that there are three distinct mechanisms for flow induced vibration. The first and second of these, turbulent buffeting and vortex shedding, are understood sufficiently to allow accurate predictions of tube response. The third FIV mechanism, fluidelastic instability, can itself be devided into two separate phenomena. Stiffness controlled FEI requires several flexible cylinders in the tube array and can be predicted reasonably well with a steady model of the fluid mechanics. i.e. the fluid force depends primarily on the position of the tubes. The damping controlled mechanism, which can cause instability in an array with only one flexible cylinder, requires an unsteady model of the fluid and depends not only on the position of the tube, but also its velocity. There are several models for this type of FEI which have enjoyed some success in qualitative analysis of the problem. These models are mainly linear and, in general, offer poor quantitative predictions. Since the credibility of these models is based on predicted tube response, rather than on comparison with experimentally measured unsteady fluid

forces, it is difficult to assess their applicability. In recent years, there have been several papers produced investigating non-linear effects in the fluid structure system. However, with the exception two studies, in all these papers, the only significant non-linearity has been due to the structure.

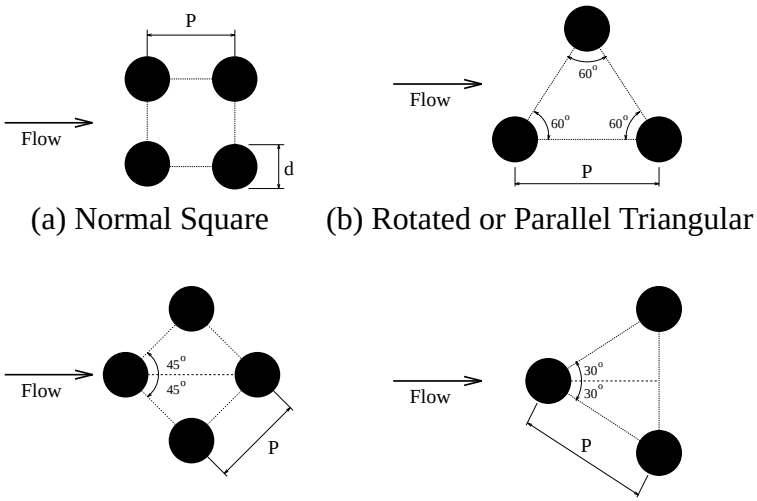

(a) Normal Square (b) Rotated or Parallel Triangular

(c) Rotated Square (d) Normal Triangular

Figure 2.1: Standard tube array configurations.

Author(s)	year	Array geom.	P/d	FIV Mechanism
Grover and Weaver	1978	△	1.375	$\mathbb{T}$, $\mathbb{V}$, $\mathbb{F}$
Pettigrew and Gorman		□ ◇ △ ◁	varied	$\mathbb{T}$, $\mathbb{V}$, $\mathbb{F}$
Zukauskas and Katinas	1980	◁ □	1.15-2.68	$\mathbb{T}$, $\mathbb{V}$, $\mathbb{F}$
Weaver and El-Kashlan	1981	△	1.375	$\mathbb{T}$, $\mathbb{V}$, $\mathbb{F}$
Tanaka and Takahara		□	1.33	$\mathbb{F}$
Tanaka et al.	1982	□	1.33	$\mathbb{F}$
Weaver and Koroyannakis		◁	1.375	$\mathbb{T}$, $\mathbb{V}$, $\mathbb{F}$
Goyder and Teh	1984	◁	1.375	$\mathbb{F}$
Savkar		□ ◇	1.5-1.7	$\mathbb{T}$, $\mathbb{V}$
Weaver and Yeung		□ ◇ △ ◁	1.5	$\mathbb{T}$, $\mathbb{V}$, $\mathbb{F}$
Weaver and Abd-Rabbo	1985	□	1.5	$\mathbb{V}$
Fitzpatrick et al.	1986	□	varied	$\mathbb{T}$, $\mathbb{V}$
Chen and Jendrzejczyk	1987	□	1.75	$\mathbb{T}$, $\mathbb{V}$
Price et al.		◇	2.12	$\mathbb{T}$, $\mathbb{V}$, $\mathbb{F}$
Andjelic	1988	◁	1.25	$\mathbb{F}$
Paidoussis et al.		◇	1.5	$\mathbb{T}$, $\mathbb{V}$, $\mathbb{F}$
Andjelic and Popp	1989	◁	1.25	$\mathbb{F}$
Andjelic et al.	1990	◁	1.25	$\mathbb{F}$
Axisa et al.		□ ◁	varied	$\mathbb{T}$
Granger		◁ (?)	1.44	$\mathbb{F}$
Price and Kuran		◇	2.12	$\mathbb{F}$
Price and Zahn	1991	◁	1.375	$\mathbb{F}$
Zukauskas and Katinas		□ ◁	varied	$\mathbb{V}$
Austermann et al.	1992	◁	1.375	$\mathbb{F}$
Price et al.		△	1.375	$\mathbb{V}$
Weaver et al.		◇	1.2-2.8	$\mathbb{V}$
Austermann and Popp	1995	□ ◇ △ ◁	varied	$\mathbb{F}$
Oengören and Ziada		◁	1.6-4	$\mathbb{T}$, $\mathbb{V}$
Hadj-Sadok et al.		□	1.5	$\mathbb{F}$

Table 2.1: Chronological summary of experimental studies.

□ = Normal Square; ◇ = Rotated Square; △ = Parallel Triangular; ◁ = Normal Triangular.

$\mathbb{T}$=Turbulent buffeting; $\mathbb{V}$=Vortex Shedding; $\mathbb{F}$=Fluidelastic instability.

Chapter 3

Experimental facility

The experimental facility consists of an open loop, draw down wind tunnel with the tube array under investigation installed in the test section. The tubes in the array are all fixed rigidly to the wind tunnel wall except for one which will be referred to as the *flexible tube.* This is a misnomer as the tube itself is rigid but it is mounted on a flexible support. The support is located outside the wind tunnel and so can be considered to be in quiescent air. Several schemes for this flexible support were considered and will be discussed below. The structural system dynamics can be modified using an electromagnetic shaker (EMS) to vary the damping. This device can also be used to provide a measurable excitation for forced response measurements. Several types of vibration sensor are used to monitor the motion of the flexible tube and to provide the necessary input data for the analysis procedures of chapter 4.

3.1 Wind tunnel specifications

All the experimentation was carried out in a purpose built draw down wind tunnel. Two decisions are implicit in this: firstly to use air as the working fluid and secondly to have a draw down open loop rather than blow down or closed loop. Air was chosen as the working fluid primarily for convenience. However, as will be discussed in the results sections, the inconvenience of a water tunnel might have been justified by substantially

larger fluid forces and the attentant improvement in signal-to-noise ratio. Once the decision to use air rather than water was taken, the confines of the space available for the new rig dictated a short open loop tunnel. Since a blow down tunnel would require a diffuser section, settling chamber and contraction before the test section, it was felt that drawing air directly from the surroundings into the test section would offer superior turbulence characteristics and a smaller footprint. Having decided the basic nature of the tunnel, well established design guidelines (e.g.Mehta & Bradshaw 1979; Downie, Jordinson, & Barnes 1984; Gibbings 1993; Rae & Pope 1984) were used to minimize pressure head losses along the length of the tunnel and the turbulence levels in the test section. A photograph of the tunnel is presented in fig. 3.1 and a dimensioned schematic is shown in fig. 3.2. The final design is $6.2m$ long, with $300mm \times 300mm \times 750mm$(length) test section.

The intake for the wind tunnel consists of a contraction section which was constructed from $3mm$ Russian Birch plywood skin shaped over a $30mm$ marine ply framework (section (A) in fig 3.2). The inlet has a $1500mm \times 1500mm$ opening reducing to the $300mm \times 300mm$ working section. This provides an area contraction ratio of 25:1. This was deemed necessary to ensure a low air velocity at the inlet and good turbulence characteristics in the test section. Initially, a screen was put in place across the inlet to further reduce turbulence levels, taking care to ensure a Reynolds number based on filament diameter less than 40 (see Rae & Pope 1984). However, it was found that the turbulence levels in the test section were not significantly higher when the screen was discarded, but the maximum flow velocity flow velocity was increased by about 30%.

A centrifugal fan driven by a 3.5 kW three phase AC motor at a constant rotational speed, manufactured by Chemsys, was used to provide the down draught for the tunnel as shown schematically as part (D) in fig 3.2. This necessitated the use of a movable baffle at the exhaust to control the flow velocity in the test section. The diffuser was constructed in a similar way to the contraction section, with a thin plywood skin and a thicker wooden skeleton. The diffuser was made in two sections. The first provides a transition from a square to an octagonal cross section as well as a slight increase in area.

The second section is straight octagonal duct. The exit of the diffuser is attached to the circular inlet of the fan with a flexible plastic seal. This has the advantage of eliminating a possible transmission path for vibrations from the fan/motor assembly to the test area.

The test section has an exterior frame made of $50mm$ aluminium angle. This frame supports the walls of the test section which are made of $10mm$ thick perspex. The test section has an internal width of $300mm$, height $300mm$ and length $750mm$. Two tube bundles were investigated in this study, both of which had five rows arranged in a normal triangular pattern (see fig 3.3). The first array had a pitch ratio ($\frac{P}{d}$) of 1.58, while the second has a pitch ratio of 1.32. The array consisted of $38mm$ diameter aluminium tubes. Each tube was cut to a length of $310mm$, slightly longer than the internal height of the test section, and plugged top and bottom. From the outset, it was intended to arrange the tube bundles vertically, so the side walls of the test section were rigidly fixed to the frame, while the floor and ceiling of the test section could be easily removed. For each pitch ratio a separate floor and ceiling was fabricated with $\phi 38mm$ holes were milled from the perspex to locate rigid tubes in the correct position. The tubes were fixed in these positions by clamping an o–ring between the end of the tube and a large washer. The compressed o–ring grips the perspex rigidly. A sketch of this scheme can be seen in fig 3.4. The advantage of this arrangement was that it allowed individual tubes to be removed, without the need for a complete disassembly of the test section while maintaining the maximum possible visibility into tube array. Another advantage was that, in the vicinity of the flexible tube, the perspex plates were identical to the site of the rigid tubes. Thus, the flexible tube could be moved easily to any location within the array.

The flow velocity was monitored using a Pitôt-static tube permanently installed upstream of the tube array and this was connected to a *Furness Control* micromanometer (model FC012) to measure freestream flow velocity in the test section. The velocity range for a clean test section is $2.5m/s - 21m/s$. When the first tube array ($\frac{P}{d} = 1.58$) was installed, the maximum upstream velocity reduced to $14m/s$ while for the second array ($\frac{P}{d} = 1.32$) it was $9.5m/s$. The difference is due to the increased blockage caused

by the second array. Using a hotwire anemometer (*DISA* 55M01) and probe (*DISA* 55P11), the turbulence levels were measured upstream of the tube bundle and were found to be less than 1% over the entire velocity range for both arrays. The hotwire was also used to verify that the onset flow approaching the tube arrays was uniform across the width of the tunnel.

3.2 Mounting scheme for the flexible tube

During the development of the rig and preliminary testing the flexible tube was mounted on a cantilever made of mild steel circular rod $0.5m$ long with a diameter of $10mm$. Both ends of the cantilever were threaded to allow fixation of the tube at one end and the base plate at the other. This type of end condition is not ideal, but it was very easy to implement. This assembly had a natural frequency of $10Hz$. Although many other researchers have used this type of support it has several inherent problems. The symmetric cross section of the cantilever offers equal flexibility in both the cross- and in-flow directions, requiring at least a two degree of freedom model for the structural behaviour. However, it is conceivable that the motion could be restricted to the crossflow direction only, by employing a nonsymmetric cantilever (e.g. a rectangular cross section), so that the structure is much stiffer in the inflow direction. A more persistent problem is that as the tube translates it also pitches. Nearly all the models dealing with flow through tube bundles assume that the fluid flow can be regarded as two dimensional. Indeed, many of the experimental studies depend on two dimensionality of the flow to reduce the amount of data necessary. If the tube is allowed to pitch this assumption is obviously violated. Furthermore, the rotation of the flexible tube will produce a centripetal acceleration on accelerometer and this acceleration will vary because both the rate and the centre of rotation varies during a cycle. Now consider an accelerometer placed in or near the flexible tube to measure the translational acceleration. The signal from such a transducer will contain artefacts from the centripetal acceleration, since every accelerometer has some cross axis sensitivity, and so will be strongly corrupted by harmonics of the

natural frequency of translational motion. Thus, the pitching motion of the flexible tube associated with a cantilever support poses problems for the execution of a testing programme as well as for the interpretation of the resulting data. For these reasons, the cantelever support was rejected as unsuitable for detailed investigation, however, some tests were conducted with this type of support.

Andjelic (1988) addressed the issue of pitching motion by suspending the flexible tube on four light springs arranged in parallel pairs at each end of the tube. This arrangement did in fact suppress the pitching motion of the tube in the cross-flow direction. It also had the advantage that the natural frequency could be modified simply by changing the tension in the springs. However, the tube was still free both to pitch and translate in the in-flow direction. Furthermore, by having the tube supported at both ends, the structural stiffness was inherently non-linear, with a strong cubic component. This type of structural behaviour could easily mask the weak non-linearity associated with the fluid force. Since the aim of this study is to quantify this non-linearity, Anjelic's arrangement was considered unsuitable.

3.2.1 The twin beam support

The mounting scheme developed in this study remedies the shortcomings of the cantilever support: the tube is free to move only in the cross-flow direction and only in pure translation. Furthermore, as will be seen below, the support is linear, at least in the displacement range of interest, and there is a large separation between the first and the second modes of vibration. The final design is illustrated by drawing in fig 3.5 and the photograph in fig 3.6. The support consists of two slender beams, $3mm$ thick, $50mm$ wide and $500mm$ long, arranged parallel to each other with a separation of $80mm$. At each end, the beams are fixed to the faces of an aluminium block, thus providing an end condition which does not allow angular deflection (i.e. a "built in" end). One of the aluminium blocks is fixed rigidly to a slab of $\frac{1}{2}''$ boiler plate while at the other end the flexible tube is attached. So that the orientation and position of the flexible tube

within the array can be adjusted, the boiler plate base is mounted on three adjustable feet, which rest on a frame made of steel box section, which in turn sits on the floor. thus the only direct path for transmission of vibration from the wind tunnel to the tube is through the concrete floor. This means the forces acting on the tube can be ascribed solely to the fluid force.

Once the position of the flexible tube is adequate, the base assembly is clamped to supporting frame by tensioning a single steel cable. The width of the shaft connecting the flexible tube to the upper aluminium block determines the maximium possible tube displacement, since it must pass through the $38mm$ hole in the wind tunnel floor. However, it was found that if the flexible tube was attached to the upper aluminium block with a slender shaft so as to allow a large displacement range, the system dynamics exhibited an additional low frequency mode of vibration due to the flexibility of this member. The problem was solved by mounting the tube on a shaft with a nominal diameter of $35mm$, but with a $15mm$ length close to the end of the tube turned down to $\phi 16mm$. This offers a maximum tube displacement of $11mm$, while ensuring that the structural flexibility is provided by the twin beams.

It was observed that if the hole in the test section ceiling immediately above the flexible tube was left open, no fluidelastic instability would occur. This was easily remedied with an aluminium plug. The hole through which the tube support passes was partially sealed by fixing a plate of balsa wood on to the flexible structure, parallel to the outer surface of the test section floor, with a clearance of less than $0.5mm$ (see the detail of fig 3.5). Since this seal was non-contact, no extra damping was introduced to the system dynamics. Trials with flexible seals made of light plastic sheeting which provided a complete blockage, were also conducted, but the additional damping was so large that fluidelastic instability for the first array ($\frac{P}{d} = 1.58$) was completely suppressed over the entire velocity range.

3.2.2 Dynamics of the twin beam system

Before the twin beam support was fabricated, a simple finite element analysis (FEA) was carried out to determine the mode shapes and natural frequencies. The numerical model consisted of 26 2D Timeshenko beam elements, all with the same mass density and Young's modulus. The cross sectional area and the second moment of area were used to differentiate between the elements comprising the twin beams, the aluminium block and the tube. Figure 3.7 shows the first four mode shapes obtained from the FEA for the configuration which was finally fabricated. The nodes of the FE model are shown on the deflected shapes and the undeformed structure is shown as a dotted line for comparison purposes. The flow direction is perpendicular to the page.

It is apparent that there is almost no angular deflection of the tube. Higher modes do in fact exhibit such displacement, but the natural frequencies associated with these modes are of the order of kiloHertz and so can reasonably be ignored. For modes 2 and 4 the tube is moving primarily in the vertical direction along its own axis. These two modes are of little importance since there are no significant fluid forces acting in this direction. Mode 1 and 3 on the other hand, produce the desired pure translation of the tube in the cross flow direction. Both these modes have been verified experimentally by using a stroboscope to freeze the motion produced by sinusoidal excitation from the EMS (which will be described below). It was was not practical to verify the 2^{nd} and 4^{th} modes in this way since it would require excitation in the vertical direction. Another important feature of fig 3.7 is that there is substantial separation between the first and subsequent modes. This would suggest that the motion of the tube mounted on this support can be sensibly analyzed using a single degree of freedom model. Furthermore, the prediction of the fundamental natural frequency agrees well with the value obtained from experimentation.

Since it implicitly assumed that the structure was conservative and linear, the finite element analysis cannot offer any information on whether the physical structure is linear nor can it predict the damping associated with the structure. A series of five tests each

with a different level of excitation were conducted to determine the system's transfer function in quiescent air. The hole in the wind tunnel floor through which the flexible tube assembly must pass restricts the tube motion to be in the range $\pm 11mm$. These tests were conducted prior to assembly of the tube array, so that the displacement of the flexible tube would not be constrained. Furthermore these tests span the range of displacement which is possible when the flexible tube is embedded in the tube array. The excitation was a band limited random force, with a passband in the range $0 - 50Hz$ and the transfer functions were constructed with 40 averages. The transfer functions were used to estimates the equivalent mass, damping and stiffness parameters. Table 3.1 summarizes this series of tests.

Test	F_{EX} (N)	$y_{RMS}(mm)$	m (kg)	c_s (Ns/m)	$k_s(N/m)$
a	0.127	0.70	0.999	2.275	1714
b	0.304	1.42	1.015	2.276	1740
c	0.403	2.03	1.015	2.200	1743
d	0.617	3.03	1.020	2.193	1752
e	0.942	5.25	1.038	2.255	1731

Table 3.1: Tests to characterize the twin beam structure

For each test the RMS of the excitation force (F_{EX}) and the tube displacement RMS (y_{RMS}) is recorded. The estimates of the modal parameters (mass, m,damping c_s, and stiffness, k_s) associated with the structure are also presented. Note that the values of damping include the effect of the shaker. The variation of the modal parameters in table 3.1 from the mean values is of the order of 2%. The fact that this spread seems to be random would suggest that the error is experimental rather than systematic. The independence of the parameters on excitation levels would indicate that the structure is linear, at least within the displacement range of interest. This result can be illustrated graphically by comparing the transfer functions from each test in the region of the natural frequency. Figure 3.8 shows the inertance (the transfer function between acceleration and force) for the highest and the lowest excitation levels. All five transfer

functions have been averaged and this average has been superimposed on the plots for comparison but is almost completely obsured because the curves match so well. As can can be seen, both the magnitude and the phase of the inertance are uneffected by the amplitude of excitation.

In conclusion, the twin beam support offers a system whereby the flexible tube is free to move only in the crossflow direction with pure translation. Furthermore, the structure is linear and can be regarded as having only one mode of deflection. This means that a simple mass-spring-dashpot type model can be used to represent the dynamics of the structure.

3.3 Development of an electromagnetic shaker

The overall aim of this work is to quantify the fluid force associated with the coupled fluid–structure system. If a known excitation force is applied to the tube, then the coupled system can be analysed using well established techniques for single-input-single-output problems. Previous studies on the forced fluidelastic response of a tube array (e.g. Tanaka & Takahara 1981 ,Chen, Zhu, & Jendrzejczyk 1994,Goyder & Teh 1984) were limited because they prescribed either the tube motion or the excitation force to be sinusoidal. Granger (1990b) did examine the forced response due to broad band turbulence, but this was limited because the excitation was unknown and low amplitude. Furthermore, the forced response of the flexible cylinder in quiescent fluid could be used to determine the modal properties of the structure, as discussed in the last section.

Although there are a variety of general purpose commercially available devices which will provide a force proportional to an input signal (either random or deterministic), none of them are completely suitable for this application. An inertial shaker, such as those manufactured by *Metravib* or an electromagnetic shaker such as a *LDS* model 200, will considerably alter the modal parameters of the system, the first will add considerable mass, while the second will add substantial stiffness and damping. This problem can be overcome by placing a force transducer between the shaker and the system, thus

quantifying the effect of the device. However, this usually produces a relatively poor signal-to-noise ratio around the resonant frequencies. For free vibration tests, the shaker must actually be removed. As well as this, a shaker such as the *LDS* type has a limited displacement amplitude. For example the *LDS* model 200, which provides a maximum force of $18N$, has a displacement range of $\pm 2.5mm$.

A simple noncontact electromagnetic shaker (EMS) was developed to provide an excitation force without significantly increasing the system mass or stiffness and without constraining tube motion. This device consists of two components, a coil and a permanent magnet (see fig 3.4). The coil, which is wound around a light cylinder of resin impregnated paper, is fixed to the structure at the excition point. The coil itself sits in the narrow annular gap between the pole caps of a permanent magnet as can be seen in fig. 3.10. When a voltage is applied across the coil, the resulting electrical current reacts with the steady magnetic field to produce a force on the structure proportional to the current in the coil circuit. If it is assumed that the capacitance and inductance of the circuit is negligible, then the force will be proportional to the input voltage. The operating principle of the EMS is identical to the *LDS* shakers or even a loud speaker. The main difference is that in both these devices the coil is suspended on a diaphragm which is fixed to the magnet, thus adding stiffness and limiting the displacement, whereas the EMS has no diaphragm. The coil of the EMS is $25mm$ long. If care is taken to position the magnet with its pole caps at the mid point of the coil while the flexible tube is at rest then the device has an effective displacement range of $\pm 12.5mm$. The EMS is not ideal though; since the annular gap between the magnetic poles is only about $2mm$ wide, the motion of the coil must be almost completely one dimensional. This is not a major limitation as the motion produced by the twin beam flexible structure described in section 3.2.1 is dominated by one dimensional translation. However, it is essential that the coil is not in contact with the magnet during any part of the oscillation cycle and since the coil and magnet are not actually connected, alignment can take some time.

The EMS was used to provide two types of excitation: broad-band random and periodic chirp. In the case of the periodic chirp, the desired input signal for the EMS was

generated in *Matlab* and then converted into an analogue signal using the DAC described in section 3.4. For the broad-band excitation a *Bruel & Kjær* white noise generator (type 1405) was used in conjunction with a lowpass filter with a cutoff frequency of $50\,Hz$. In both cases the resulting signal was amplified with an *LDS* power amplifier, the output of which was then fed into the EMS.

Another effect of installing the EMS is that the damping of the structure will be modified. This is in fact a distinct advantage as the amount of extra damping provided can be varied simply by changing the total resistance of the electrical circuit used to excite the coil. To demonstrate that the electromagnetic damping will be linearly proportional to the tube velocity consider the coil moving in the steady magnetic field of the permanent magnet. An e.m.f. is induced in the coil with a magnitude and direction governed by Lens's law:

$$\vec{\epsilon} = \vec{v} \times \vec{B} \tag{3.1}$$

where $\vec{\epsilon}$ is the induced emf vector;
$\vec{v}$ is the coil velocity vector;
and $\vec{B}$ is the magnetic field vector.

If the coil is part of a closed circuit, then this e.m.f. causes a current:

$$\vec{I} = \frac{\vec{\epsilon}}{R}$$

where R is the total resistance of the circuit, including the coil itself. However, a current carrying conductor in a magnetic field experiences a force:

$$\begin{aligned} \vec{F}_d &= \vec{I} \times \vec{B}l \\ &= \frac{\vec{\epsilon}}{R} \times \vec{B}l \\ &= \frac{\vec{B} \times \vec{v}}{R} \times \vec{B}l \end{aligned}$$

Since the coil is constrained to move perpendicularly to the magnetic field, this expression can be written in scalar notation:

$$\begin{aligned} F_d &= \frac{B^2 l}{R} v \\ &= C_{em} v \end{aligned}$$

where C_{em} is the coefficient of equivalent viscous damping due to electromagnetic dissipation.

$$\therefore C_{em} = \frac{B^2 l}{R} = \frac{G_{em}}{R} \tag{3.2}$$

Thus, the extra damping added by the EMS is inversely proportional to R, the resistance in the coil circuit. This means that if the circuit is open, the extra damping C_{em} is zero, since $R = \infty$. The implication is that the EMS need not be removed to conduct free vibration tests on the structure itself; the coil circuit need only be opened. The subscript *em* denotes that the quantity is related to the EMS. Note that the values of B and l depend on the properties of the magnet as well as the geometry of the coil and pole caps. The effect of these parameters can be gathered into a constant G_{em}. No effort has been made to determine the value of this constant directly since measuring the magnetic flux density in a confined space (the gap between the pole caps) is difficult and unwarranted for this testing programme.

To ensure that the added damping is in fact inversely proportional to the circuit resistance a series of tests were conducted to measure the apparent damping for different circuit resistances. For each resistance considered the flexible tube was given an initial displacement and released. Using the motion of the tube itself to trigger the data acquisition the resulting motion was recorded using a sample rate of 2048Hz and a record length of 4 seconds. A complete description of the instrumentation can be found in section 3.4. Each test produced a decaying sinusoid which could be analysed using the downhill simplex fitting technique described in chapter 4. The variation of the logarithmic decrement (which is indicative of the total equivalent viscous damping) with circuit

resistance can be seen in figure 3.11. A line of the form

$$\delta_{total} = \frac{G_1}{R} + G_0$$

has been fitted to the data points. The constant G_0 corresponds to the damping of the structure alone, while the constant G_1 corresponds to G_{em} in equation 3.2. As can be seen, there is good agreement between the experimental points and the predicted functional form. More importantly, the other modal parameters (mass and stiffness) appear to be unaffected by changing the circuit resistance. This can be seen in figure 3.12 where the frequency of oscillation is plotted against the resistance. Since the damping is so low this frequency can be regarded as the natural frequency. There is some deviation from a constant value, but this scatter can reasonably be attributed to experimental error.

3.4 Instrumentation for vibration monitoring

Since the coupled fluid structure system under consideration is being treated as a single degree of freedom linear system (only pure translation of the tube in the cross-flow direction is considered and the tube is assumed to undergo rigid body motion) there are only four quantities of interest that need to be measured: the tube displacement, velocity & acceleration (the tube response) and the applied force (the tube excitation).

Although the response quantities are linearly related, by the differential operator, it is difficult to obtain a reliable signal by numerical differentiation since high frequency noise will by amplified and so swamp the desired signal. Similarly, with numerical integration, the low frequency noise is amplified. These problems can be overcome by applying low and high pass filters respectively, however this solution will introduce further distortion to the signal due to the filter characteristics, particularly in the phase. Even in the absence of line noise, the numerical differentiation or integration can yield unreliable results (see Worden 1990. Therefore it is desirable to use a variety of instruments to measure the response and so obtain direct independent measurement of the tube displacement, velocity and acceleration.

For each test the relative phase angle between the responses can be estimated easily either in the frequency or the time domain and compared to the theoretical value. Numerical differentiation of the displacement and integration of the acceleration can be used to yield two new estimates for the velocity. Although both these derived velocity signals may be strongly contaminated by noise due to the numerical process, the resulting time records are sufficiently good to verify consistency in the magnitudes with directly measured velocity. In other words, for each data set, by examining the relative phase and magnitude of the measured tube response signals, it can be verified that the appropriate calibration constants were applied, that no overloads occurred and that the data is generally self consistent. This ability to check the integrity of the data obtained further reinforces the need for measuring tube displacement,velocity and acceleration separately.

The displacement was measured in two ways, depending on the tube support. When the tube was mounted on the cantilever $2mm$ foil strain gauges were used to measure displacement of the tube. The gauges were affixed to the cantilever close to the root, on flats which were machined at 90^o to each other. The gauges were calibrated by applying a range of static displacements. This allowed measurement of displacement in both the in-flow and cross-flow direction. The strain gauges are certainly applicable to the twin beam support in principle, but experience with the strain gauges on the cantilever showed that they were prone to electrical noise and drift. This was most likely due to the associated wheatstone bridge circuit rather than the strain gauges themselves. So for the twin beam tube mount, a non-contact capacitive displacement transducer (ncdt) manufactured by $\mu - \varepsilon\ Messtechnik$ was employed. The model used was an S600-5 with a DT620 single channel oscillator/demodulator. This transducer has a stated linearity of $< 0.2\%$ for displacements in the range $0 - 5mm$. Since the tube is free to vibrate with an amplitude of up to $11mm$ (i.e. a peak-to-peak amplitude of $22mm$) the transducer could not be used directly on the tube mount close to the tube the way the accelerometer and velocimeter were. Instead, it was set up close to the fixed end of one of the beams, where the displacement amplitude is lower. The beam provides

a suitable target for the ncdt, as it is flat and metallic. Ideally the surface of the beam would remain parallel to the face of the ncdt. Although this is not the case, this was not a problem as the curvature of the target is negligible. Furthermore, the sensor was positioned so that no part of the target would deflect outside the range for linearity, thus ensuring a linear relationship between the deflection of the tube and the voltage output from the ncdt. The linearity of the response was verified with static calibration tests. One of the disadvantages with using part of the beam as a target is that vibration modes of the beam were present in the ncdt output, while not in the accelerometer or velocimeter readings (these correspond to vertical displacement of the tube, to which the other to transducers were relatively insensitive).

The tube velocity was measured by focusing a *Dantec* 55X-laser vibrometer on the accelerometer casing, which was installed on the rigid blocks at the top of the twin beam assembly. Together with the *Dantec* 55N10 frequency shifter and the *Dantec* 55N20 Doppler frequency tracker, this instrument allows non-contact instantaneous measurements of the surface velocity component in the direction of the laser beam. This sensor provides an analogue voltage signal which is linearly proportional to the instantaneous velocity right down to DC. There are, however, several disadvantages with the system. Firstly, the measured quantity is the velocity of the target *relative* to the receiving optics. This means that the signal can be contaminated by additional sources of noise such as vibration of the vibrometer itself. Furthermore, since the transmitting optics are also the receiving optics, alignment can be tedious. This task is made more difficult because ideally the line of the laser beam should be coincident with the direction of the velocity to be measured. Any deviation from this line will introduce an attenuation of $\cos\theta$, where θ is the angle between the line of the laser beam and that of the direction of motion. Notwithstanding these considerations, this instrument has proved invaluable.

The acceleration was measured using a *Bruel & Kjær* 4370 delta-shear piezoceramic based accelerometer. A *PCB* charge amplifier (model 422E03) and a power source/amplifier (model 482A16) converted the charge to a voltage which is proportional to the acceleration.

All the instruments used to measure the tube response were calibrated at a single frequency using a *Bruel & Kjær* calibration exciter (type 4294). The relative phase distortion between the three transducers was measured by calculating the cross spectra of the measured signals due to a broadband excitation.

For forced response tests a *Bruel & Kjær* piezoceramic force transducer (type 8200) was placed between the EMS coil and the structure. This transducer will measure the sum of the two forces generated by the EMS. One is due to the excitation voltage supplied by the *LDS* amplifier, the other is due to the velocity of the coil itself. Consider the situation when the *LDS* amp is presented with a band limited white noise spectrum. The excitation force due to the input signal will have a flat spectrum (the power amp has been tested and shown not to attenuate any frequencies significantly). On the other hand, the structural response will have a peak at the natural frequency, so the force due to electromagnetic damping will be a maximum at this frequency. As a result, the measured force between the coil and the structure exhibits a drop out around the resonant frequency of the structure, rather than a flat spectrum. This can be seen clearly in figure 3.13 which shows a typical PSD of the input voltage to the amplifier and the corresponding measured excitation force from the force transducer. The spectra are offset by 20 dB for clarity. If the output from the force transducer were to be used as the measure of the excitation the signal-to-noise ratio at the natural frequency would be worse than elsewhere making reliable modal parameter estimation more difficult. The solution is to measure the input voltage to the power amplifier directly. Effectively, the damping behaviour of the EMS is being regarded as part of the structure. The calibration factor necessary to convert the excitation voltage to units of force was determined by conducting dynamic tests and examining a transfer function between the force transducer and the input voltage.

All the dynamic data was digitised and recorded using a HP35650A mainframe fitted with an 8 channel acquisition board (designation HP35655A). A programmable DAC module (HP 35656A) was used to generated the periodic chirp signal that was used in some of the forced response tests. This hardware was controlled by a HP 300

series unix workstation running the *Cada-X* (version 2.8) software package from *Leuven Measurement Systems (LMS)*. This system is capable of synchronous measurements on up to 8 differential voltage inputs using 14 bit analogue/digital conversion (ADC). Each channel has independent programmable analogue amplification and a DC offset (in the range $\pm 4volts$) can be applied so the resultant signal makes as much use of the voltage range of the ADC as possible, thus minimizing the quantization error inherent in any digitization process. Although the HP system has the capability for AC coupling the cutoff is at $1Hz$ with a roll off of $3dB$ per octave. Since the natural frequency of the tube structure is about $6.5Hz$. Experience has shown that the phase distortion caused by the AC filters dramatically changes the estimates for the damping. This issue will be examined in more detail in chapter 4. Since damping estimation features prominently in this work it was necessary to always use DC coupling. The sample frequency can be set easily within the software package subject to the constraint that it must be a power of 2. Anti-aliasing (low pass) filters are present on each input and have a cutoff which is automatically set equal to 80% of the Nyquist frequency (i.e. 40% of the sample frequency). Many of the tests described later have used a sample frequency of $128Hz$ and 8192 points per average, so the effective frequency span is $0 - 51.2Hz$ with a resolution of $\frac{1}{64}Hz$.

The acquired data can be stored directly to the disk of the workstation using on board cache memory as a temporary buffer so that the data is logged continuously during a test (so called Throughput Acquisition or *TPA*). This means that there was effectively no limitation on the quantity of data which could be measured during each test. Alternatively, the data can be stored in the cache memory until the test is complete when it is transferred to the workstation (Block Input Acquisition or *BIA*). Although in this acquisition mode a maximum of 8192 data points per channel can be acquired, the time or frequency domain functions which have been calculated on line can be ensemble averaged, thus reducing the total amount of data which has to be saved. The main advantage of this mode is that it provides an immediate presentation of results. This capability proved useful during the development of the rig and testing procedures. Whether the

data is obtained using TPA or BIA, the time records and spectral functions (power spectra, transfer functions and coherences) can be interrogated within the Cada software to provide a “quick check” of the quality of the data

Figure 3.15 shows a schematic of the instrumentation and acquistion setup described above. Once the data was acquired, codes which were developed specifically for this project, were used export the data from the Cada system to *Matlab*, for further analysis. The analysis techniques used will be dicussed in the next chapter.

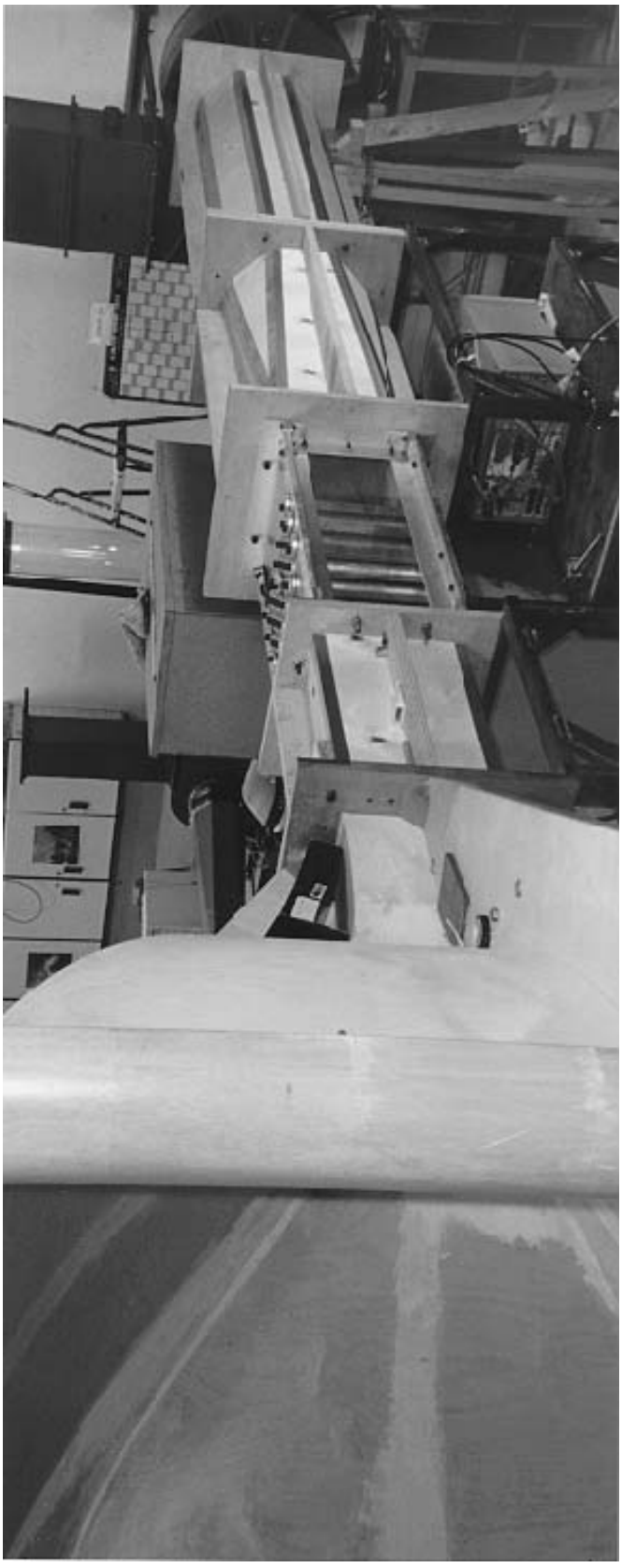

Figure 3.1: A photograph of the assembled wind tunnel.

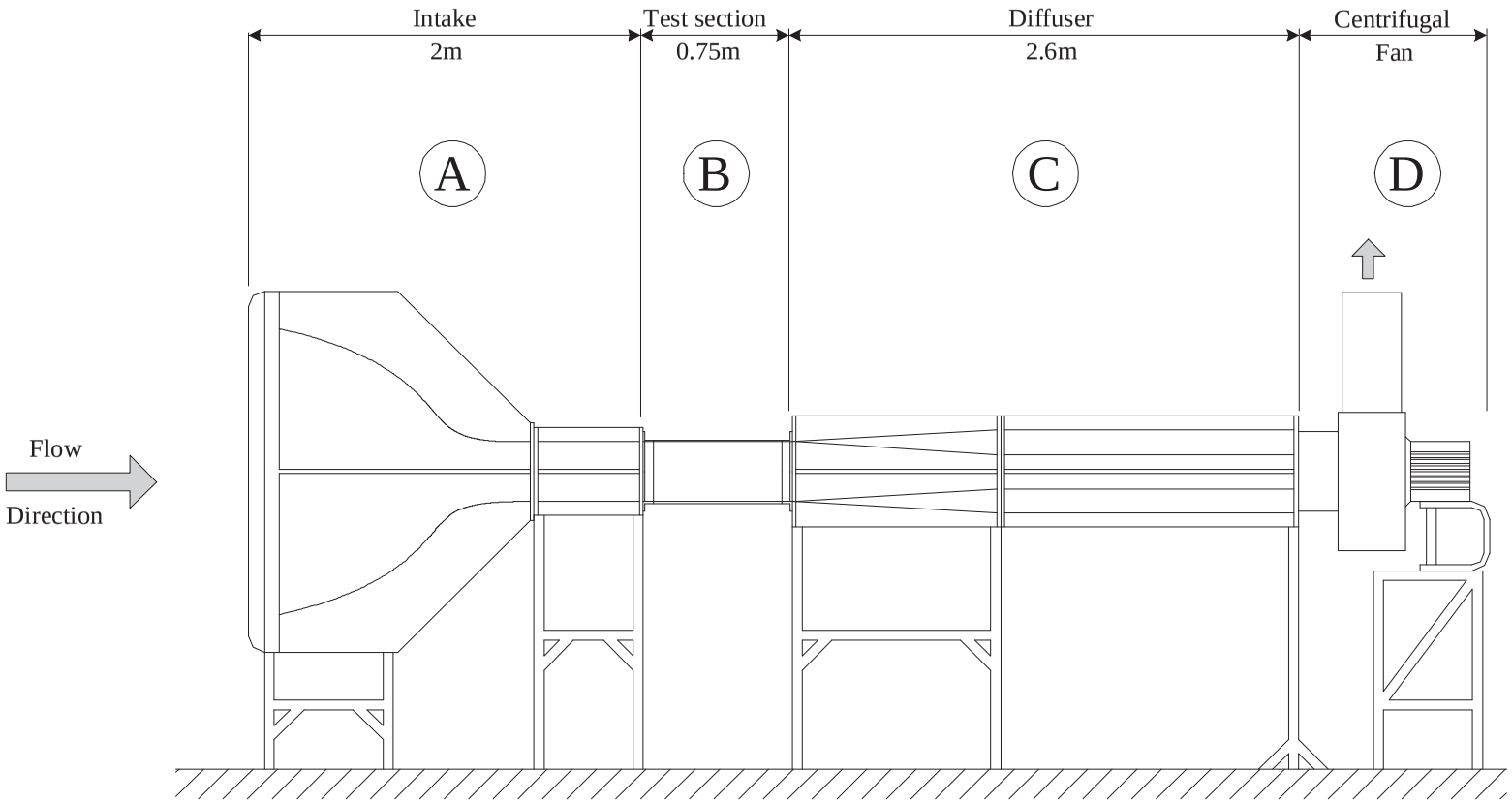

Figure 3.2: A schematic of the assembled wind tunnel.

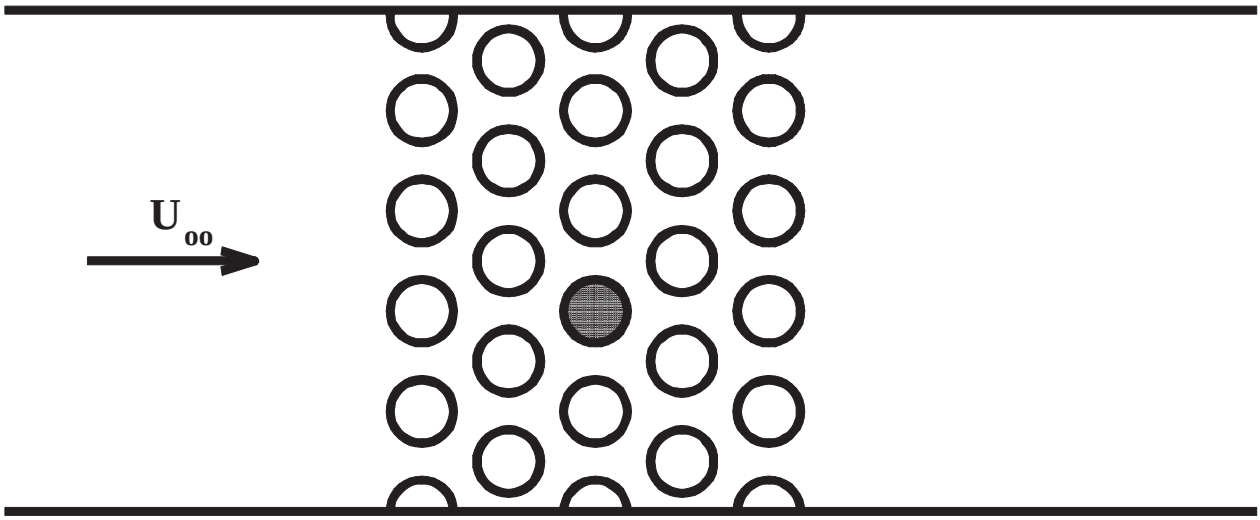

Figure 3.3: A schematic of the normal triangular tube array.

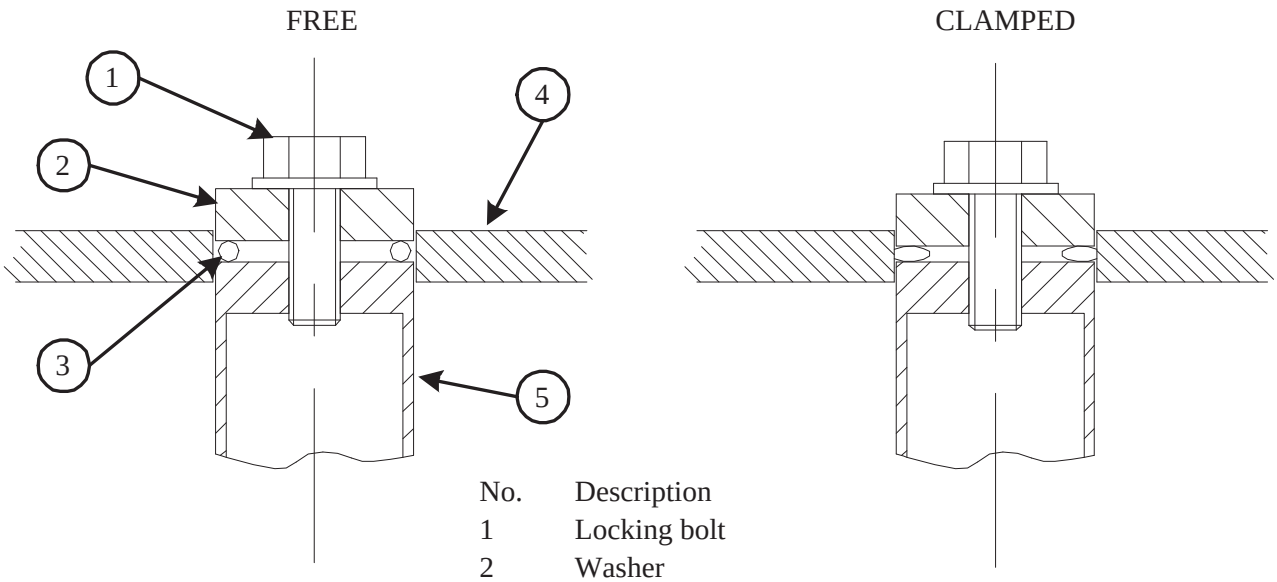

No.	Description
1	Locking bolt
2	Washer
3	Rubber o-ring
4	Wind tunnel ceiling
5	Rigid tube

Figure 3.4: The clamping scheme for the rigid tubes.

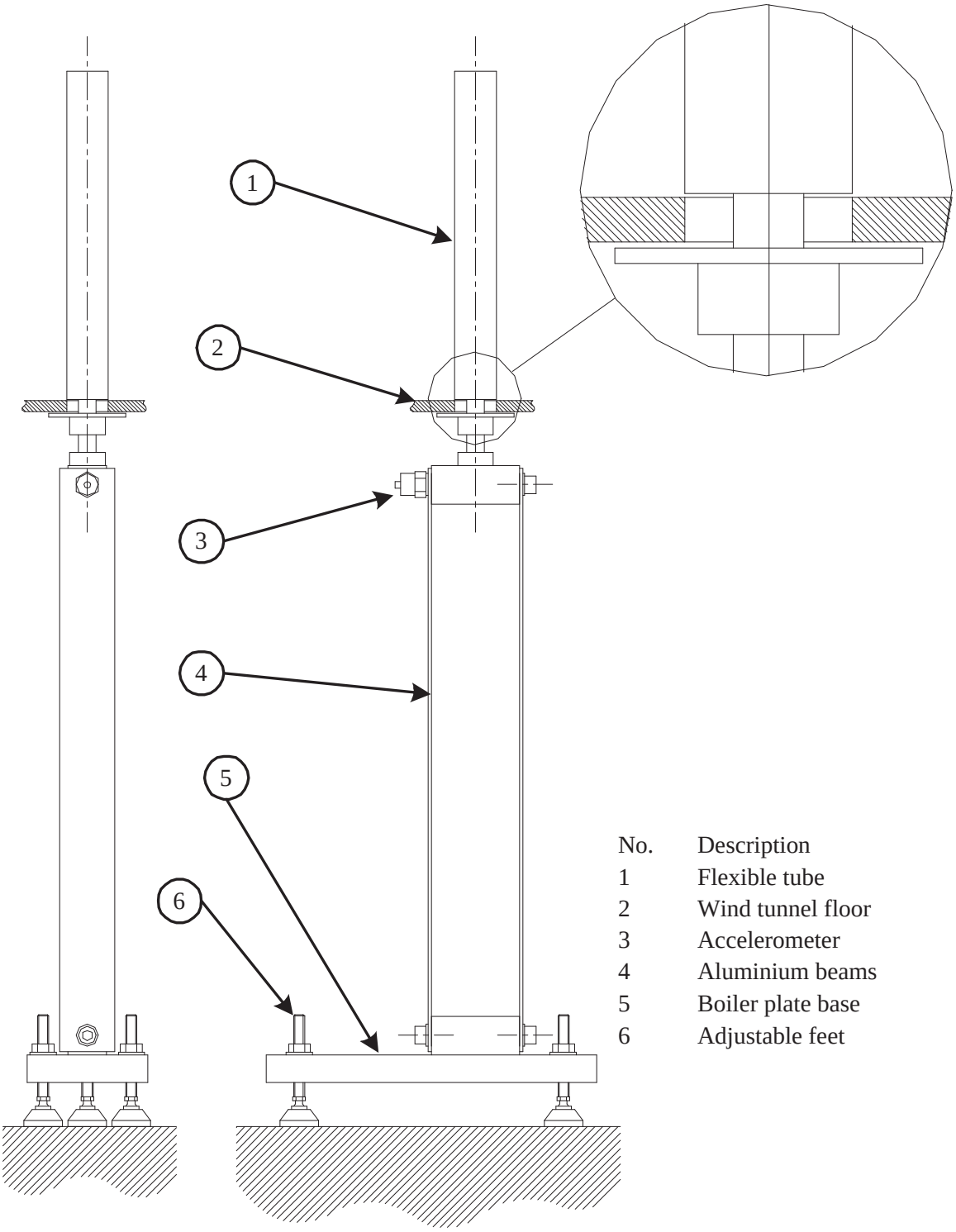

Figure 3.5: Assembly drawing of the twin beam flexible tube support.

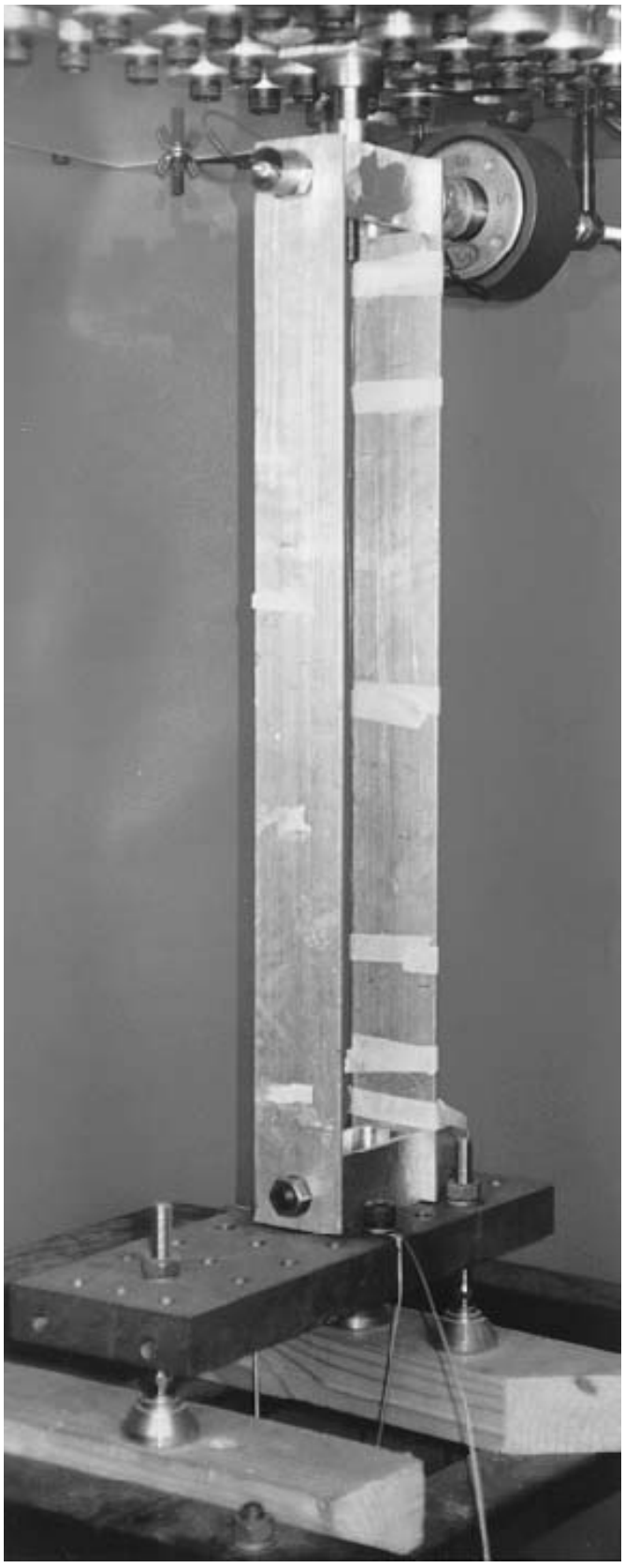

Figure 3.6: A photograph of the flexible tube support.

Mode 1, f_1=6.7Hz.

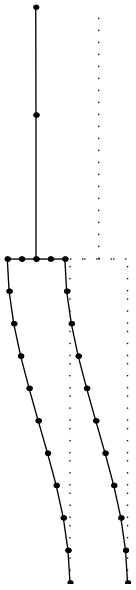

Mode 2, f_2=77.5Hz.

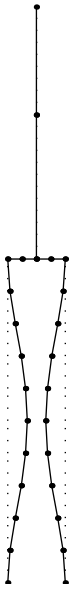

Mode 3, f_3=79.2Hz.

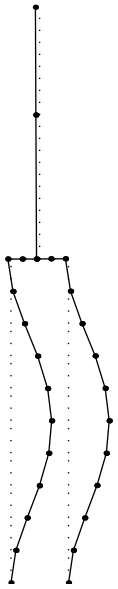

Mode 4, f_4=212.2Hz.

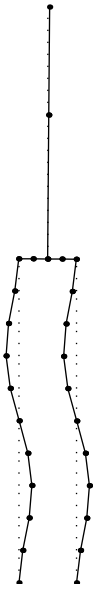

Figure 3.7: First four modes predicted by FEA.

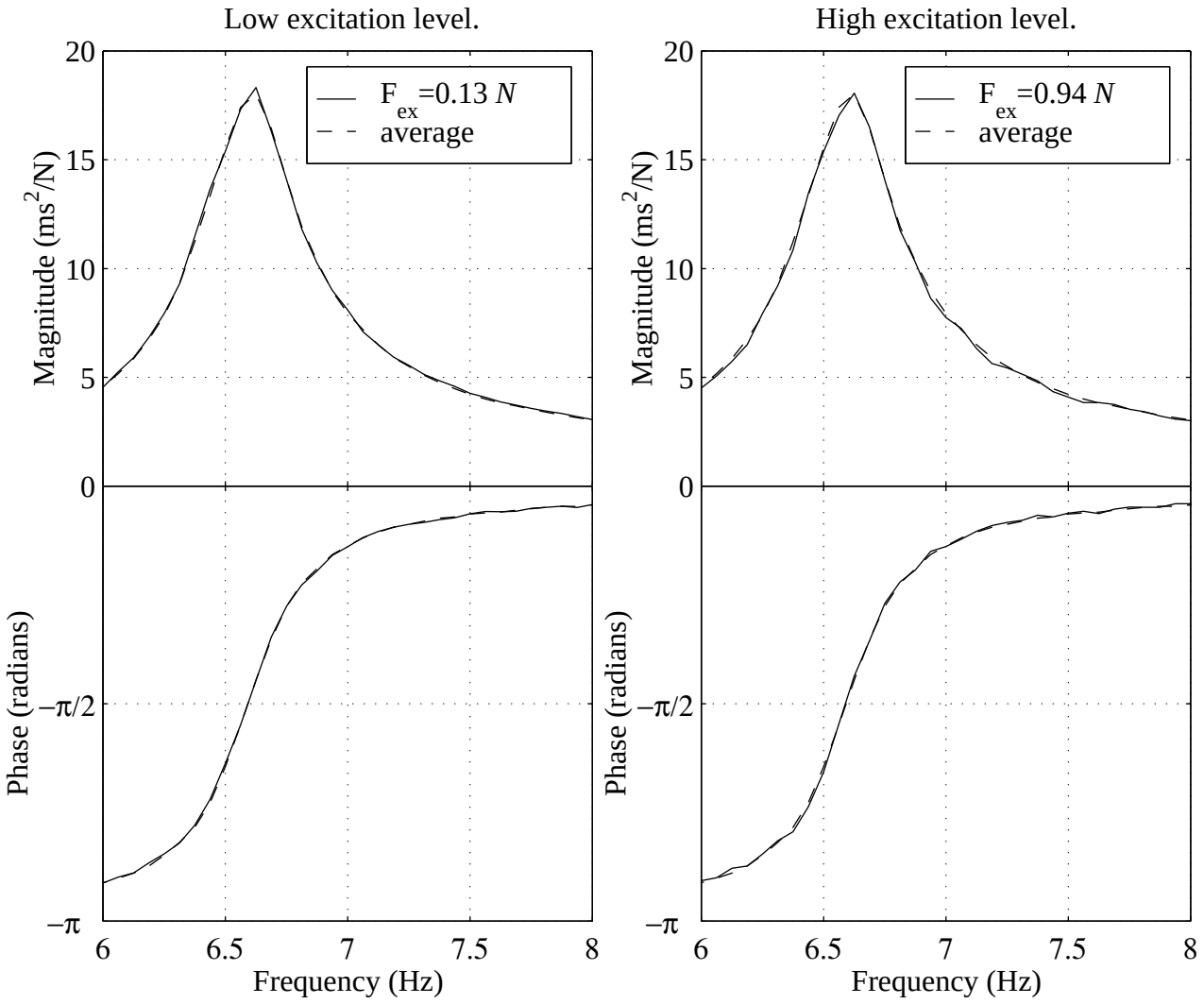

Figure 3.8: System transfer function at two levels of excitation.

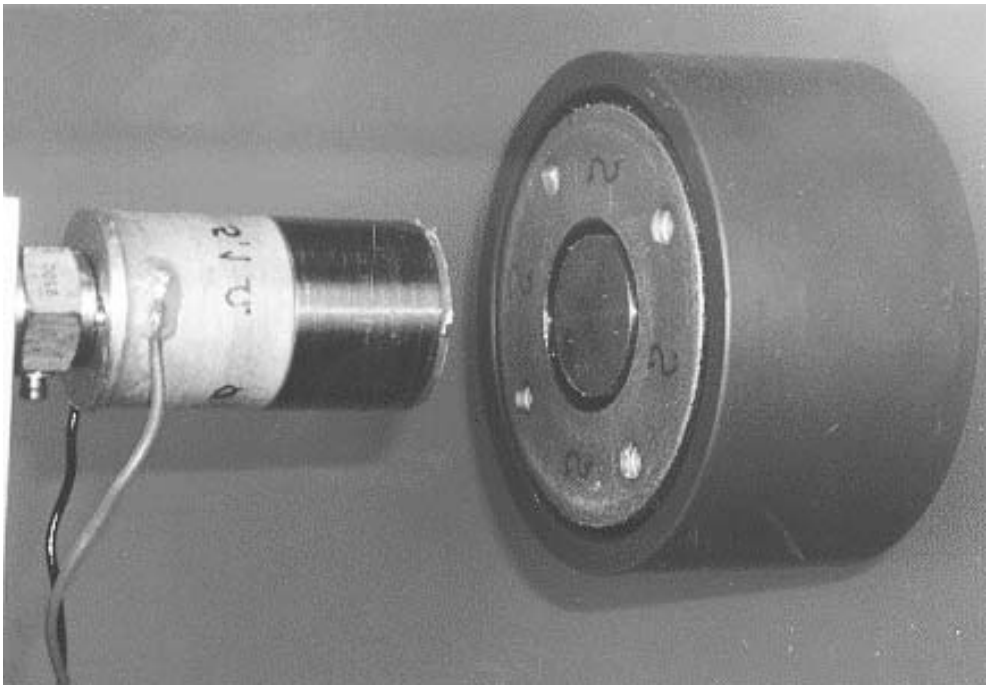

Figure 3.9: Coil and magnet of the EMS.

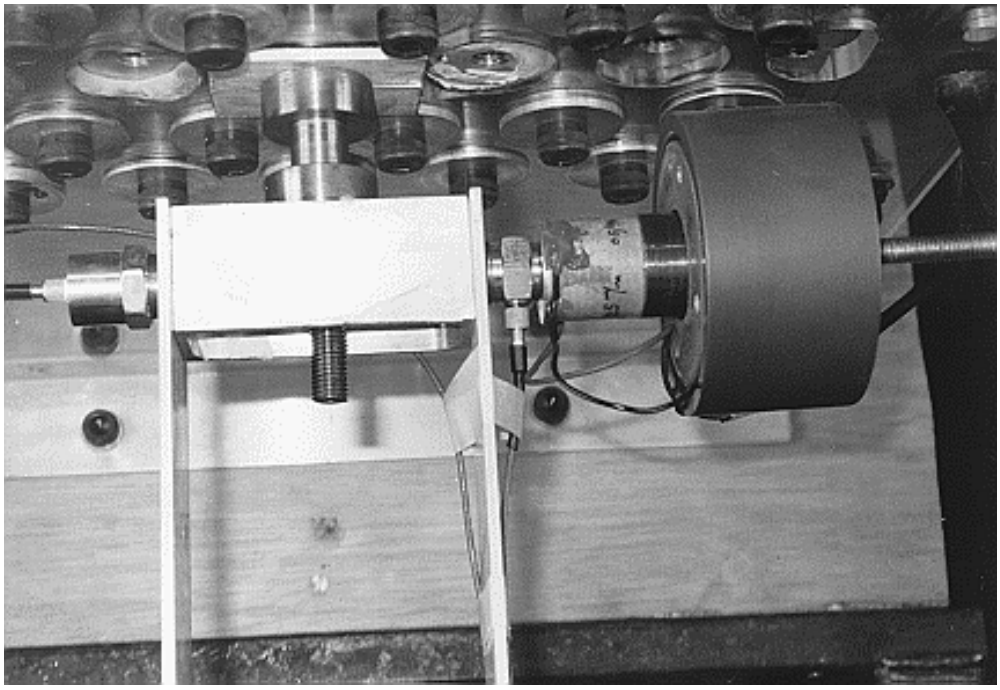

Figure 3.10: EMS *in situ*.

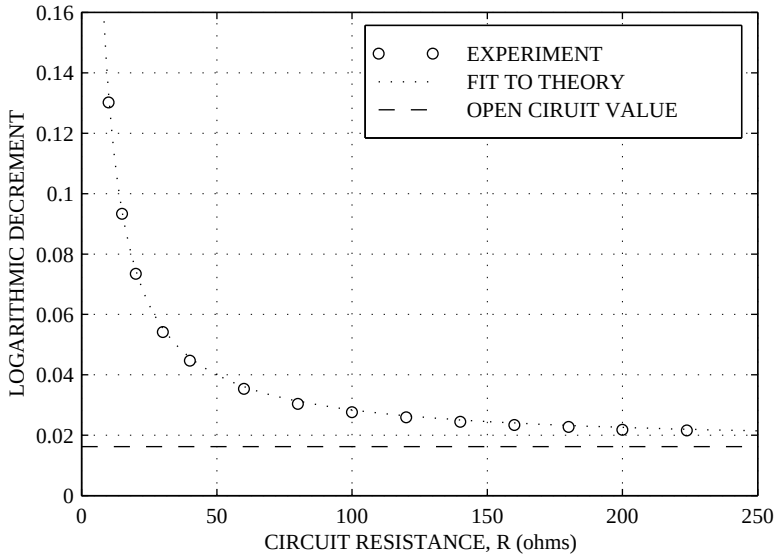

Figure 3.11: The total damping of the flexible tube (in quiescent fluid) as coil circuit resistance is varied.

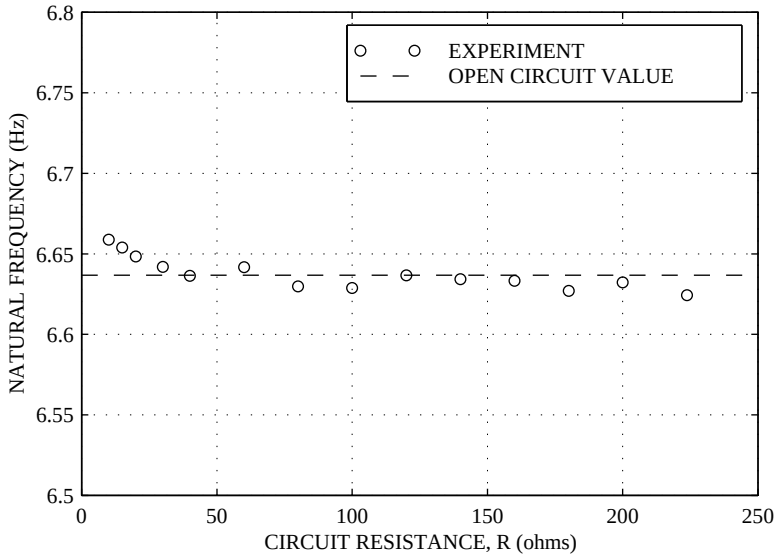

Figure 3.12: The natural frequency of the flexible tube (in quiescent fluid) as coil circuit resistance is varied.

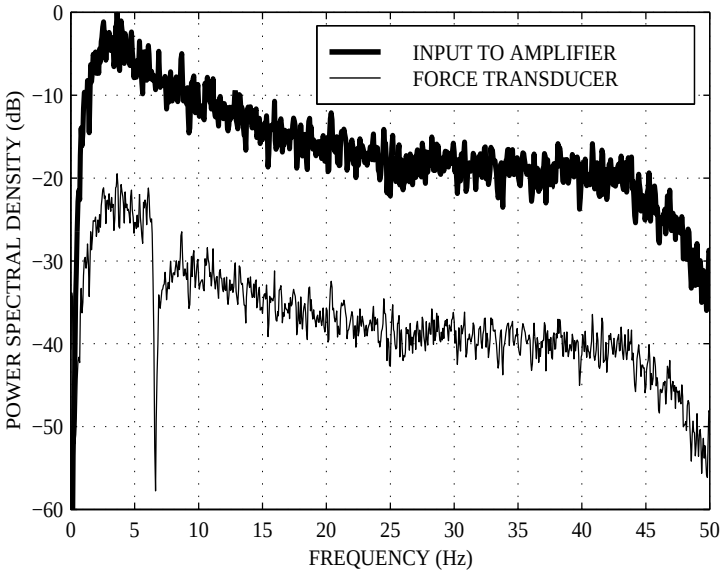

Figure 3.13: Typical power spectrum of the excitation force measurement.

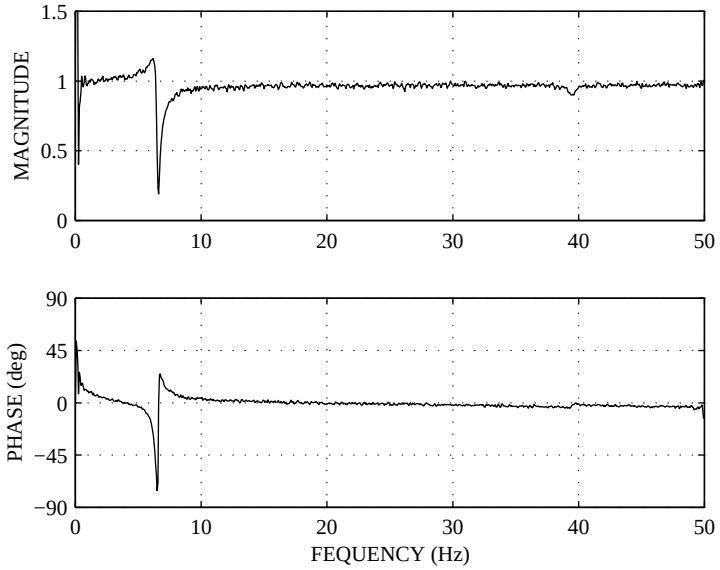

Figure 3.14: Transfer function between the two measures of excitation force.

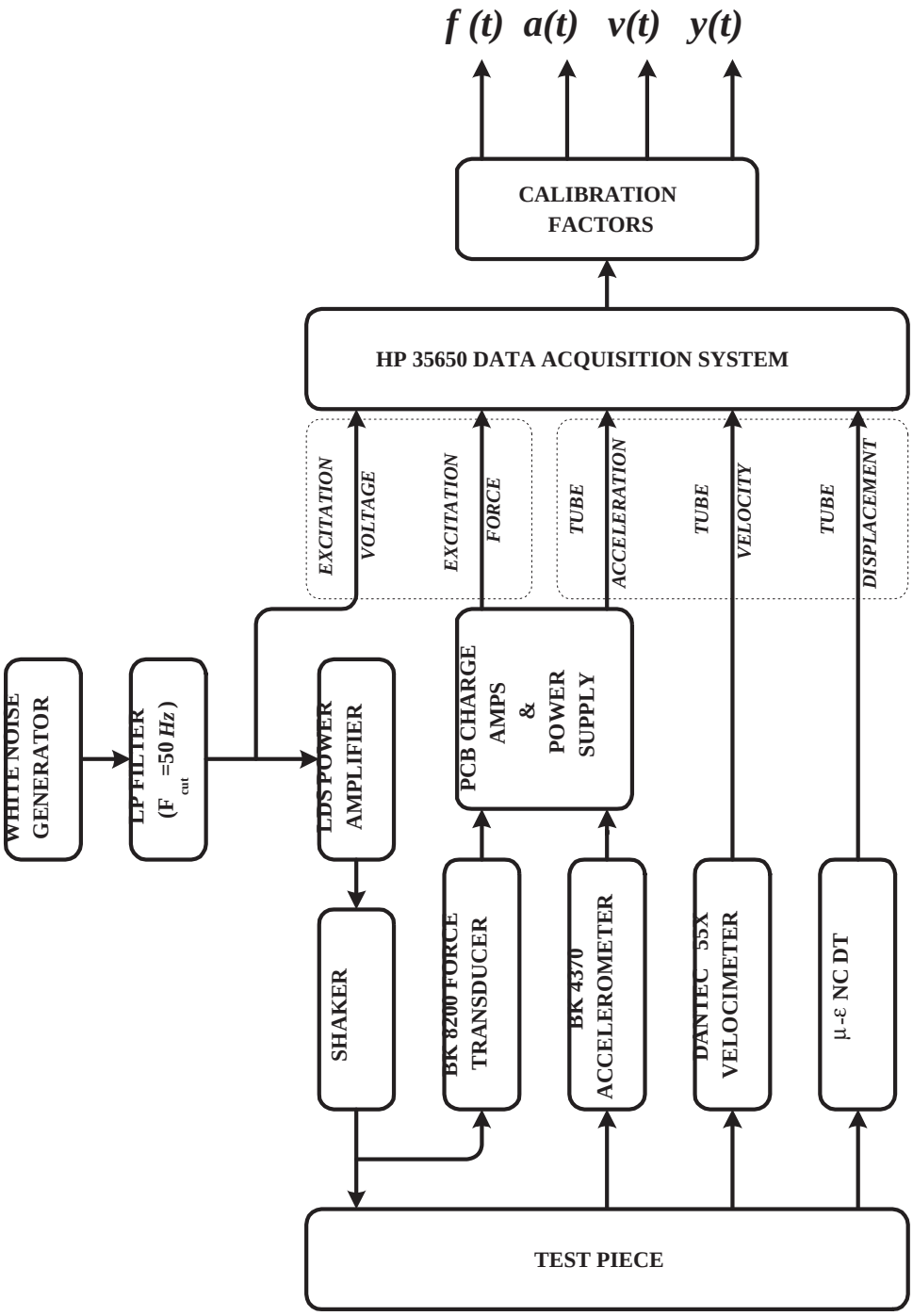

Figure 3.15: Schematic of instrumentation and data acquisition setup.

Chapter 4

Data analysis procedures

The main thrust of this work is concerned with the quantitative identification of the coupled fluid-structure system. There are a wide variety of techniques available for identification of both linear and non-linear systems (se.g. Schoukens & Pintelon 1991; Jezequel & Lamarque 1992). These techniques can all be classified by whether they identify either a parametric or a non-parametric model of the system. Non-parametric models attempt to design a "black box" representative of the system. This model will have the same input/output characteristics as the physical system but not necessarily the same internal structure. These schemes require a large amount of data and produce a large number of identified parameters which have little or no physical meaning. Notwithstanding this, they have enjoyed much success (e.g. Billings & Tsang 1989). In the area of fluidelasticity, Granger (1990b) has successfully used a non-parametric identification technique to model the linear behaviour of a tube array with a single flexible cylinder subject to cross-flow, but this study was limited to low amplitude motion. Conversely, parametric schemes depend on fitting the behaviour of a system to a mathematical model with only a few parameters. The model is assumed based on knowledge of the system. This approach has the benefit that the parameters obtained can be compared with those from other techniques and the identified model can be assessed in a qualitative way, since the nature of the sytsem has also been determined. The three parametric identification techniques which have been used in this study, will be described below.

4.1 Linear Frequency Response Function (FRF)

In the previous chapter, an electromagnetic shaker was described which could be used to excite the flexible tube support with a measurable force. Such a test without fluid excitation is shown schematically in fig 4.1. The transfer function, which is indicative of the system is given by:

$$H(\omega) = \frac{Y(\omega)}{F(\omega)}$$

where Y and F are the Fourier transforms of the tube response and input force respectively. The effect of line noise, R_1 and R_2, on the measured signals, Y_m and F_m, can be reduced by using the ensemble averaged auto- and cross-spectra of the measured signals. This gives two possible estimates for the transfer function $H(\omega)$:

$$\text{either } H(\omega) \approx H_1(\omega) = \frac{S_{FY}(\omega)}{S_F(\omega)} \tag{4.1}$$

$$\text{or } H(\omega) \approx H_2(\omega) = \frac{S_Y(\omega)}{S_{YF}(\omega)} \tag{4.2}$$

In both cases the auto-spectrum will be biased upwards by the line noise.

When the system is subject to fluid loading, the effects of fluidelasticity can be accounted for within the transfer function, but the turbulent buffeting must be treated as an additional external excitation. This situation is depicted in fig 4.2. The cumulative loading G is the sum of the known excitation force F and the unknown turbulent excitation T. If the system is assumed to be linear, the total response Y can be considered to be comprised of Y_F and Y_T, the response due to each of the input forces. Thus the cross spectrum between known input force and tube response can also be separated into two components as can the auto-spectrum of tube response:

$$S_{FY} = S_{FY_F} + S_{FY_T}$$

$$S_Y = S_{Y_F} + S_{Y_T}$$

Substituting these expression into eqn 4.1 & 4.2:

$$H_1(\omega) = \frac{S_{FY}(\omega)}{S_F(\omega)} = \frac{S_{FY_F}}{S_F} + \frac{S_{FY_T}}{S_F} \tag{4.3}$$

$$H_2(\omega) = \frac{S_Y(\omega)}{S_{Y_F}(\omega)} = \frac{S_{Y_F}}{S_{FY_F} + S_{FY_T}} + \frac{S_{Y_T}}{S_{FY_F} + S_{FY_T}} \tag{4.4}$$

If it is assumed that the turbulent excitation T and the input force F are uncorrelated and that the system is linear, then F and Y_T are also uncorrelated, i.e.:

$$\gamma^2_{FT} = 0 \Leftrightarrow S_{FY_T} = 0$$

$$\Rightarrow H_1 = \frac{S_{FY_F}}{S_F} \tag{4.5}$$

$$H_2 = \frac{S_{Y_F}}{S_{FY_F}} + \frac{S_{Y_T}}{S_{FY_F}} \tag{4.6}$$

The extra term in eqn 4.6 implies that the H_1 estimator of eqn 4.1 is more accurate than the H_2 estimator, when the system is subject to fluid excitation.

In practice, the acceleration is used as the measure of tube response. For a single degree of freedom linear system, the transfer function between acceleration and input force is :

$$H(\omega) = \frac{\omega^2}{(\omega^2 m - k) - \jmath\omega c} \tag{4.7}$$

The values of the linearized parameters m, c and k can be determined by fitting eqn 4.7 to the inertance which was estimated experimetally using eqn 4.1. Some manipulation of eqn 4.7 will allow ordinary least squares to be used for the line fitting operation. This method of quantifying the system parameters generates an estimate of the modal mass, but it does necessitate the linearization of the model describing the fluidelastic force. An attempt to relax this constraint was made by employing the non-linear spectral estimation technique descibed by Rice & Fitzpatrick (1988, 1991). These attempts were unsuccessful due to the low contribution of the non-linearities to the total force.

4.2 Downhill Simplex Method (DHS)

The free response of a linear system to a perturbation from equilibrium at time t_q is:

$$y(t_q) = y(q) = A\mathrm{e}^{-\zeta\omega_n t_q}\cos\left(\omega_n t_q + \phi\right) \tag{4.8}$$

In general, the left hand side can be measured, but on the right hand side the amplitude A, damping ratio ζ, natural frequency ω_n and phase ϕ are unknown. The frequncy ω_n could be estimated from examining the time between peaks, and the reduction in subsequent peak values is related to the damping ζ by the logarithmic decrement. Estimating the linear system parameters in this way does not make full use of the the data set and since it depends on identifying the location of peaks, the procedure is prone to large errors due to noise. An alternative is to fit the data $y(t_q)$ with a curve of the form:

$$y_{FIT}(q) = \alpha_1\mathrm{e}^{\alpha_2 t_q}\cos\left(\alpha_3 t_q + \alpha_4\right)$$

Due to measurement errors and noise, $y_{FIT}(q)$ cannot be a perfect representation of the data $y(q)$. Thus, if the error is λ:

$$\begin{aligned} y(q) + \lambda(q) &= y_{FIT}(q) \\ \Leftrightarrow \lambda(q) &= y_{FIT}(q) - y(q) \end{aligned}$$

The problem is now to choose parameter values α_i such that the cost function, ε is minimized:

$$\varepsilon = \| \lambda(q) \|_2 \tag{4.9}$$

It can be seen from eqn 4.8 that y_{FIT} is non-linear in the parameters α_i impling that the cost functin ε is also non-linear in the parameters. This means that the minimization problem is non-linear, so least squares regression is not applicable. Instead an iterative minimization procedure is required.

There are many numerical optimization techniques which could be applied here, but they all have two things in common. Firstly, an initial estimate of the parameters is required to initiate the procedure, and secondly, although the cost function is minimized,

there is no gaurantee that a global minimum has been achieved. In other words, the final estimates of the parameters may depend on the initial guess. These techniques can be classified by the highest order of derivative, with respect to the parameters, of the cost function that is needed. In this study, a zero order technique called the downhill simplex scheme (Nelder & Mead 1965) was used. Gradient (or first order) techniques were rejected because they may take longer than DHS, as the gradients must be calculated at every time step. Furthermore, for some choices of starting values, the gradient techniques may minimize on a subset of the parameter space. Geometrically this is equivalent to converging on a saddle point rather than a local minimum. Although second order techniques, such as Newton-Raphson, do converge more quickly than the other classes, they are more difficult to code and may be divergent for some starting guesses. In comparison, the DHS is easy to code, robust and the fact that only one function evaluation is required per iteration means that, despite the small steps towards the minimum, convergence is achieved in a relatively short time.

For the sake of completeness, the underlying concept is outlined below. A more detailed description of the technique can be found in Press et al. (1992).

A simplex is the geometric figure in n dimensions, comprised of $n + 1$ points and all the interconnecting line segments, polygons, volumes, etc. For example, in two dimensions a simplex is a triangle. In the downhill simplex method each parameter represents an independent dimension. The optimization is initialised with $n + 1$ points where n is the number of parameters. In practice this is achieved by constructing a small simplex with a single starting guess as one vertex. The algorithm then takes a step in which the cost function at each vertex is compared and the point with the largest value of ε is orthographically reflected through the opposite side of the simplex. This operation preserves the area of the simplex. At the next step, the cost function need only be evaluated at the new point since it is already known at the other vertices. Depending on the rate of change of the maximum cost function value with each step, the algorithm may contract or expand the simplex in one or more dimensions. This helps to increase the convergence rate while ensuring that the solution is stable.

Since the downhill simplex method is an iterative algorithm, it must be forced to terminate. This can be achieved by applying several criteria:

- the change during the last step in the sum of the cost function at each vertex is less than some predefined tolerance;
- the change in the vertex position is less than than some specified value;
- a fixed number of iterations have been completed.

In pratice a combination of these criteria is used.

As with any iterative optimization, the initial estimate of the solution set can dramatically affect the final values of the parameters. Experience has shown that for the exponentially decaying sinusoid of this problem, there are only two local minima in the cost function. One is the required solution set, offering a good approximation to the measured data. An example of the y_{FIT} generated with the parameters at the undesired local minimum is shown in fig 4.3. Fortunately, this solution set is not robust and only appears if the initial guess for the phase α_4 is almost exactly π radians removed from the actual phase ϕ. Interestingly, the estimate for the frequnecy is still accurate and the value of damping α_2 is correct, albeit scaled by -1. The estimates of damping and frequency for the structure in quiescent air are used as starting guesses for α_2 and α_3. The maximum value in the measured data set yields the starting guess for the amplitude. The time at which this peak occurs is multiplied by the starting value of the frequency α_3 to provide an initial estimate for the phase α_4. In this way, the initial estimate is never too far removed from the solution set of parameters, and so the DHS converges towards the desired local minimum.

Once estimates of the parameters α_i have been obtained, the total stiffness and damping coefficients can be obtained from α_2 and α_3 by assuming a value for the modal mass. Any error in the calibration factor of the instrumentation will be absorbed by the parameter α_1 and any phase distortion will effect only parameter α_4. Neither of these parameters effect the estimates of the damping and stiffness. Hence, the the DHS identification technique is less susceptible to systematic errors.

4.3 Force Surface Mapping (FSM)

The force surface method (also called the force state mapping) was first proposed by Masri & Caughey (1979) as a non-parametric identification procedure for single degree of freedom non-linear systems, although it has been extended to multi-degree of freedom systems (Masri, Sassi, & Caughey 1982). The underlying concept is straightforward and is best illustrated by means of an example.

Consider the system shown in fig. 4.4. The mass is fixed to ground by two linear elements and a general non-linear element, in which the force is some arbitray function of the displacement and velocity, $E(y, \dot{y})$. Only the mass of the system is known, so the parameters for linear elements, k_s & c_s, must be quantified. In addition, to describe the system, the functional form of the non-linear function must be determined and any relevant parameters estimated. If the system is disturbed from equilibrium, the equation of motion will be:

$$\begin{aligned} m\ddot{y}(t) &= -c_s\dot{y}(t) - k_s y(t) - E(y(t), \dot{y}(t)) \\ &= F(t) \end{aligned}$$

Since a value for m is readily available and the acceleration $\ddot{y}$ can be measured, $F(t)$ is known. At time t, the displacement and velocity can also be measured, so that the restoring force F can be plotted as a surface above the plane of y & $\dot{y}$. Hence, if the system had a cubic stiffness and a cubic damping (i.e. $E = \beta_1 y^3 + \beta_2 \dot{y}^3$), the restoring force surface would look like fig 4.5. At this stage Masri & Caughey (1979) map the state space $(y, \dot{y}, F)$ onto a new space $(\cos^{-1}(y), \cos^{-1}(\dot{y}), F')$. The transformed force surface is then approximated with a series of Cheyshev polynomials, increasing the order until the required accuracy is obtained.

Al-Hadid & Wright (1989) argued that the benefit of the orthogonal nature of Cheyshev polynomials is minimal and increases the likelihood of unacceptable errors due to the coordinate mapping necessary. Their alternative was to use ordinary polynomials so

that the force surface could be expressed as follows:

$$\begin{aligned} F(y,\dot{y}) = &\quad N_1(y) &+ &\quad N_2(y,\dot{y}) &+ &\quad N_3(\dot{y}) \\ = &\quad \sum_{p=0}^{h} \alpha_p y^p &+ &\quad \sum_{p=1}^{r}\sum_{q=1}^{s} \beta_{pq} y^p \dot{y}^q &+ &\quad \sum_{p=1}^{n} \gamma_p \dot{y}^p \end{aligned}$$

The order of the polynomials, n, r, s, h, are chosen to approximate the force surface to the required accuracy.

This is still a non-parametric identification procedure, since non-polynomial non-linearities must be approximated by polynomials. For example, if Coulomb damping is present, r in the equations above would have to be large to give a resonable approximation to the characteristic step change in restoring force around $\dot{y} = 0$. Since the force surface is approximated by a function of the state variables, y and $\dot{y}$, rather than some mapping of these variables, it is straightforward to fit the force surface to any assumed function of y and $\dot{y}$.

Both of these approaches have the advantage of being generally applicable, even if there are cross terms present. Indeed in both cases the authors chose a van der Pol oscillator, which has a strong cross term, to demonstrate their scheme. Both papers consider simulated data so that noise is not an issue. The technique has been successfully applied to experimental data, but invariably the signal-to-noise ratio was high and the non-linearities were strong (e.g. Xu & Rice 1998). In a fluidelastic system, the measured signals may be degraded by unknown turbulent excitation, and the system will be predominantly linear because of the structural support. Furthermore, the total damping force, including the non-linear fluid damping of interest, is expected to be an order of magnitude smaller than the stiffness. This is an issue since the non-linear aspect of the damping is physically of greatest signifigance, but from the point of view of surface fitting, the opposite is true. These difficulties can be alleviated by examining the force surface only in the region close to zero displacement.

This is achieved by calculating the intersection of the force surface with the $y = 0$ plane. In this plane, the total stiffness force N_1 and cross-term N_2 are zero, so the curve obtained is simply the total damping N_3 against velocity, $\dot{y}$. A similar curve for N_1

versus displacement can be obtained by slicing the force surface at the $\dot{y} = 0$ plane. For the example of a system with cubic damping and stiffness, the slices through the force surface and the resulting curves are shown in fig 4.5 and 4.6, respectively. The nature of the cross-term can be investigated by slicing the force surface with a series of planes at constant displacement and subtracting $N_1(y)$ and $N_3(\dot{y})$ which have already been identified. One of the advantages of this approach is that the functional form of N_1, N_2 and N_3 can be determined by examining simple two-dimensional plots.

Once the experimental data has been acquired, the data is discrete and so the force state mapping will not be available as a continuous surface as depicted in fig 4.5. Several interpolation schemes exist to generate a force surface above equispaced points in the state plane (e.g. Masri & Caughey 1979; Worden 1990). However, these techniques are time consuming for large data sets and they tend to smooth the force surface to such an extent that the subtle non-linearities which are of interest in this study may be masked. Therefore, the slices through the force mapping have been achieved by first locating zero crossings in the raw data, and then applying linear interpolation between the two points on either side of the plane. Tracing the system trajectory through the state space in this way obviates the need for surface interpolation and so is computationally inexpensive, even for a large number of samples.

This approach will produce a scatter of points in the plane, which can be fitted by an appropriate curve using a least squares technique. The force axis is derived from a direct measurement of acceleration, while the horizontal axis is either the measured displacemnet or velocity. Since all the data is measured in a similar way, errors are equally likely in the displacement (or velocity) data as they are in the force data. Therefore, an ordinary least squares approach, which assumes that errors are present in only one measurement, is inappropriate. Section 4.4 describes a total least squares algorithm which overcomes this difficulty.

4.3.1 Error due to a phase distortion in measured signals

It is implicit in the discussion of the force surface method above that the displacement, velocity and acceleration must be measured synchronously. Although the acquisition system described in chapter 3 captures the data from its input channels simultaneously, phase distortion in the individual instruments may violate the assumption of synchronization. In this section the effect of a phase error between the measured signals on the identified parameters will be examined. Since the signals are dominated by a single frequency, the phase error will be regarded as a time lag (or lead). The following arguement will be restricted to a linear system. As any non-linearity in the coupled fluid-structure system will be small, it is assumed that the general error trends obtained in this section will be broadly applicable to the non-linear problem at hand.

Appendix A gives the expressions for the free response of a single degree of freedom system. Substituting eqns A.2 into eqn A.1 yields the equation:

$$m\omega_n^2 \left[\cos(\psi + 2\theta) + \jmath \sin(\psi + 2\theta)\right] + c\omega_n \left[\cos(\psi + \theta) + \jmath \sin(\psi + \theta)\right] + k \left[\cos(\psi) + \jmath \sin(\psi)\right] = 0$$

where $\theta = \tan^{-1}\left(-\frac{\sqrt{1-\zeta^2}}{\zeta}\right)$ and $\psi = (\omega t + \phi)$.

This equation can be represented graphically as a vector diagram, with the basis vectors aligned along the real and imaginary axes. Fig 4.7 depicts the equivalent closed vector triangle rotating around the origin with radial frequency ω. The three instantaneous forces (inertia, damping and stiffness) are given by the real components. Note that the common scaling factor $A\mathrm{e}^{-\zeta\omega_n t}$ has been omitted for clarity. In fact, if the exponential envelope is assumed to change slowly with time (i.e. low damping) then this factor can be ignored completely, since the argument which follows is based on the relative size of the vectors.

The error in the parameter estimates due to a phase error in the velocity signal can be assessed by examining the situation when the measured velocity is delayed relative

to the actual velocity by a time Δt. The velocity vector will be rotated clockwise by an angle $\tau = \omega \Delta t$. (Note that a positive angle is a time lag). The force diagram for this scenario is shown in fig 4.8.

The error in the estimated value of the stiffness k' can be estimated by considering the triangle PQS :

$$\frac{k}{\sin(\pi - \theta + \tau)} = \frac{k'}{\sin(\pi - \theta - \tau)}$$
$$\Rightarrow \frac{k'}{k} = \frac{\sin(\pi - \theta - \tau)}{\sin(\pi - \theta + \tau)}$$

Define the signed normalized error in the estimated stiffness k':

$$\varepsilon_k = \frac{k' - k}{k} = \left[\frac{\sin(\theta + \tau)}{\sin(\theta - \tau)} - 1\right]$$

Some manipulation yields:

$$\varepsilon_k = \frac{2 \tan \tau}{\tan \theta - \tan \tau} \tag{4.10}$$

For the error in the estimated value of damping c', consider the triangle QRS:

$$\frac{c\omega_n}{\sin(\pi - \theta - \tau)} = \frac{c'\omega_n}{\sin \theta}$$
$$\Rightarrow \frac{c'}{c} = \frac{\sin \theta}{\sin(\theta + \tau)}$$

Define the normalized error in estimated damping c':

$$\varepsilon_c = \frac{c' - c}{c} = \left[\frac{\sin \theta}{\sin(\theta + \tau)} - 1\right]$$

After some manipulation:

$$\varepsilon_c = \frac{\tan \theta \, (1 - \cos \tau) + \sin \tau}{\tan \theta \, \cos \tau - \sin \tau} \tag{4.11}$$

Fig 4.9 shows a similar situation to fig 4.8, but now the time lag is applied to the displacement. To evaluate the error in the estimated stiffness associated with a phase

error in the displacement signal, consider the triangle PQS in fig 4.9

$$\begin{aligned} \frac{k'}{\sin(\pi-\theta)} &= \frac{m\omega_n^2}{\sin(\pi-\theta-\tau)} \\ \Rightarrow \frac{k'}{\sin(\pi-\theta)} &= \frac{k}{\sin(\pi-\theta-\tau)} \\ \Rightarrow \frac{k'}{k} &= \frac{\sin(\theta)}{\sin(\theta+\tau)} \end{aligned}$$

Using the same definition of ε_k as before

$$\varepsilon_k = \frac{\tan\theta\,(1-\cos\tau)-\sin\tau}{\tan\theta\,\cos\tau+\sin\tau} \tag{4.12}$$

Finally, the error in the damping estimate due to a time lag in displacement can be evaluated by first working on triangle PQR in fig 4.9 :

$$\begin{aligned} \frac{c\omega_n}{\sin(2\theta-\pi)} &= \frac{m\omega_n^2}{\sin(\pi-\theta)} \\ c\omega_n &= -m\omega_n^2\frac{\sin(2\theta)}{\sin(\theta)} \end{aligned} \tag{4.13}$$

And then on triangle PQS :

$$\begin{aligned} \frac{c'\omega_n}{\sin(2\theta-\pi+\tau)} &= \frac{m\omega_n^2}{\sin(\pi-\theta-\tau)} \\ c'\omega_n &= -m\omega_n^2\frac{\sin(2\theta+\tau)}{\sin(\theta+\tau)} \end{aligned} \tag{4.14}$$

With the same definition of the error in the estimated damping e_c, eqns 4.13 & 4.14 yield:

$$\varepsilon_c = -\frac{\sin\tau\,\sin\theta,\tan\theta+\sin\tau\cos\theta}{2(\sin\theta\,\cos\tau+\sin\tau\,\cos\theta)} \tag{4.15}$$

Equations 4.10, 4.11, 4.12, 4.15 represent the error in the parameter estimates using the FSM technique due to phase distortion of the measured signals. The exact level of error depends strongly on the actual values of the parameters c, k, m since θ depends on all these system parameters. So to further investigate the error, consider a specific case which is similar to the system under scrutiny.

Assume that $m = 1kg$, $c = 2.5Nsm^{-1}$ and $k = 1600Nm^{-1}$. This yields a damping ratio ζ of 0.031 and a natural frequency of $6.4Hz$. The equations derived above have been used to calculate the errors in the estimated parameters due to phase distortion for the parameter values assumed for a time delays in in the range $\pm 2.2ms$. The results are shown in fig 4.10, 4.11. The vertical axis is the signed error as a percentage of the exact value. It is interesting to note that the estimated stiffness is robust, varying by less than 1% regardless of which signal is distorted. Similarly, the damping is insensitive to time delays in the velocity signal. However, the error in the damping associated with a distortion in the displacement signal is huge. A very modest time delay of $1ms$ causes a 70% overestimation of damping. This result has been verified numerically by applying FSM to time series generated using eqn A.2 but with a time lag applied to the displacement.

Putting the problem in perspective, the periodic time for this case is of the order of $150ms$ and so a time delay of $1ms$ represents a 2^o phase shift between the displacement and acceleration instrumentation. Therefore, if FSM is to be used (or indeed any time domain technique which depends on all three measured quantities) it is crucial that the instruments be calibrated with particular attention paid to the relative phase distortion.

4.4 Total Least Squares (TLS)

The result of the FSM technique is a two-dimensional plot of restoring force against either displacment or velocity. It was pointed out in the last section that this data may have errors in both axes, so an ordinary least squares regression is not suitable to fit a curve to the data. Consider the restoring force data, from a slice through the $\dot{y} = 0$ plane (the arguemnt is equally valid if the independent variable is to be the velocity $\dot{y}$). In the absence of errors, the instantaneous force at time t_q is related to the displacement by:

$$F(q) = -N_1(y(q)) \tag{4.16}$$

where $F(q) \equiv F(t_q)$ and $y(q) \equiv y(t_q)$. The functional form of the right hand side can be determined by inspection of the graph and approximated by a sum of n simple nonlinear functionals in y:

$$N_1(q) = \sum_{i=1}^{n} \beta_i z_i(q)$$

β_i are the system parameters to be determined and the functionals are given by z_i. So for example $z_2(q)$ might be $(y(t_q))^3$ or $|y(t_q)|$. Since there are n unknowns ($\beta_1 \ldots \beta_n$), the number of data points p must be at least n. The parameters can be gathered into a row vector with n entries:

$$\underline{B} = [\beta_1, \beta_2, \ldots, \beta_n]$$

The measured response and the derived non-linear functionals can be gathered into a $p \times n$ matrix $\underline{Z}$ and the column vector of the measured restoring force $\underline{F}$ with p elements:

$$\underline{Z} = [z_1(q), z_2(q), \ldots, z_n(q)]$$
$$\underline{F} = [F(q)]$$

The measured data can be further grouped by defining the augmented matrix:

$$\underline{D} = [\underline{Z}\ \underline{F}]$$

In the presence of measurement errors, equation 4.16 becomes:

$$F(q) + \lambda_{n+1}(q) = -\sum_{i=1}^{n} \beta_i \left(z_i(q) + \lambda_i(q)\right) \tag{4.17}$$

Defining the unkown error matrix, with dimensions $p \times (n+1)$

$$\underline{\Lambda} = \left[\lambda_1(q), \lambda_2(q), \ldots, \lambda_(n+1)(q)\right]$$

equation 4.17 can now be expressed in terms of the measrued data:

$$\left[\underline{B} \quad 1\right] (\underline{D} + \underline{\Lambda}) = 0$$

The system can be identified by choosing an optimal parameter set $\underline{B}_o$ such that the Frobenius norm, $\| \underline{\Lambda} \|_F$, is minimized. Golub & van Loan (1983) have shown that the solution to this problem can be obtained from the singular value decomposition of the augemented matrix $\underline{D}$.

The SVD of $\underline{D}$ is:

$$\underline{U}^T \underline{D} \, \underline{V} = \text{diag}\,(\sigma_1, \sigma_2 \ldots \sigma_{n+1}) = \underline{\Sigma}$$

Note that U and V are not in any way related to the flow velocity. Unfortunately, U and V are standard notation for the orthogonal matrices associated with SVD. The matrix $\underline{V}$ can be subdivided into four partitions:

$$\underline{V} = \begin{bmatrix} \underline{V}_{11} & \underline{V}_{12} \\ \underline{V}_{21} & \underline{V}_{22} \end{bmatrix}$$

where $\underline{V}_{12}$ is a $n \times 1$ vector and $\underline{V}_{22}$ is a scalar. Once the augmented matrix $\underline{D}$ has been decomposed and $\underline{V}$ partitioned, the solution set to the TLS problem is

$$\underline{B}_o = \underline{V}_{12} \underline{V}_{22}^{-1} \tag{4.18}$$

and the error matrix associated with this parameter set is

$$\underline{\Lambda}_o = -\underline{D} \begin{bmatrix} \underline{V}_{12} \\ \underline{V}_{22} \end{bmatrix} \begin{bmatrix} \underline{V}'_{12} & \underline{V}'_{22} \end{bmatrix}$$

Thus, a measure of the total residual error is given by the expression:

$$\varepsilon = \| \underline{\Lambda}_o \|_F \tag{4.19}$$

This algorithm has the advantage that it is linear in the parameters β_i even though it fits a non-linear model to the data. The benefit of this characteristic is that different models can be quickly fitted to the system and their accuracy compared. The major flaw in the technique is that the error in each of the functionals, z_i is indepentent. Although this is not physically accurate, since one would expect some correlation between two non-linear functions of the same data, there is no technique, linear in the parameters, which can account for the dependent nature of the errors.

4.5 Summary

Three techniques have been described for system identification.

- The first, which is based on the frequency response (FRF) of the flexible tube to a measurable excitation, has the advantage that it yields an estimate of the modal mass allowing the effect of added fluid mass to be assessed directly. Estimates for the stiffness and damping are also obtained. However, this procedure is limited to linearized parameter estimation.

- The downhill simplex (DHS) scheme can provide estimates of linearized parameters from the free response of the tube. Since this technique requires just one measurement of the response, it is not prone to errors caused by relative phase or magnitude distortion in the instrumentation. It is theoretically possible to extend the DHS method to identify a non-linear model, but this would require an analytical expression for the free response of the model. In general, such an expression can not be easily obtained for non-linear systems. Furthermore, it would be difficult to assess the applicability of the assumed model.

- The last identification method considered (FSM) provides a qualitative assesment of the extent and nature of the non-linearities from free response data. Used in conjunction with the total least squares algorithm (TLS) it can also quantify the parameters of a non-linear model. The drawback with this technique is that it requires simultaneous measurements of all three response variables, and so is susceptable to both phase and magnitude distortion in these signals.

These techniques have been applied to experimental data of the tube response under the influence of fluid loading. The linearized parameter estimates obtained with the first and second (FRF and DHS) methods will be discussed in chapter 5, while the non-linear model identified with the third method (FSM) will be described in chapter 6.

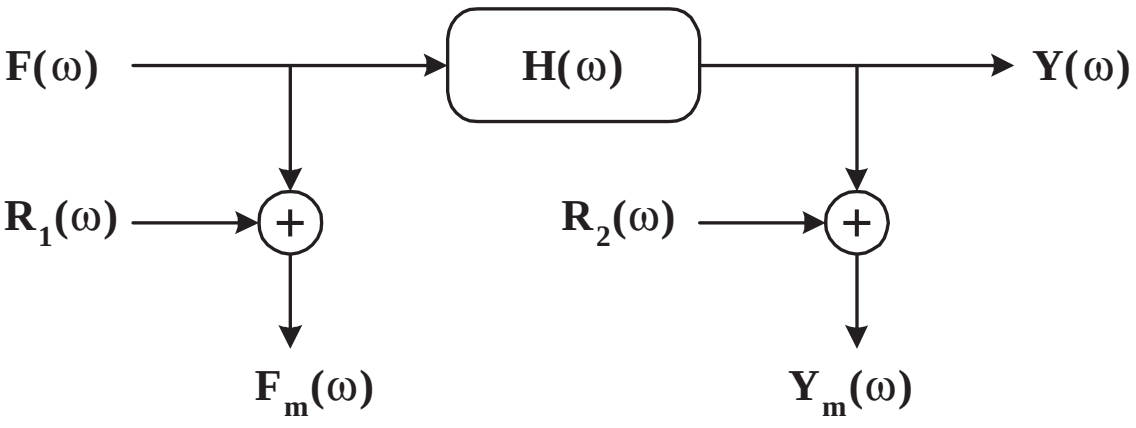

Figure 4.1: Block diagram of system with line noise on measured signals.

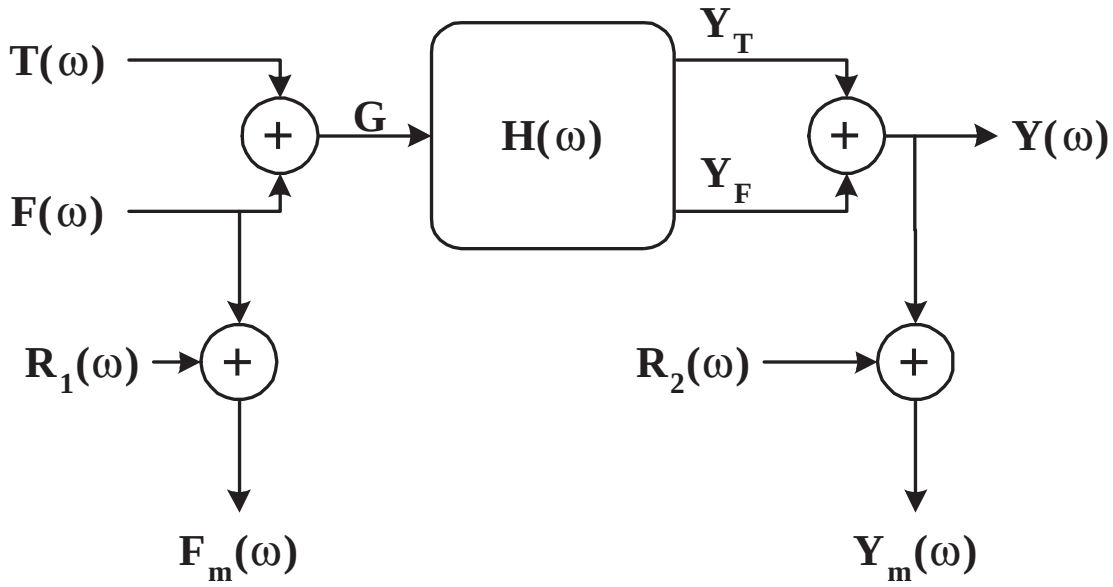

Figure 4.2: Block diagram of system with turbulent excitation.

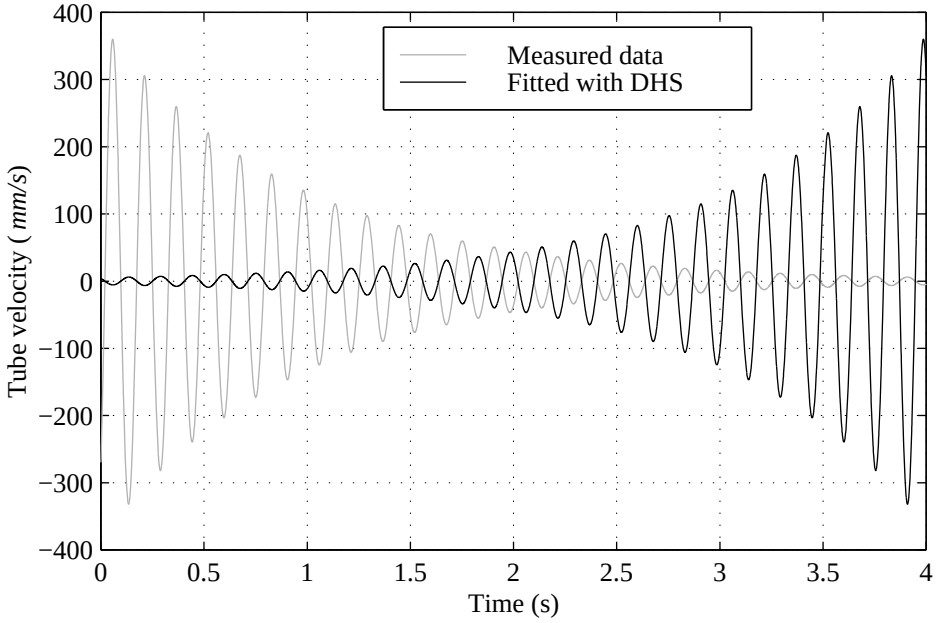

Figure 4.3: Erroneous line fit using the downhill simplex method.

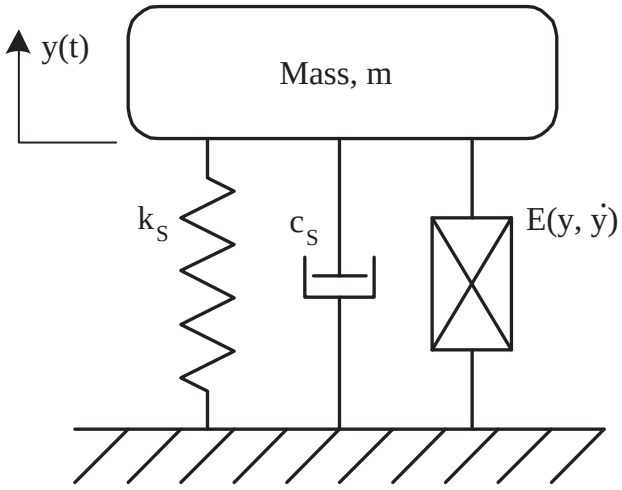

Figure 4.4: Schematic of single degree of freedom non-linear system.

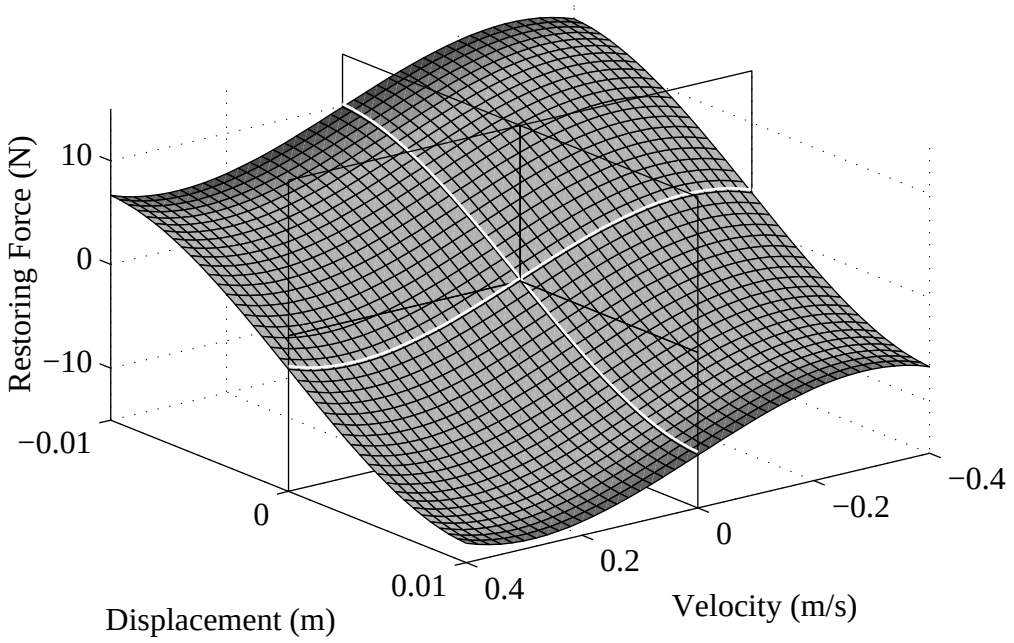

Figure 4.5: Restoring force surface.

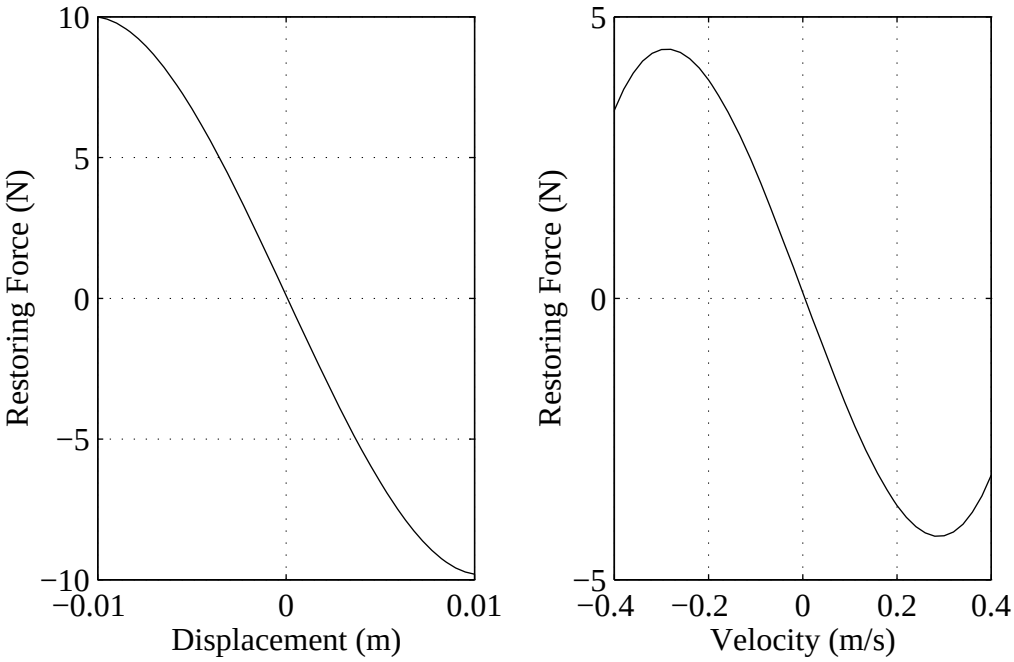

Figure 4.6: Slices through the force surface.

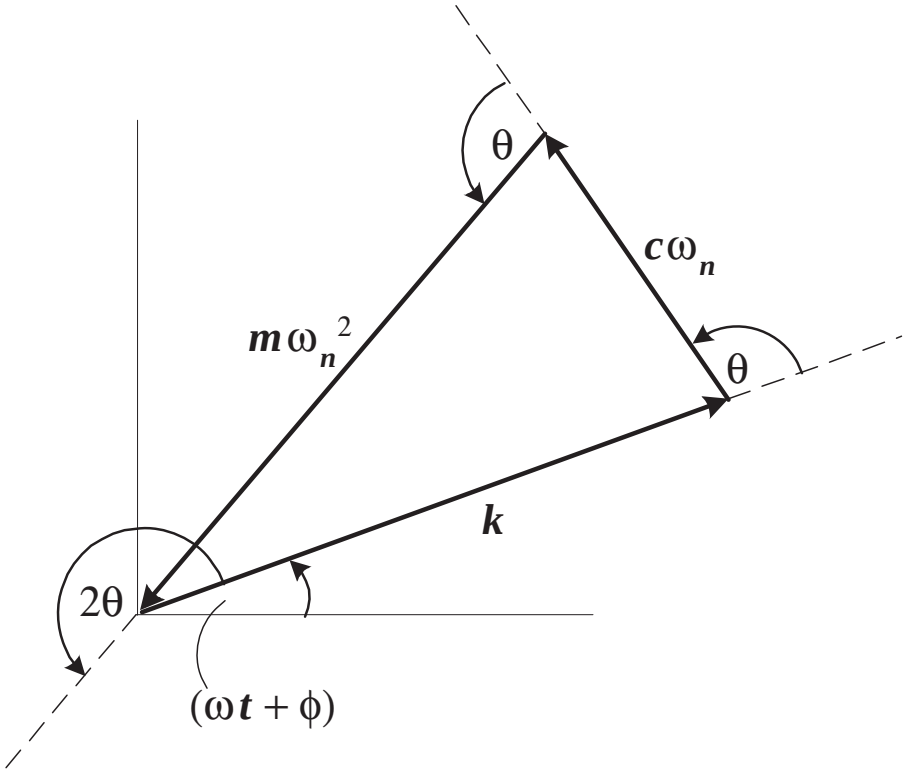

Figure 4.7: Force diagram for free response

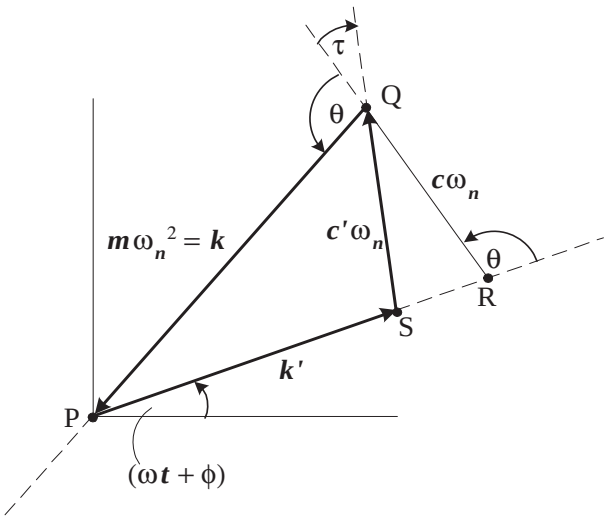

Figure 4.8: Force diagram for free response with a time lag in velocity

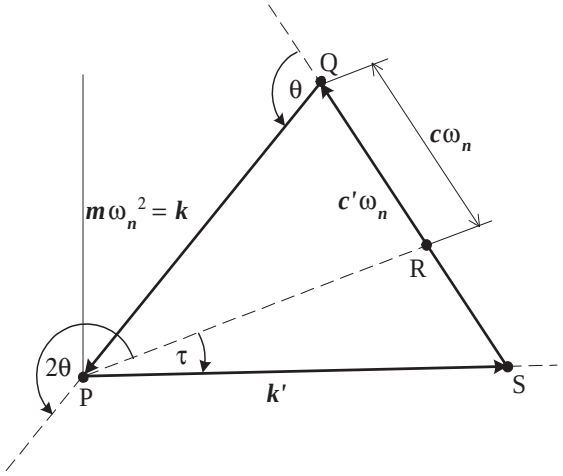

Figure 4.9: Force diagram for free response with a time lag in displacement

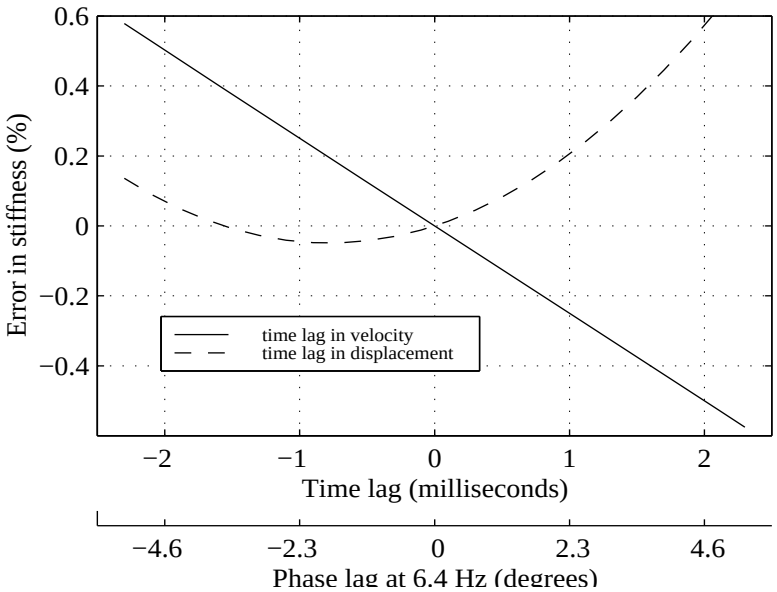

Figure 4.10: Errors in the estimated stiffness due to phase distortion of the measured signals

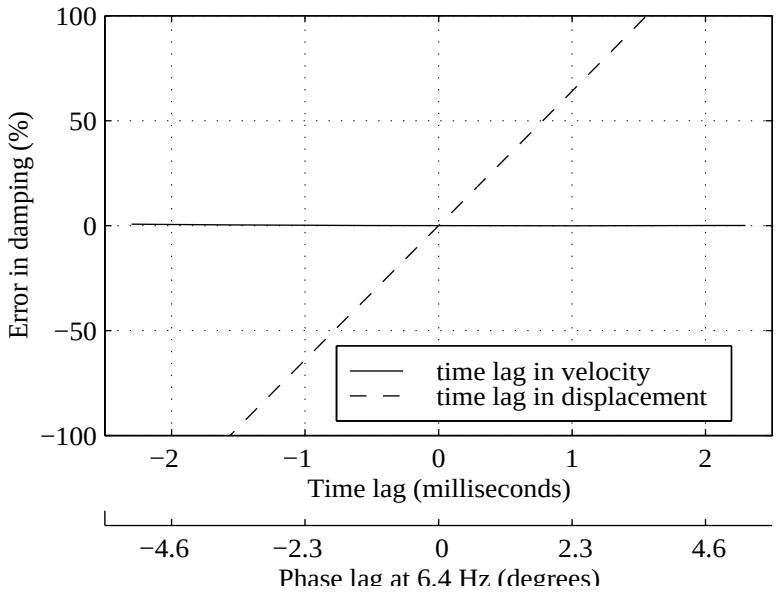

Figure 4.11: Errors in the estimated damping due to phase distortion of the measured signals. Note the vertical scale; 100% error!

Chapter 5

A linear model

Preliminary tests were conducted with the flexible tube in the third and fourth row of a five row array. Broadly similar results have been obtained for linearized parameters at both locations. Therefore, all the results presented in this chapter and the next are for tests with the flexible tube mounted in the third row.

5.1 Vortex shedding

The flexible tube was mounted on the twin beam support detailed in chapter 3. This mounting scheme allows motion only in the cross flow direction. The flexible tube was given an initial displacement and the motion was allowed to decay. The time records were ensemble averaged to minimize the effect of turbulence. Fig 5.1 & 5.2 show the power spectra for the tube acceleration obtained from these transient tests using the accelerometer. For both arrays, the flexible tube was in the third row and the damping was at the maximum possible level. The spectra have been scaled and offset for clarity. The first mode of vibration is at about $7Hz$. In fig 5.1, higher modes are clearly visible around $100Hz$, $200Hz$ and $400Hz$. In fig 5.2, there is also a peak at 50Hz. This can be attributed to interference from the electric mains. When the two graphs are compared it is obvious that the relative strengths of the modes are different. This is most apparent when the mode just above 200Hz is examined in each figure. One might expect the

structural chracteristics to be identical for both tests. However two different levels of electromagnetic damping were applied in each set of tests so as to ensure that fluidelastic instability did not occur. A feature which cannot be attributed to the structural dynamics is the peak denoted by the symbol $\circ$ on each spectrum. The frequency of this peak tends to increase as the flow velocity increases, suggesting a Strouhal periodicity. If the vortex shedding frequencies are plotted against the flow velocity a straight line is obtained (see fig. 5.3). The Strouhal number based on the freestream velocity can be estimated from the slope of the straight line fitted through each data set. The Strouhal number for $P/d = 1.58$ was estimated at 1.4 while for $P/d = 1.32$ a value of 2.18 was calculated.

Polak & Weaver (1995) suggest that the data from Pettigrew & Gorman (1978) could be discarded on the basis that it was obtained from large amplitude oscillation in water flow, but do not explain why this data should be unreliable. The two new data points from this study would tend to suggest that the results of (Pettigrew & Gorman) are valid. The values estimated here are not inconsistent with hotwire measurements in rigid arrays with similar pitch ratio. For example, for a pitch ratio of 1.6, (Polak & Weaver) report a Strouhal number of 1.42, while for a ratio of 1.33 they have obtained a Strouhal number of 2.51. Furthermore, these two new values for Strouhal number are in agreement with the empirical curves for normal triangular arrays determined by Oengören & Ziada (1995). Therefore, when viewed with all the other available data, it would appear that the vortex shedding frequencies determined here are typical of those observed in other studies.

As well as providing new data for vortex shedding, these tests suggest that the fluid flow within the tube arrays under investigation behaves in a similar fashion to other experimental facilities which have been documented in the literature. It is also clear that the vortex shedding frequencies are sufficiently high that Strouhal periodicity can be sensibly ignored when considering the system dynamics around the first natural frequency (6.5Hz) as the lowest vortex shedding frequency in the velocity range considered is at $160Hz$.

5.2 FEI for an array with two degrees of freedom

The flexible tube was mounted on the cantilever support and placed in the third row of the array with pitch ratio of 1.58. This provides at least two degrees of freedom for the tube array: translation in the crossflow and inflow directions. The flow velocity was systematically varied over the entire operating range of the wind tunnel. At each flow velocity the tube was allowed to develop a steady motion. In practice this was achieved by allowing the system 300 seconds to settle. This is comparable to the settling time allowed by other researchers (e.g. Andjelic & Popp 1988 allowed 600 seconds). Furthermore, several tests have been conducted allowing longer settling times. In these tests the RMS of the tube motion was found to be unaffected. Once this settling time had elapsed, the tube motion was recorded using the 2 strain gauges mounted on the cantilever. The data was acquired at a rate of $256Hz$ and the record length was 32 seconds. This yields a minimum frequency resolution of $0.03Hz$

In fig 5.5, the RMS of tube displacement measured with the strain guages is plotted against the onset flow velocity measured upstream of the tube bundle. It is apparent from the trace for cross-flow motion that the tube array has developed fluidelastic instability. This is characterised by the very rapid increase in RMS displacement in the region of $U_\infty = 6.0m/s$. It is noteworthy that there is only a slight increase in inline motion. This is further emphasised by figure 5.4 which depicts a typical trajectory for the tube after the onset of instability. Although the amplitude of inline motion is substantially smaller than that of the cross flow motion, the inline motion is phase locked to the cross flow motion (in fact it is 90^o out of phase). The other feature to note in fig 5.5 is that even before the onset of fluidelastic instability, the amplitude of the cross flow motion is larger than that of the inline motion. It might be expected that these motions should be similar since they are both excited by a similar turbulent field. However, as will be seen in later sections, the force associated with the coupled fluid-structure system can modify the total damping even before the onset of the instability threshold. If it is assumed that the tube is excited in the two directions by two different random forces with the same

statistical properties (or indeed exactly the same broadband random force), the reduction in damping in the cross flow direction would account for the larger response amplitude in that direction.

Several researchers (e.g. Rzentkowski and Lever 1992; Andjelic et al. 1990) have reported a hysteretic effect with respect to flow velocity, when investigating vibration amplitude. However, whether the tube has been brought to rest or given a large initial displacement before being allowed to establish steady motion appears to make no difference to the RMS response in the current tests. This would imply that there is no hysteretic behaviour for this array and range of parameters.

These observations are generally in agreement with reports in the literature (e.g. Price & Zahn 1991 and Andjelic & Popp 1988) and imply that fluidelastic instability can be explored with just one degree of freedom. While this assumption is used widely as the basis for theoretical models and data reduction, it has not previously been tested experimentally.

5.3 Fluidelastic instability threshold

The flexible tube was again mounted on the twin beam arrangement described in chapter 3. This support scheme allows motion only in the crossflow direction. All subsequent results presented have been obtained using this setup.

A series of tests have been conducted to investigate the stability thresholds of the two array geometries with the 1 degree of freedom tube placed in the third row. As with the 2 degree of freedom system, at each flow velocity the tube is brought to rest and then allowed 300 seconds to establish a steady motion. The resistance in the EMS circuit was varied to obtain three different levels of damping for each array so that the instability thresholds lay within the wind tunnel velocity range. Initially the denser array ($\frac{P}{d} = 1.32$) was tested at the the same damping levels as the first array ($\frac{P}{d} = 1.58$). However, at these low levels of damping the flexible tube exhibited fluidelastic instability at even the lowest flow velocity ($2.5m/s$). For this reason, higher total damping levels were

used for a pitch ratio of 1.32.

Fig 5.6 and 5.7 show the RMS of the tube displacement for array pitch ratios of 1.58 and 1.32 respectively. The rapid increase in vibration amplitude characteristic of fluidelastic instablity is apparent and it is obvious that the value of damping determines the flow velocity at which this "step" occurs. This is the instability threshold or critical velocity, U_c. An abrupt drop in amplitude at around 9 *m/s* can be seen in fig 5.7 for the pitch ratio of 1.32. Unlike the critical velocity, this drop does not depend on damping. A loud acoustic resonance was clearly audible at this velocity the frequency of which was found to be 1053Hz. This frequency was determined with a microphone outside the windtunnel, downstream of the array. No such resonance was observed for the pitch ratio of 1.58, suggesting that the resonance is particular to this array, rather than to the wind tunnel. Unfortunately the limit of the wind tunnel velocity range with this array is 9 *m/s* so it was impossible to explore the behaviour of the array at higher velocities and so verify that the instability would in fact re-establish itself after the conditions for acoustic resonance had been exceeded. A similar effect was reported by Price & Zahn (1991). Their observations indicate that the interaction between the acoustics and the structural dynamics could augment instability as well as suppressing it. No mechanism for this phenomenon has been suggested but it is puzzling how an acoustic standing wave can so dramatically effect the flow regime at a frequency nearly two orders of magnitude lower.

Determining exactly the critical velocity, U_c is problematic. For example, for $\delta = 0.015$ in fig 5.6, the critical velocity could be anywhere from 6 *m/s* to 8 *m/s*. Several criteria have been proposed to determine the value of U_c. Andjelic & Popp (1989) proposed the so-called "transient-time criterion" based on the time taken for steady state motion to become established. Other techniques are based on amplitude criteria. The one used here is that outlined by Austermann & Popp (1995). The variation of tube response amplitude with flow velocity is idealised as two straight lines, one for below U_c and one for above. The point of intersection of these two lines gives the critical velocity. Regardless of what method is used, there will always be some degree of

subjectivity associated with determining the instability threshold from the tube response alone, particularly for higher values of pitch ratio where the onset of large amplitude oscillations is more gradual. The critical velocities obtained from figures 5.6 & 5.7 are shown in table 5.1.

Pitch ratio (P/d)	1.58			1.32		
Log. Dec., δ	0.015	0.023	0.031	0.093	0.106	0.114
Critical velocity, U_c (m/s)	7.1	8.5	10.3	4.1	5.5	6.5
Reduced velocity, $\frac{U_c}{f_n d}$	28.1	33.6	40.8	16.2	21.8	25.7
Reduced gap velocity, V_r	33.9	40.5	49.1	57.3	77.1	90.8

Table 5.1: FEI Thresholds for 3^{rd} row

The reduced velocity is simply the non-dimensionalized critical velocity. The reduced *gap* velocity, which was proposed by Chen (1984) in an attempt to compare data from different array geometries and pitch ratios, has become the standard way to present such data. it is define on page 13.

The stability threshold in terms of the reduced gap velocity is shown in figure 5.8 together with data from Austermann & Popp (1995) and Price & Zahn (1991). These two sources are by no means the only data available, but they have similar a set-up (normal triangular array with a single flexible cylinder in air). As can be seen, the current results compare favourably with the data available from these studies.

5.4 Linearized fluid force parameters: Free response

The motion of the single degree of freedom system subject only to fluid loading is governed by the general equation:

$$m\ddot{y} + c_s\dot{y} + k_s y = E(y, \dot{y}) + T(t) \tag{5.1}$$

where c_s is the system damping in quiescent fluid;

k_s is the system stiffness;

$E(y, \dot{y})$ is the fluidelastic force which is a function of tube motion ;

$T(t)$ is the turbulent excitation.

Assume that the response can be decomposed into the sum of the response to the fluidelastic excitation and the random turbulent excitation.

$$y(t) = y_E(t) + y_T(t)$$

where $y_E(t)$ and $y_T(t)$ can be defined by the equations:

$$m\ddot{y}_E + c_s\dot{y}_E + k_s y_E = E(y_E, \dot{y}_E)$$
$$m\ddot{y}_T + c_s\dot{y}_T + k_s y_T = T(t)$$

This implicitly assumes that there is no interaction between the excitation mechanisms. Strictly speaking this is not valid, since the fluidelastic excitation depends on tube motion which will inturn be influenced by the turbulent excitation. However, in the absence of a non-linear model for $E(y, \dot{y})$ and instantaneous measurements of $T(t)$, this asssumption is a necessary expedient. Furthermore, if the tube motion is large, the effect of turbulent buffetting will be small. If n tests are conducted with exactly the same initial conditions, one would expect $y_E(t)$ to be identical for each test. The turbulent response y_T however will vary randomly from one test to the next. Thus if the ensemble is averaged, only the fluidelastic response will be left:

$$\begin{aligned}\bar{y}(t) &= \sum_{i=1}^{n} y(t) \\ &= \sum_{i=1}^{n} y_E(t) + \sum_{i=1}^{n} y_T(t)\end{aligned}$$

But, since $y_T(t)$ is random, as $n \to \infty$, $y_T(t) \to 0$

$$\Rightarrow \bar{y} = \sum_{i=1}^{n} y_E(t) = \bar{y}_F(t)$$

Thus the equation of motion asociated with the ensemble average is:

$$m\ddot{\bar{y}} + c_s\dot{\bar{y}} + k_s\bar{y} = F(\bar{y}, \dot{\bar{y}}) \tag{5.2}$$

If the fluidelastic force is assumed to be a linear function of tube motion then:

$$E(y, \dot{y}) = -k_f y - c_f \dot{y}$$

where k_f is the fluid stiffness and c_s is the fluid damping. The equation of motion for linearized free response can be written as:

$$m\ddot{y} + (c_s + c_f)\dot{y} + (k_s + k_f)y = 0 \tag{5.3}$$

From appendix A the response of the tube to an inital displacement is:

$$y(t) = Ae^{-\zeta\omega t}\sin(\omega t + \phi) \tag{5.4}$$

where A, ϕ depend on the initial conditions
$\zeta = \frac{(c_s+c_f)}{2\sqrt{m(k_s+k_f)}}$
and for low damping, $\omega \approx \sqrt{\frac{k_s+k_f}{m}}$

To provide data to fit to the linear response of eq. 5.4, a series of free decay tests have been conducted for each array. The tube was given an initial deflection and then released. The damping levels are such that fluidelastic instability does not occur. The tube displacement, velocity and acceleration are recorded using data acquisition triggered by the tube velocity. For each flow velocity and level of damping, an ensemble of time records was collected and averaged to eliminate the effect of turbulent buffeting at the natural frequency. Bendat & Piersol (1980) have shown that the amplitude of Gaussian noise associated with a measuement is reduced by a factor of $\frac{1}{\sqrt{n}}$, where n is the number of ensemble averages taken. Hence, ten averages would reduce the tube

response to turbulent buffeting by a factor of 3. This was deemed to be a reasonable compromise between accuracy and practicality, since the error due to turbulence was already small. This is based on the small amplitude of vibration observed before the onset of instability, where the dominant excitation mechanism is turbulent buffeting (see fig 5.6 and 5.7).

Each time record is 4 seconds long with 8192 samples (i.e. a sample frequency of 2048Hz and a frequency resolution of $\frac{1}{4}Hz$). The high sample rate offers good time domain resolution but the signals, particularly the acceleration, may have significant high frequency components due to vortex shedding or higher modes excited by turbulent buffeting. A digital filter was applied off line to attenuate components at frequencies higher than 50 Hz although it was noted that the filtered signals yielded only marginally different results. The ensemble averaged experimental response data can be approximated by the expression:

$$y_{FIT}(t) = \alpha_1 e^{\alpha_2 t} \sin(\alpha_3 t + \alpha_4) + \alpha_5$$

using the downhill simplex curve fitting scheme described in chapter 4. The extra parameter, α_5, is included to allow for any DC offset in the measured data. A typical ensemble average of tube velocity is shown in fig 5.9. The decaying sinusoid which has been fitted to the data is also shown, but has been decimated by a factor of ten for clarity. It can be seen that the fitted curve underestimates the measured data at high amplitudes (fig 5.10(a)), while it overestimates the data at lower amplitudes (fig 5.10 (b)). This would imply that the logarithmic envelope associated with the fitted curve has a slightly smaller exponent than that of the measured data. In other words the instantaneous equivalent linear damping ratio ζ is higher than the fitted value at higher amplitudes while the reverse is true at lower amplitudes of vibration. This type of behaviour is typical of a mildly non-linear system. The data in figures 5.11-5.16 have been generated using the velocity data but it has been found that the tube displacement and acceleration yield very similar results for the parameters of interest, namely the damping (α_2) and the frequency (α_3).

5.4.1 Pitch ratio 1.58

If the parameter α_2 estimated in the downhill simplex scheme is scaled by a factor of -2, the mass normalised damping $2\omega\zeta$ is obtained (in fact the mass normalised damping is $2\omega_n\zeta$, but for low damping $\omega \approx \omega_n$). The total estimated damping is plotted against flow velocity in fig 5.11 for three different levels of damping. By subtracting the damping associated with the no flow condition from each data set, the equivalent linear damping coefficient, c_f, associated with the fluid force can be estimated. This is shown in fig. 5.12. As can be seen, the three data sets collapse reasonably well. The coefficients are negative, indicating that the fluid is imparting energy to the structure, rather than dissipating it. Initially, at low flow velocity, there is some evidence that the net damping is increased by the fluid loading. This is supported by Granger (1990b) who measured a fluid damping 6 times larger than the structural damping at low velocities, but that study was in water. This increase is caused by the fluid dynamic drag which occurs even in quiescent fluid. The magnitude of this drag force increases quadratically with the flow velocity while the direction of the drag force rotates from the transverse direction at zero flow to close to the inline direction when $\dot{y} \ll U$. The result is that the component of this force in the transverse direction initially increases rapidly with the flow velocity and then continues linearly. At intermediate velocities, the destabilizing components of the fluid elastic force begin to dominate and the fluid damping decreases linearly with velocity.

This pattern of variation is consistent with the quasi-steady assumptions proposed by Price & Paidoussis (1986). However, for higher velocities (above about 12 *m/s*) the fluid damping no longer follows a linear variation, suggesting that the quasi-steady model is not completely applicable. The model proposed by Lever & Weaver (1986), although not based on a quasi-steady assumption, yields a similar variation of fluid forces with flow velocity. An alternative interpretation of the results can be inferred by comparing the data with the quadratic curve (shown as a dashed line) which has been fitted. The data follows this trend reasonably well suggesting that the damping estimates for this

array may vary with dynamic pressure head, $\frac{1}{2}\rho U^2$ as proposed by Chen *et al.* (Chen, Zhu, & Jendrzejczyk 1994; Chen 1987).

Applying a scaling factor of 2π converts the parameter α_3 into the frequency of oscillation. As can be seen in fig 5.13, there is good agreement between the three data sets for the estimates of the fluidelastic frequency. The fluidelastic frequency varies by less that $\frac{1}{4}Hz$ over the entire flow velocity range considered. Had a frequency domain analyis been employed, the effect of fluidelastic stiffness on the frequency would have been masked as the minimum frequency resolution for this data is $\frac{1}{4}Hz$. It was not feasible to improve frequency domain resolution by extending the sample time of 4 seconds since the tube motion is decaying. Therefore only a time domain analysis is appropriate for this data.

The fluid stiffness has been extracted from the raw parameter estimates of α_3 in a similar way to the fluid damping (fig 5.14). A quadratic curve has been fitted for comparison purposes. The fluidelastic stiffness follows this curve closely, reinforcing the conclusion that Chen's *et al.* model is appropriate. There is less scatter in the fluid stiffness data than the damping, but this could be attributed to the fact that the fluid damping force is nearly an order of magnitude smaller than the fluid stiffness force: if the flow velocity is 14 *m/s*, the frequency is $40rad/s$ and the tube displacement amplitude is $10mm$, the fluid spring force has an amplitude of about $1.5N$ while that of the fluid damping force is about $0.2N$ and the total force amplitude is approximately $18N$.

5.4.2 Pitch ratio 1.32

The fluid damping coefficient and fluid stiffness coefficient for a pitch ratio of 1.32 are shown in fig 5.15 and fig 5.16 respectively. In this case only two levels of damping were tested. As will be seen in the next chapter, the effect of fluid dynamical non-linearities is far more pronounced for this array than for the other. This may explain why there is more variation in the parameters, c_f and k_f, when comparing the two damping

levels. The fluidelastic damping coefficients are much larger than before, indicating that for a given level of total structural damping, the array with pitch ratio of 1.32 will exhibit fluidelastic instability at a lower flow velocity than the array with pitch ratio of 1.58. This behaviour was observed in section 5.3. Neither the fluid stiffness, k_f, nor the fluid damping, c_f, for this array follow the quadratic trend which has been superimposed on figures 5.15 & 5.16. This suggests that Chen's assumption that the fluid force coefficients vary with dynamic head is not applicable to this array.

The effect of acoustic resonance discussed above can be seen clearly in these graphs at a flow velocity of 9 *m/s*: the magnitude of both the fluid stiffness and damping drop suddenly. Fig. 5.7 indicates that the amplitude of tube motion at this flow velocity is about the same as for subcritical flow velocities. This suggests that the total damping at $U = 9m/s$ must be at least equal to that value at around 4 *m/s*.

5.5 Linearized fluid force parameters: Forced response

The forced response of flexible tube under fluid loading was investigated to complement the linearized model identified from the free decay tests. The excitation force was generated by the EMS which was fed a band limited periodic chirp signal. The frequency range excited was $2Hz$-$40Hz$ and the period of the chirp was 16 seconds. The averaged power spectrum of the periodic chirp can be seen in fig. 5.17. The sharpness of the cut-off frequencies ($2Hz$ and $40Hz$) is one of the advantages of a deterministic signal. Band limited white noise was also used for some tests, but it was found that the periodic chirp produced spectra and transfer functions which were comparable to those obtained with white noise, but with half as much data.

Since the periodic chirp attempts to excite each frequency individually, the acquisition sequence should not be triggered by excitation nor should a single long block of data be recorded as both these strategies will lead to substantial dropout at some frequencies. Instead, at each flow velocity, a series of 20 records were obtained, each 16 seconds long with a sample frequency of $128Hz$. This offers a frequency resolution of

$\frac{1}{16}$ Hz. The data was then used to generate the linear transfer functions between the tube response and the input force using eq 4.1. In the region of the natural frequency, the admittance, mobility and inertance transfer functions are mutually consistent. The admittance and to a lesser extent the mobility FRF become gradually contaminated with noise as the frequency increases above the natural frequency. This can be attributed to a lower response amplitude, and so a poorer signal-to-noise ratio at these frequencies. The inertance (the transfer function between acceleration and excitation force) is relatively immune to this as the sensitivity of an accelerometer to low amplitude vibration increases with frequency. For this reason the inertance transfer function has been used.

Figure 5.18 (a-l) plots the inertance in the region of the natural frequency as the flow velocity is increased for the 1.58 pitch array. For comparison purposes, on each set of axes the transfer function in quiescent air is drawn as a broken line. For a flow velocity between $3.4m/s$ and $5m/s$, the transfer function is largely unchanged (a-c). The increase in the peak of the transfer function under fluid loading which is barely perceptible in (d), is indicative of a reduced net damping. The fact that the peak has shifted to the right, indicating an increased fluidelastic frequency of vibration, is consistent with a increase in the total stiffness. This effect becomes more pronounced as the flow velocity is increased. As discussed in chapter 4, a single degree of freedom system can be fitted to the complex FRF data obtained. The estimates for stiffness agree with the stiffness estimates obtained from the free response tests (see fig 5.20). In fig 5.19 it can be seen that the damping follows a similar trend to the data obtained from the free response tests. Notwithstanding this similarity, the damping from the forced response tests differs from the free response data by as much as 20%. Since an estimate of a frequency response function requires two calibrated measurements (one for the excitation, the other for the response) any phase distortion or calibration error in the instrumentation will affect the estimates of the linear parameters. On the other hand, the downhill simplex scheme is immune to this problem since it requires only a single uncalibrated measurement. However, as the linear parameters for the structure in quiescent fluid obtained from the two estimation techniques are in good agreement, it seems likely that the discrepancy

between the estimates with flow in fig 5.19 is primarily due to the assumptions associated with the fluid force model. The contribution of the non-linear components of the fluidelastic force to the total fluid force will depend on whether the tube is in free or force response. Since these non-linear elements have not been modelled here, their contribution will be accounted for within the equivalent linear damping. The effect of turbulent buffeting on the total fluid force may also depend on the tube motion. These two factors may explain why the identified linear parameters depend on the type of test conducted.

An interesting feature of the forced response data (fig 5.19) is the very definite increase in total damping at low velocities, indicated by a positive fluid damping. This coupled with the linear variation at intermediate velocities would suggest that the quasi-steady model of Price & Paidoussis (1986) is applicable, although this model cannot explain why the fluid damping seems to level off at a constant value above $12m/s$.

Similar tests have been conducted with the closer packed array ($\frac{P}{d} = 1.32$), the results of which are shown in fig 5.21 (a-l). Again the transfer function in quiescent air is drawn as a broken line for comparison purposes. In contrast to the transfer functions obtained for a pitch ratio of 1.58, the influence of fluid load is immediately obvious even at the lowest velocity. In fact, at a flow velocity of $5m/s$ the peak of the FRF is comparable to the other array for $U = 14m/s$. The general trend though is the same: the amplitude of the peak is increasing as is the natural frequency of the coupled fluid-structure system, indicating a reduction in total damping and an increase in total stiffness. The peak value of the FRF falls off dramatically $U = 9m/s$, under the influence of the acoustic resonance.

The linear modal parameters associated with this array estimated from the transfer functions of fig 5.21 can be found in figs 5.22 & 5.23. There is good agreement between the free and forced response stiffness estimates. The two methods have yielded similar estimates for damping at both low and high velocities, but at velocities around 6 *m/s* there is substantial scatter between the two methods and even between the two data sets from the free response tests. There is no apparent reason for this deviation, but the

persistance of the discrepancy in repeated tests would rule out experimental error. It is possible that the coincidence of the Strouhal periodicity with the structural mode around $400Hz$ in this velocity range (see fig 5.2) may be responsible.

As a consequence of the flat excitation force spectrum the tube response spectra exhibit a large peak at the natural frequency. In other words, the amplitude of response depends heavily on the frequency. This implies that the effect of the non-linearities in the fluid-structure system also depends on the frequency making a linear FRF approximation unreliable. This problem might have been minimised by using a prewhitened excitation signal i.e. one which will produce the same response amplitude across the frequency range examined. However, as a similar argument could be applied to the free response data, there is no reason to prefer one data set to the other.

The estimates of the total modal mass obtained from the FRF method for both arrays is shown in fig 5.24. The fluctuations about the mean value of $1.02kg$ are small and can be attributed to experimental error. This shows that the added fluid mass is negligible or at least independent of flow velocity.

5.6 Prediction of stability threshold

It has been seen while interpreting the results above, that the data for a pitch ratio of 1.58 might be described with Chen's framework whereby the fluid forces vary with dynamic head. This model cannot support the results obtained from a pitch ratio of 1.32. However, it was noted that the quasi-steady theory of Price & Paidoussis (1986) or that of Lever & Weaver (1986) might be appropriate for either pitch ratio although the data at higher flow velocities did not conform. The conclusion is that no consistent theory has been proposed which describes the functional form of the relationship between flow velocity and the linearized fluid force coefficients. Therefore, a cubic curve has been fitted through each set of parameter estimates (figures 5.19, 5.20, 5.22, 5.23) subject only to the condition that it must pass through the origin. This is a physical constraint, since there can be no fluid force when there is no flow. Since the measurement of

the flow velocity is reliable in comparison to the estimates of the force coefficients conventional least squares estimation was used.

The variation of fluid force parameters with flow velocity can now be used in a simple linearized model of the fluid-structure dynamics to predict the instability threshold. The fluid stiffness is always positive, which means that a static divergence is impossible in this velocity range. Furthermore, a linearized stiffness must, by definition, be conservative. Therefore, the fluid stiffness can be ignored when estimating the critical velocity.

For a linearized model, instability is caused by a dynamic divergence. This means that the tube motion will be oscillatory, but with a increasing amplitude of vibration. A limit cycle is not possible, except at the stability threshold itself. This will occur when the fluid damping exactly counteracts the dissipation within the structure:

$$c_s = -c_f \tag{5.5}$$

Combining this condition with the empirically determined expressions describing the variation of c_f with flow velocity obtained from figs 5.19 & 5.22, a prediction for the stability boundary for each array is obtained. These stability boundaries are plotted in fig 5.25 & 5.26. The values of reduced critical gap velocity which were obtained by direct experimentation (see table 5.1) are marked for comparison. The general trend is accurate, but the threshold is systematically overestimated. The extent of this error can be assessed from table 5.2.

Pitch ratio	1.58			1.32		
Log. Dec., δ	0.015	0.023	0.031	0.093	0.106	0.114
Mass damping parameter, δ_r	28.2	43.3	58.42	175.3	199.8	214.8
Reduced gap velocity, V_r	33.9	40.5	49.1	57.3	77.1	90.8
Predicted reduced gap velocity	38.2	47.7	60.1	104.9	120.3	127.3

Table 5.2: Predictions for FEI Thresholds using a linearized model

An obvious source of error is the interaction of turbulent buffeting with the fluidelstic forces which has not been accounted for in eqn 5.5. Lever & Rzentkowowski (1988) demonstrated that linear interaction of turbulent buffeting with the fluidelastic dynamics would reduce the apparent stability threshold. The effect of turbulence on the stability boundaries predicted here has been assessed using turbulence levels determined by Axisa et al. (1990), but the improvement was found not to be significant. Rzentkowski & Lever (1995) went on to show that non-linear interactions would further reduce the critical velocity, though not substantially. Hence, the effect of turbulence on the stability boundaries can be ignored.

The predictions for a pitch ratio of 1.58 systematically overestimate the experimentally determined values of critical velocity by 20%. It might have been expected that the predictions would have been closer, since the fluid force coefficients were measured experimentally. However, in light of the low contribution of the damping force to the total force (about 1%) this level of error is acceptable, particularly when compared to the theoretical predictions of Rzentkowski & Lever (1998) which indicate a critical velocity twice that observed here. It is true that other researchers (e.g. Tanaka & Takahara 1981; Granger 1990b) have obtained closer agreement between linear models with experiemntally determined parameters and the experimental stability thresholds, but these studies have been conducted in water, and so the both magnitude and relative contribution of the fluid damping was more significant.

The situation is considerably worse for a pitch ratio of 1.32. At the lowest level of mass damping parameter the critical velocity from the linear model is nearly 100% in excess of the actual value observed, improving to an error of 40% at the highest level of damping considered. This large error can not be attributed simply to systematic experimental error as the contribution of fluid damping forces is about 4 times more significant than in the other array. It is likely that the assumption of linearity itself is responsible for the large discrepancy in the predictions. Since the fluid force is inherently non-linear, any effective linear parameter estimate will include some contribution from non-linear components. It might be argued that the use of the DHS scheme which utilizes data

from large amplitude tube motions exacerbates this problem. Indeed, it has already been noted that the discrepancy observed between the DHS parameter estimates and those from the FRF method, which uses relatively low amplitude response data, might be in part due to the non-linear fluid force terms which have been ignored. However, the difference between the two data sets (those from DHS and FRF) is not great enough to account for the failure of the linear model to accurately predict critical flow velocities with a pitch ratio of 1.32.

These results imply that a linearized model, while acceptable for a pitch ratio of 1.58, is not appropriate for a more densely packed array. The next chapter will show that the non-linearity is much stronger in the array with a pitch ratio of 1.32. This may explain why predictions from a linearized model are more accurate for a pitch ratio of 1.58 than for a ratio of 1.32.

5.7 Summary

It has been demonstrated at the start of this chapter that the Strouhal numbers associated with vortex shedding in the two arrays considered are consistent with published data. It has also been shown that a single 2 degree of freedom flexible tube mounted in the third row of an array exhibits the same fluidelastic behaviour as has been observed in other test facilities. Having established that the experimental rig is comparable with those previously documented, it has been demonstrated experimentally that an array with a single degree of freedom can develop fluidelastic instability in the cross flow direction. Although this assumption has been implicit in several theoretical models and experimental studies it has not, until now, been validated.

Estimates of effective linear fluid damping and stiffness have been obtained at several levels of damping using both the FRF and DHS approaches described in chapter 4. The parameters estimated from the forced response tests were in general agreement with those from the free vibration tests. However, the observed trends in the linearized parameters with flow velocity can not be accounted for by one of the available theoretical

models alone.

Based on these parameter estimates, predictions of the stability threshold have been made. The predictions for the $\frac{P}{d} = 1.58$ array were within 20% of the critical velocities determined experimentally, suggesting that a linearized model is applicable to this array. For the second array ($\frac{P}{d} = 1.32$) the predictions obtained overestimated the critical velocity for the onset on instability by 100%. The FRF methodology is based on continuous low amplitude tube response, while the DHS technique relies on large amplitude transient data. This fundamental difference in the techniques used implies that the erroroneous predictions of the linear fluid force model in this case can not be attributed to the method of linearization, but rather must be caused by the assumption of linearity itself. In other words, although a linear model can be successfully applied to the first array, the second array requires a non-linear model to describe even its most basic behaviour. In the next chapter a non-linear model is proposed to address this issue.

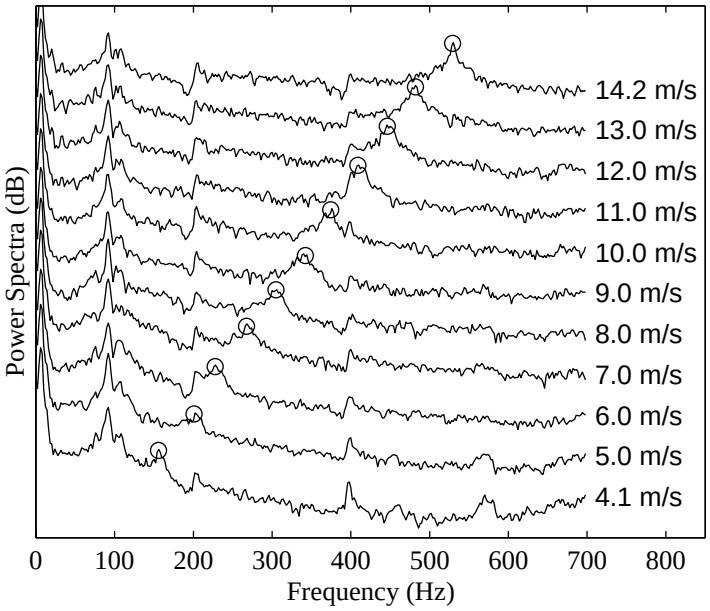

Figure 5.1: Power spectra of tube acceleration ; $P/d = 1.58$.

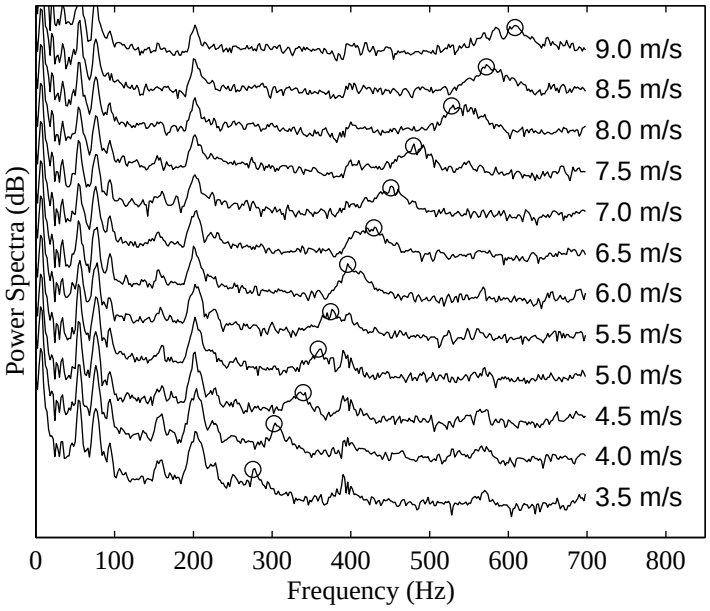

Figure 5.2: Power spectra of tube acceleration ; $P/d = 1.32$.

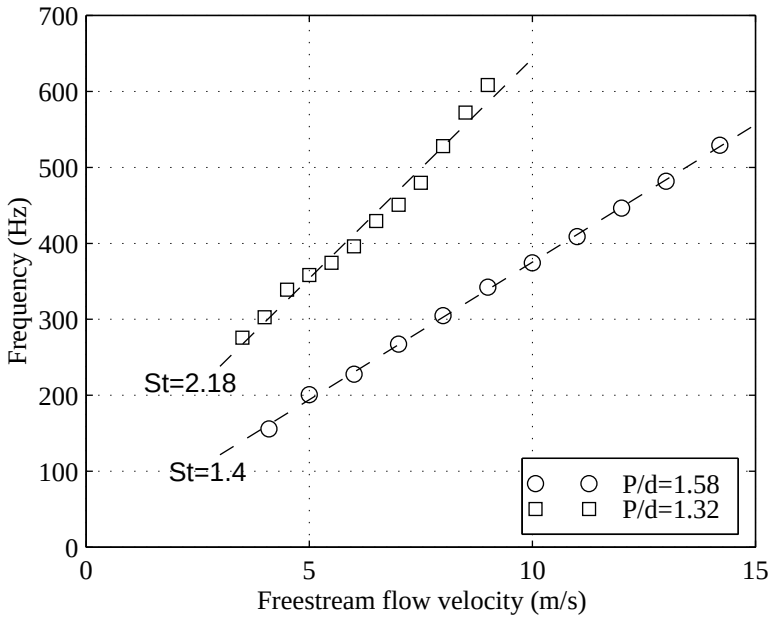

Figure 5.3: Vortex shedding frequency against free stream flow velocity (U).

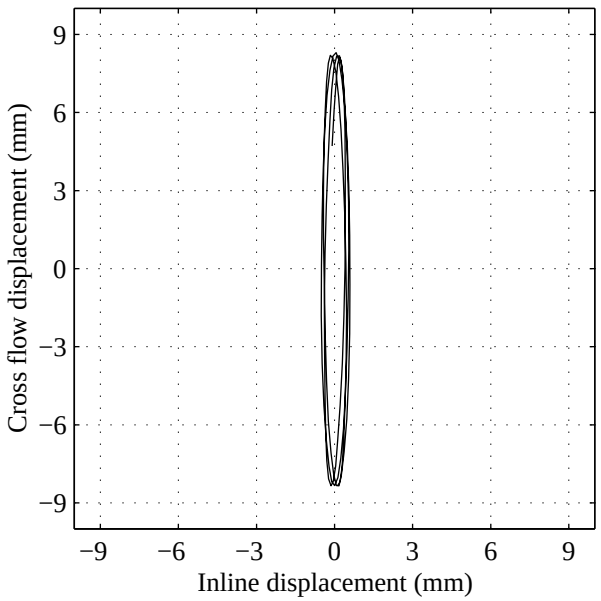

Figure 5.4: A typical trajectory for the 2dof flexible tube with $U = 9m/s$

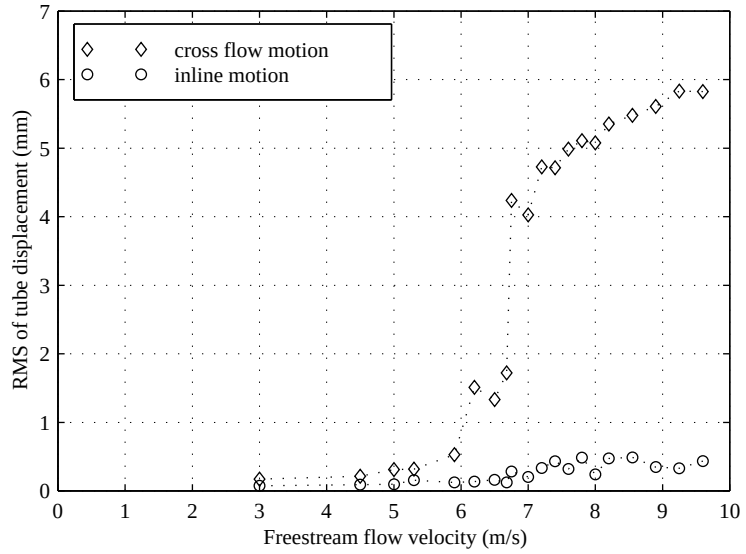

Figure 5.5: Variation of tube displacement RMS with onset flow velocity, U.

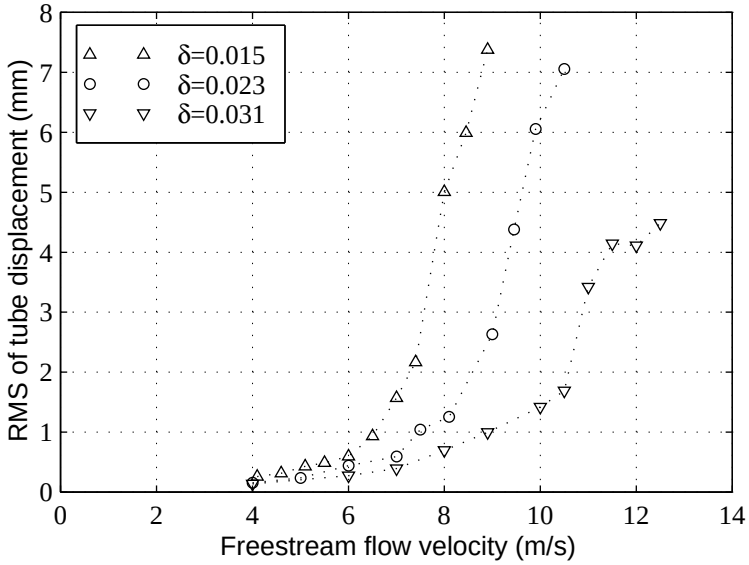

Figure 5.6: RMS of tube motion. $P/d = 1.58$, flexible tube in 3^{rd} row.

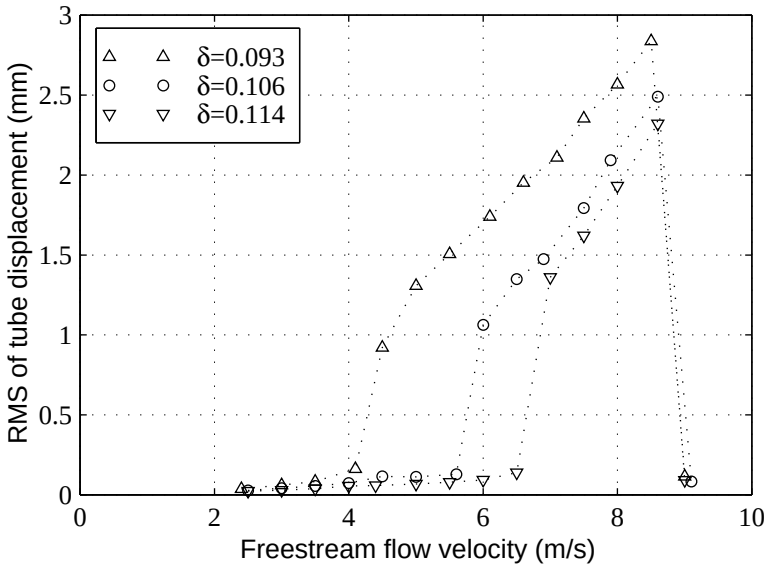

Figure 5.7: RMS of tube motion. $P/d = 1.32$, flexible tube in 3^{rd} row.

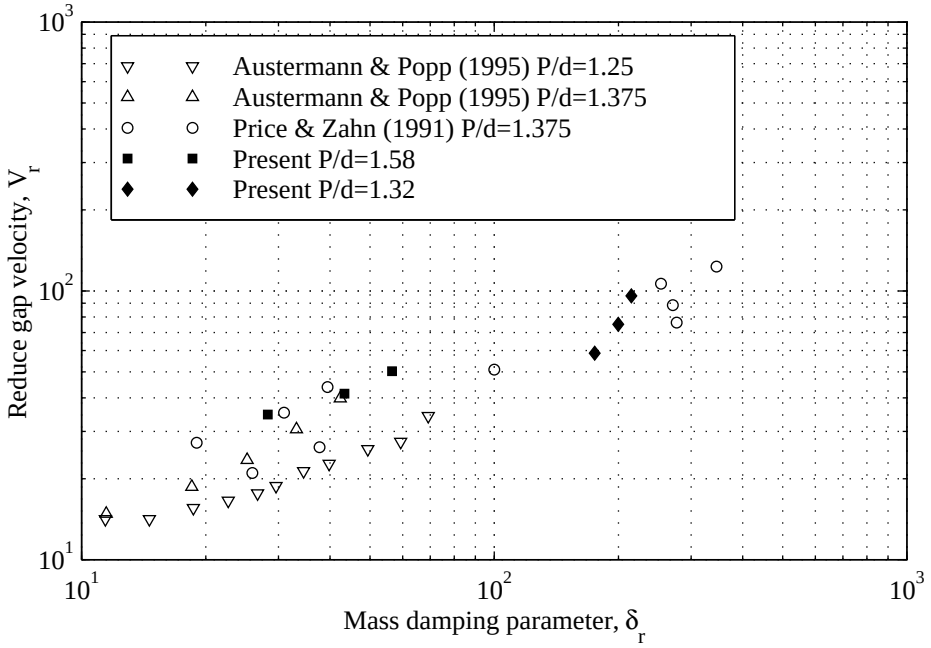

Figure 5.8: Comparison of measured stability threshold for the 3_{rd} row.

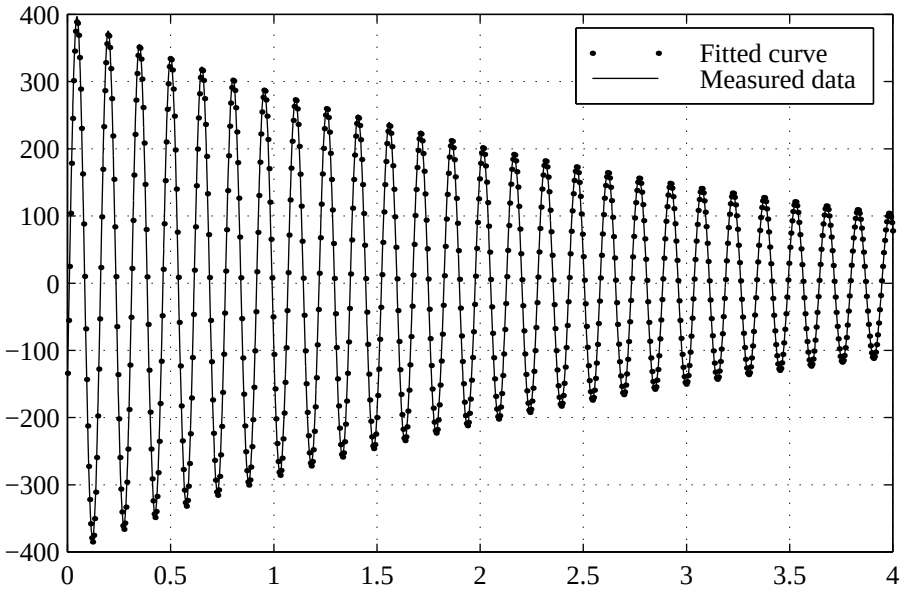

Figure 5.9: A typical ensemble average of free response and the curve fitted with the Downhill Simplex scheme. $P/d = 1.58$; $U = 12m/s$

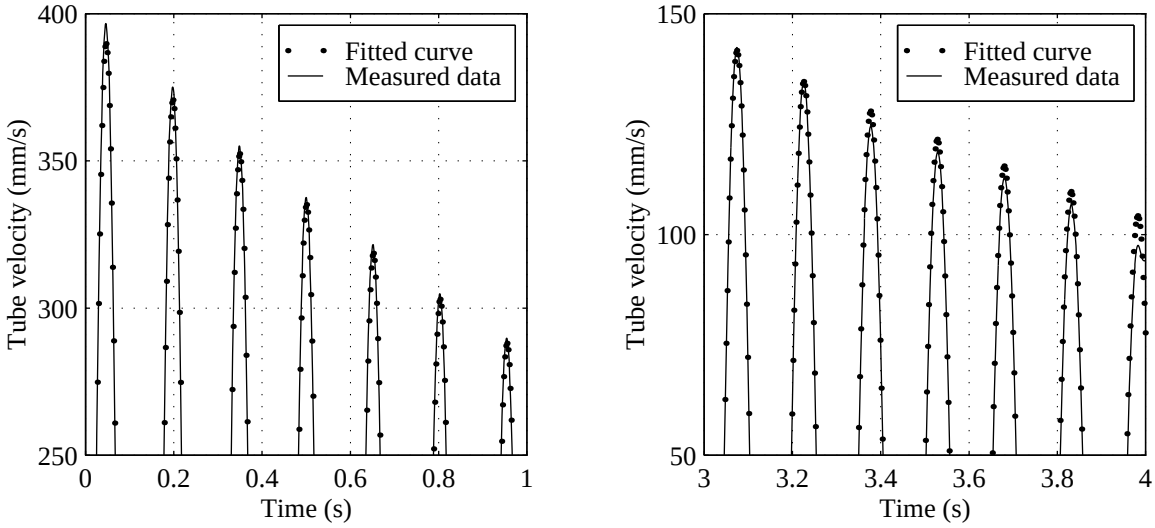

(a) High amplitude (b) Low amplitude

Figure 5.10: Detail of figure 5.9

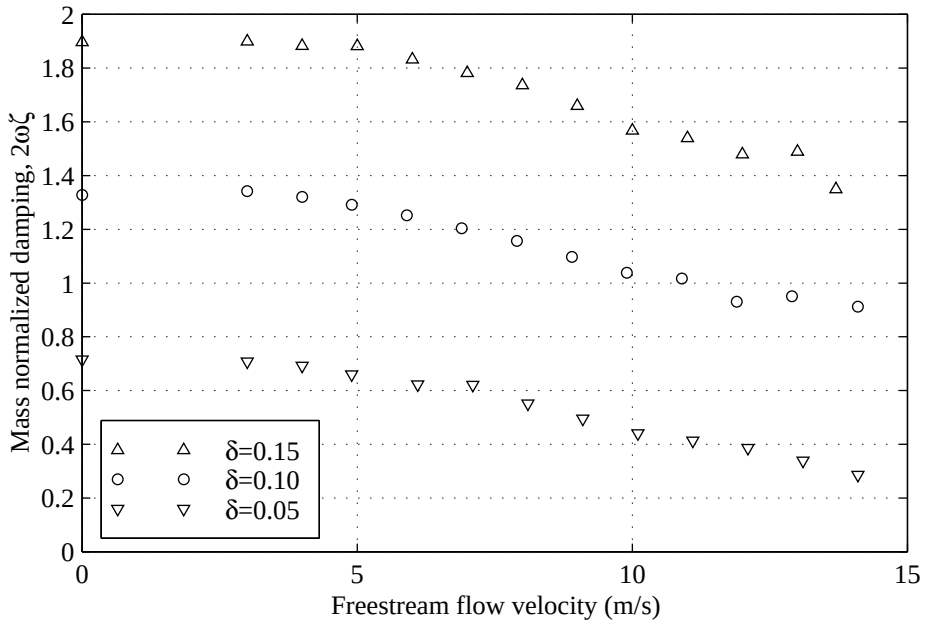

Figure 5.11: Total equivalent linear damping estimated form the downhill simplex scheme. $P/d = 1.58$, flexible tube in 3^{rd} row.

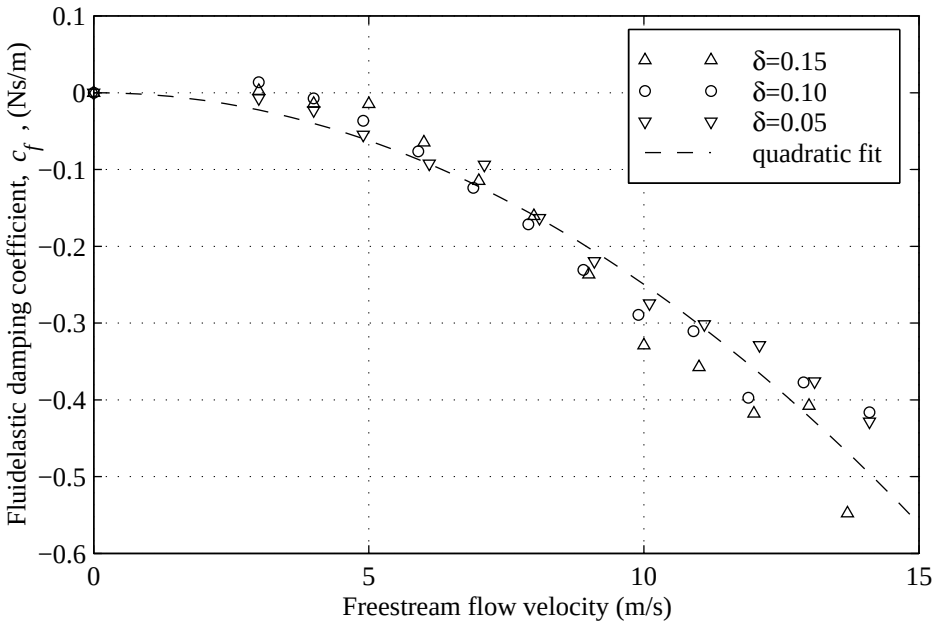

Figure 5.12: Equivalent linear damping, c_f, attributable to the fluid force. $P/d = 1.58$, flexible tube in 3^{rd} row.

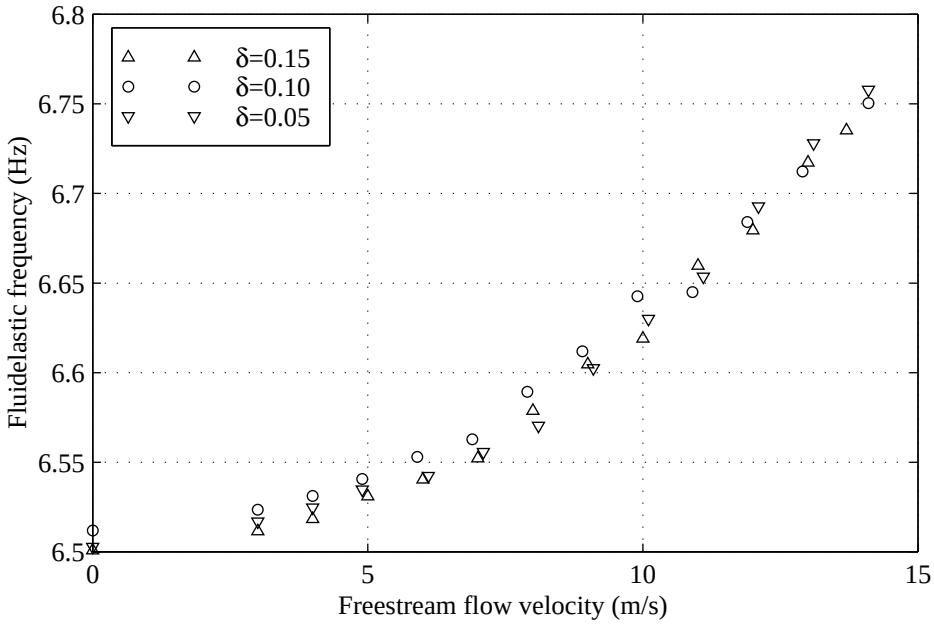

Figure 5.13: Frequency of oscillation under fluid loading, from downhill simplex. $P/d = 1.58$, flexible tube in 3^{rd} row.

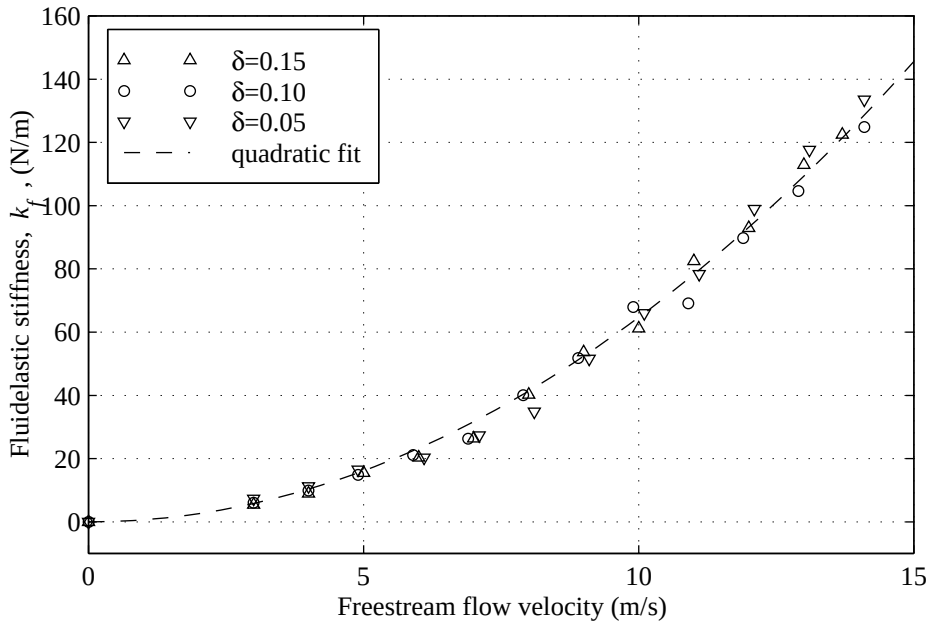

Figure 5.14: Equivalent linear stiffness, k_f, attributable to the fluid force. $P/d = 1.58$, flexible tube in 3^{rd} row.

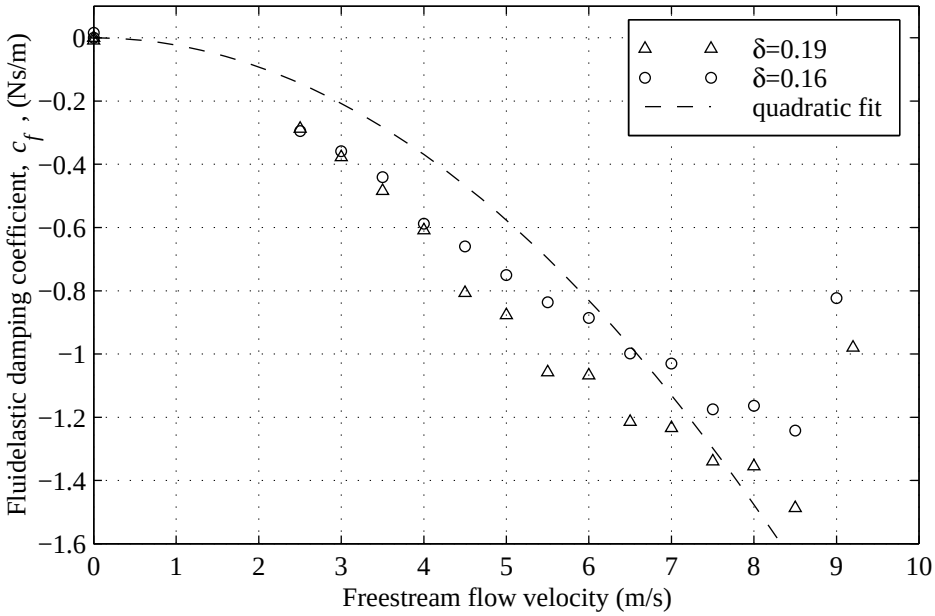

Figure 5.15: Equivalent linear damping, c_f, attributable to the fluid force. $P/d = 1.32$, flexible tube in 3^{rd} row.

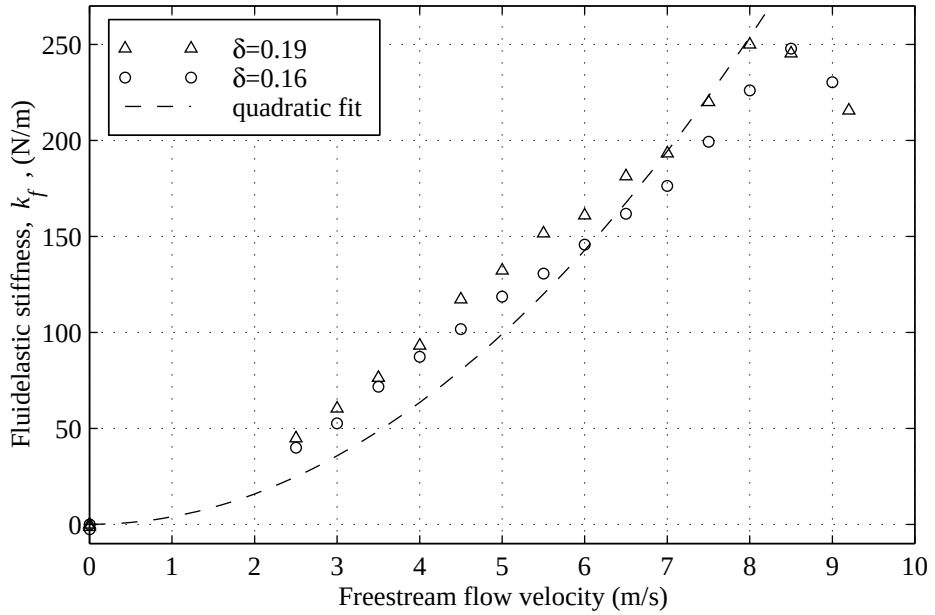

Figure 5.16: Equivalent linear stiffness, k_f, attributable to the fluid force. $P/d = 1.32$, flexible tube in 3^{rd} row.

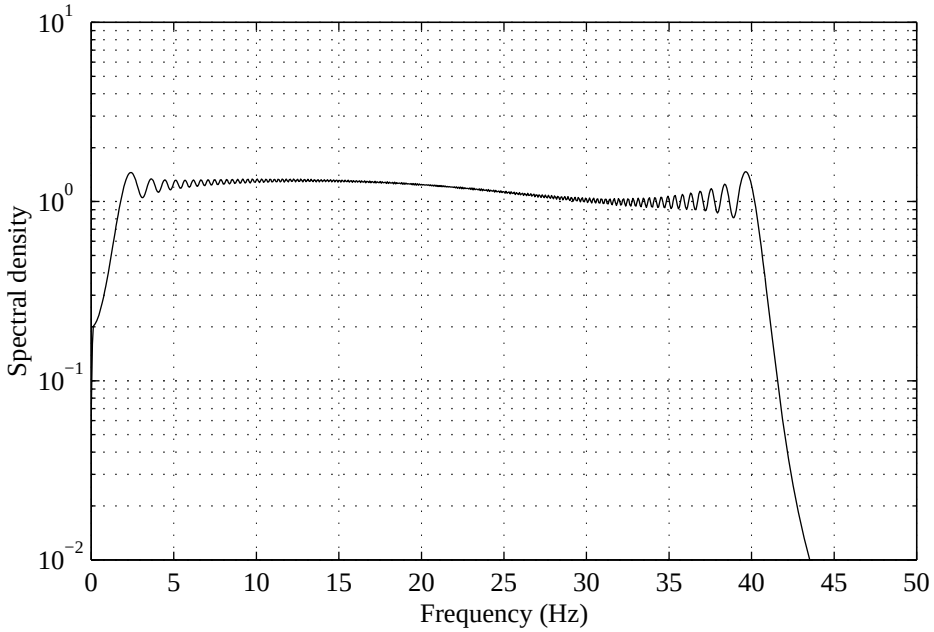

Figure 5.17: Spectrum of excitation force.

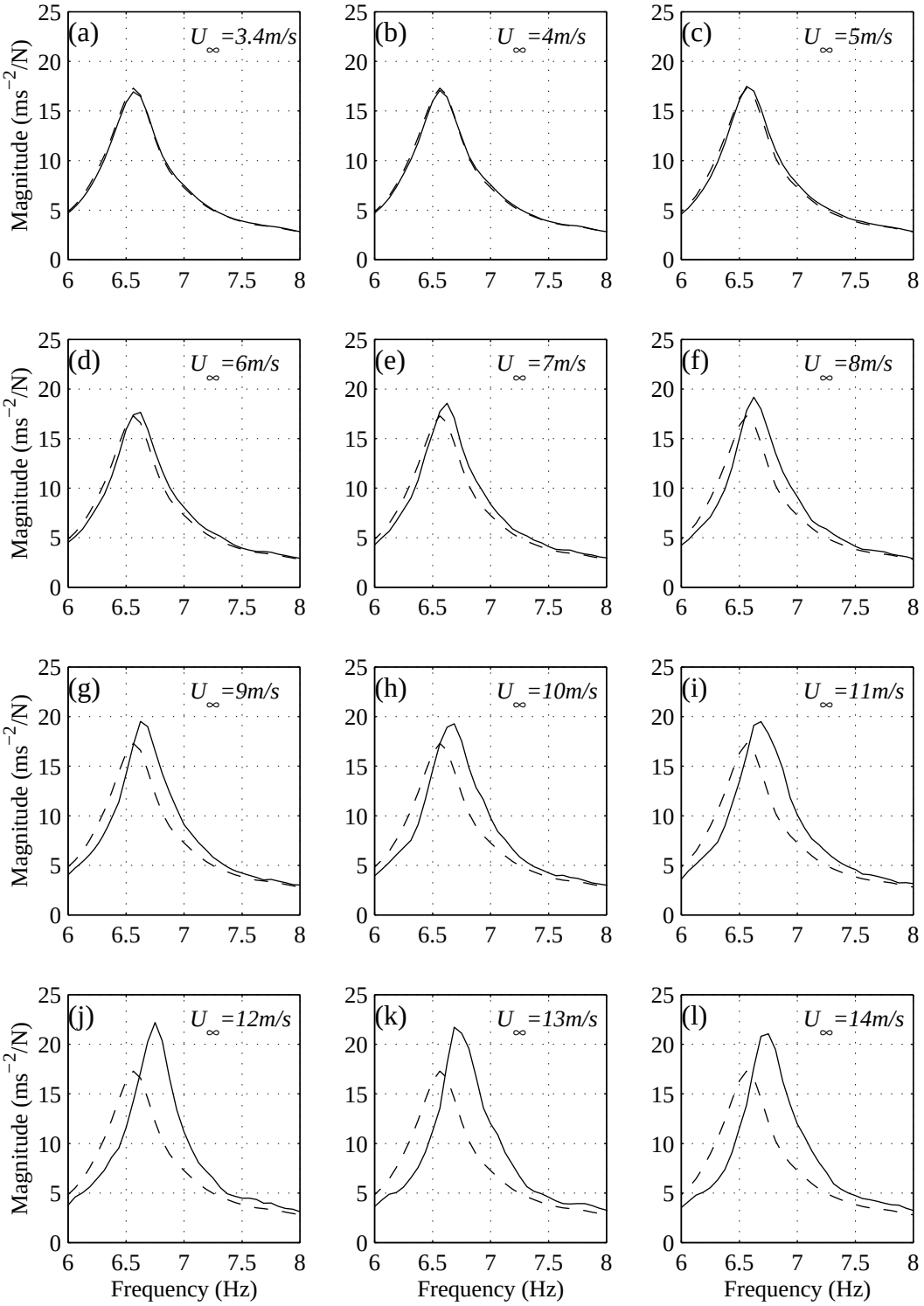

Figure 5.18: Variation of inertance function. Flexible tube in 3^{rd} row, $\frac{P}{d} = 1.58$. (— with flow; – – in quiescent air)

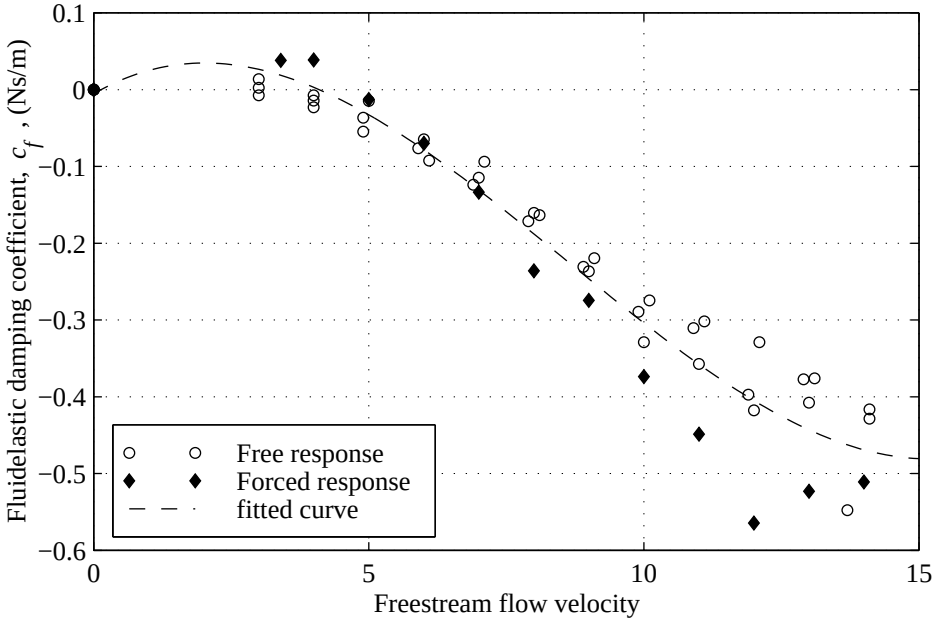

Figure 5.19: Fluid damping, c_f, calculated from the forced and free response. P/d=1.58

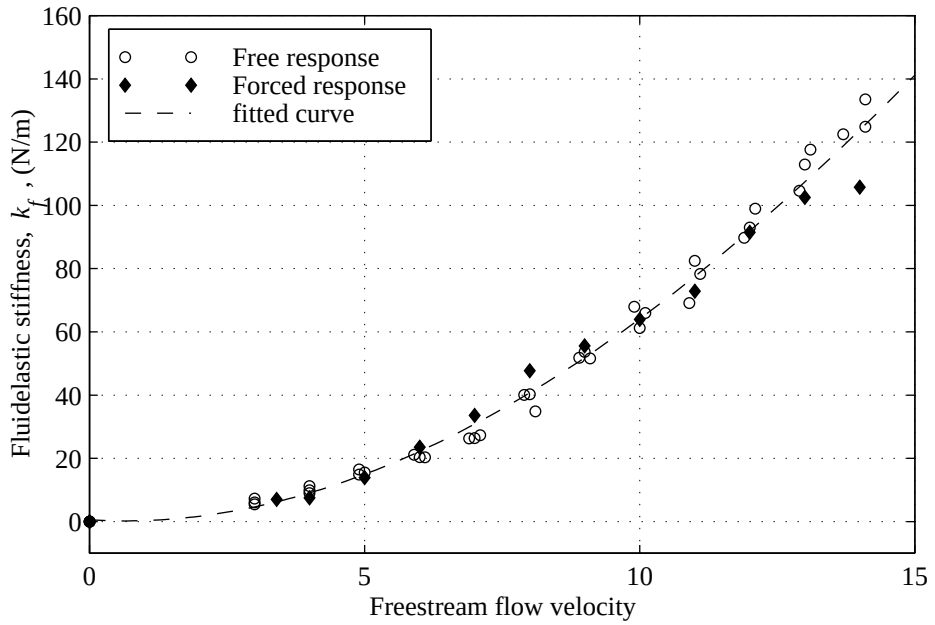

Figure 5.20: Fluid stiffness, k_f, calculated from the forced and free response. P/d=1.58

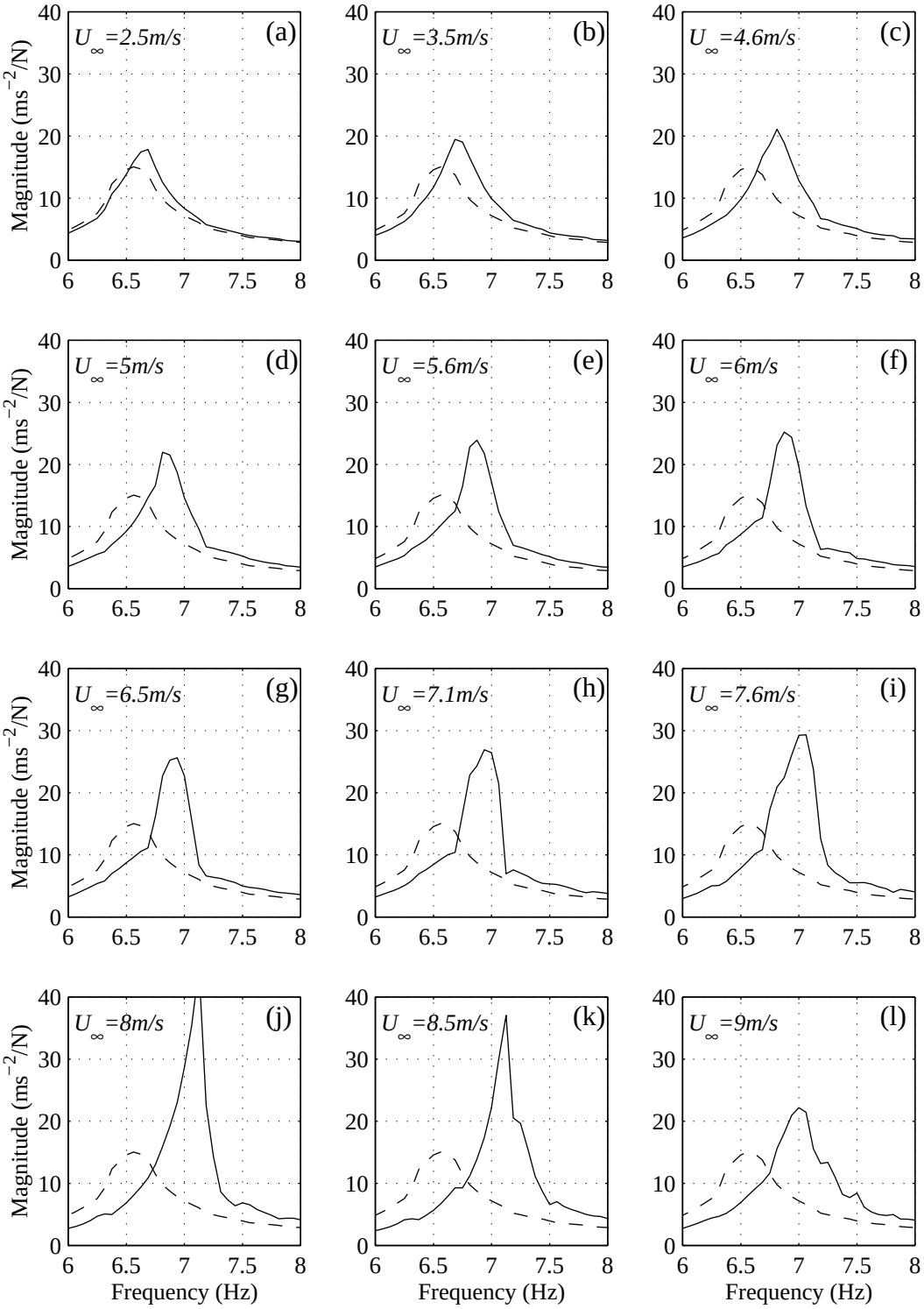

Figure 5.21: Variation of inertance function. Flexible tube in 3^{rd} row, $\frac{P}{d} = 1.32$. (— with flow; – – in quiescent air)

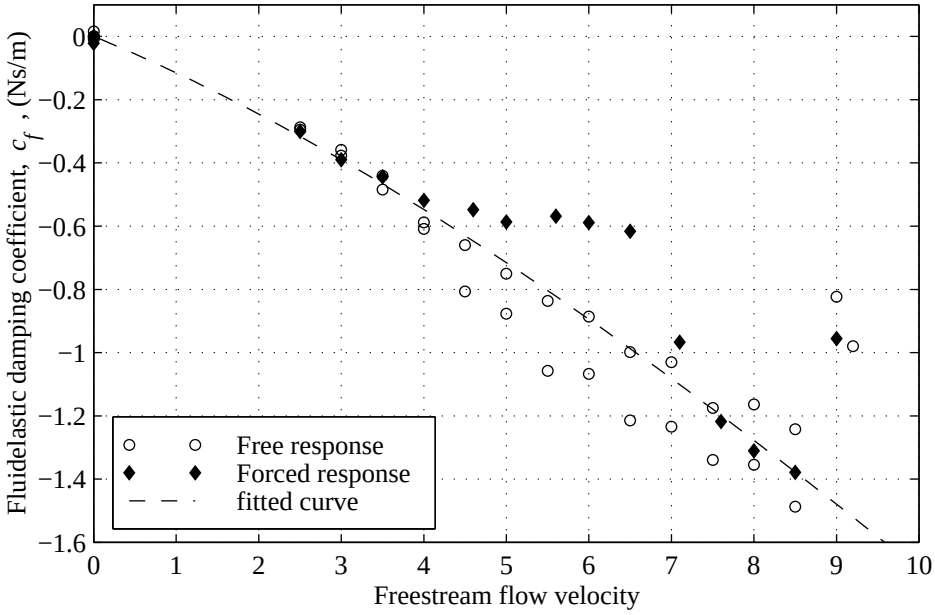

Figure 5.22: Fluid damping, c_f, calculated from the forced and free response. P/d=1.32

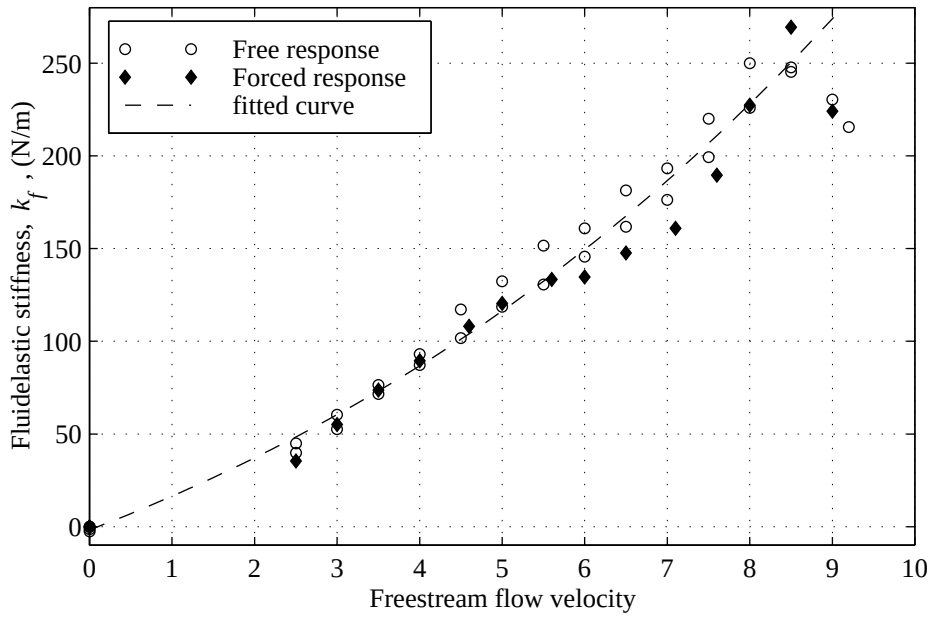

Figure 5.23: Fluid stiffness, k_f, calculated from the forced and free response. P/d=1.32

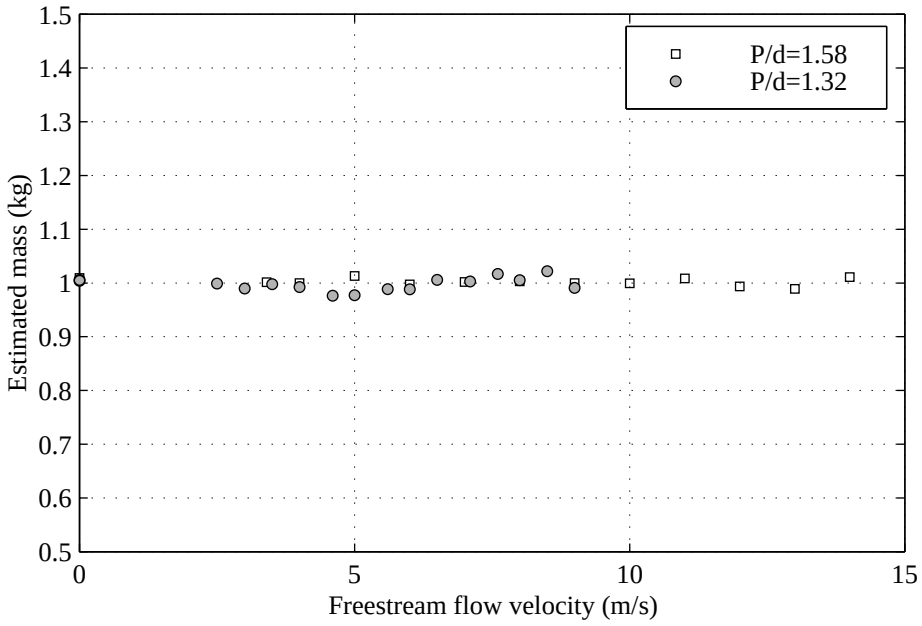

Figure 5.24: Mass estimate from the FRF method for both arrays.

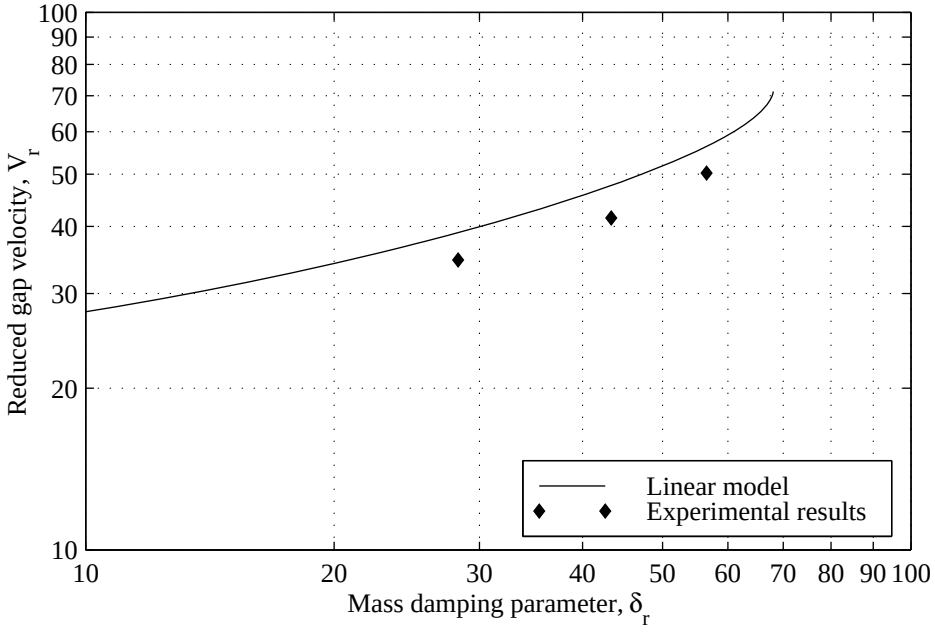

Figure 5.25: Prediction of stability threshold using linear model. P/d=1.58

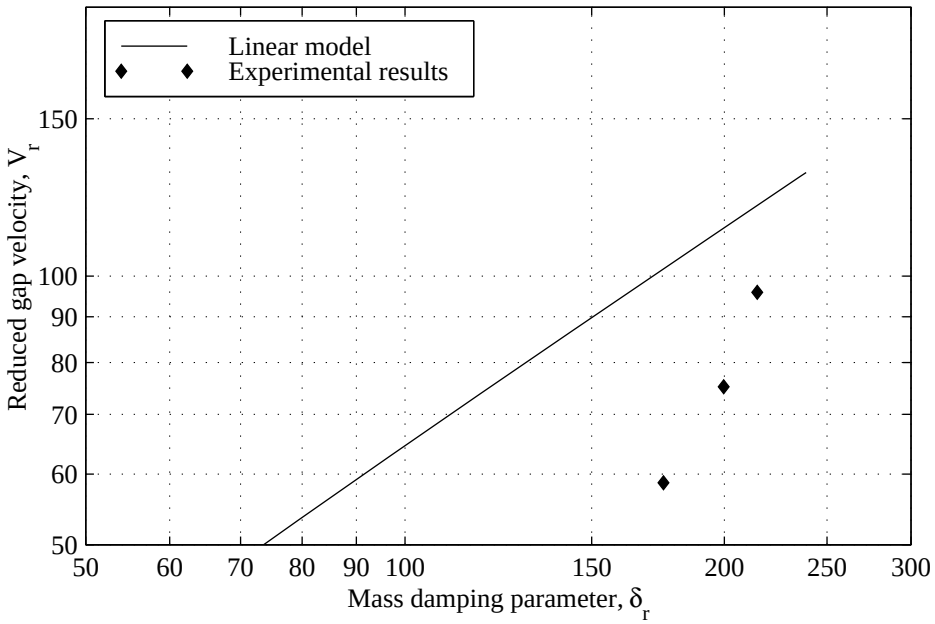

Figure 5.26: Prediction of stability threshold using linear model. P/d=1.32

Chapter 6

A non-linear model

The fluidelastic instability phenomenon is not only self exciting, it is also self limiting. This is demonstrated by the finite limit cycle amplitude observed in the post stable regime (see fig 5.6 & 5.7). If the fluid load produced only linear negative damping, after the critical velocity the net damping would always be less than zero and the flow would continue to transfer energy into the structure until failure,impacting or some other structural limitation was met. In fact, several researchers have attributed the self limiting nature of fluidelastic vibration to structural non-linearities. However, since the flexible tube considered here is mounted on a linear structure (at least within the displacement range possible), the limiting behaviour must be due to a non-linear interaction between the tube motion and the fluid force. For this reason, the simple linearized fluid model described in the last chapter can only predict tube motion in the subcritical velocity range and the limit of this range. The substantial difference between measured stability threshold and the value predicted from the linear model for the more densely packed array suggests that the linearized model is not reliable even in this range. It could be argued that in practical applications, a structural non-linearity will limit the motion at a much lower amplitude, making the non-linear nature of the fluid force irrelevant. For example Paidoussis & Li (1992) considered the effect of tube impacting on a loosely fitted baffle. However, Price (1995) noted that even in the case of tube impacting, a non-linear fluid model is still required to determine how much energy is available at

impact.

There have been several attempts to extend the linear theoretical framework to a full non-linear model (Price and Valerio 1990; Lever and Rzentkowski 1992; Austermann et al. 1992). None have enjoyed much success in predicting both FEI stability threshold and limit cycle amplitudes when the structure is linear and therefore not the limiting factor. Thus, there is no clear description of the non-linear mechanisms at work or their functional forms. In this chapter the functional dependence of the fluid force on the tube motion is explored using a variety of techniques. The Force State Mapping (FSM) technique described in chapter 4 is applied to the same free response data that was used for the linearized model allowing a quantitative non-linear model for the fluid force to be evaluated.

6.1 Evidence of non-linearity

A series of forced response tests was conducted with various levels of excitation amplitude, to demonstrate the non-linear behaviour in the fluid force. The excitation waveform was a band limited periodic chirp similar to the type used in section 5.5. The transfer functions obtained for $\frac{P}{d}$=1.58 and $\frac{P}{d}$=1.32 are shown in fig. 6.1 and 6.2 respectively. The FRF for pitch ratio of 1.58 does exhibit some amplitude dependence. The resonant peak value drops by about 20% (from $22.5ms^{-2}/N$ at low excitation to $18.5ms^{-2}/N$ at high excitation). The second array also shows a dependence on the excitation amplitude, but here it is more apparent. The effective damping clearly changes with excitation level (a reduction in FRF peak value), but so too does the apparent natural frequency, implying non-linear elements in both stiffness and damping. Since the more closely packed array exhibits more significant non-linear behaviour, the discussion will focus solely on the array with a pitch ratio of 1.32.

The reduction in natural frequency with increased excitation amplitude suggests an asymmetric spring force-displacement curve (see Rice et al. 1998) which can be attributed to a component with an even functional form (i.e. quadratic). Alternatively,

the shift in natural frequency could be caused by a softening spring effect. This would manifest itself as a high order odd component in the displacement force curve with a negative coefficient (e.g. a cubic stiffness term).

Another indication of the non-linear aspect of the fluid force can be gleaned from the tube's free response in a supercritical regime (i.e. after the onset of instability). The velocity power spectrum for such a situation is shown in fig 6.3. The flow velocity (U) is 7.5*m/s* and the logarithmic decrement (δ) has been set at a value of 0.093. An arbitrary reference velocity of 1 *mm/s* was used to represent the power spectrum on a convenient *d*B scale. The peaks at the harmonics are almost certainly genuine components of the tube response (rather than artefacts of the instrumentation) since they are also present in the acceleration and displacement spectra, albeit closer to the noise floor. The persistence of the odd harmonics (third, fifth and seventh) indicates that the functional form of the fluid force must have a strong anti-symmetric or odd componenet (i.e. either $E(-y) = -E(y)$ or $E(-\dot{y}) = -E(\dot{y})$). Conversely, the presence of the second harmonic implies that there must also be an even element in the relationship between fluid force and tube motion, though the absence of higher even harmonics suggests that this term is relatively weak. Physically, the second harmonic means that the fluid-structure system behaves differently when displaced in one direction rather than the other. This asymmetry in the relationship between fluid force and tube motion might be caused by geometric deviation from the ideal array configuration in quiescent fluid. Several researchers have found that a displacement of the equilibrium position does not effect the main stability threshold, but it may suppress any multiple stability boundaries or change the limit cycle amplitude. (Andjelic et al. 1990; Paidoussis et al. 1995).

When the magnitude of the FRF for the tube at the same flow velocity as in fig 6.3 is examined (fig. 6.4) there is no evidence of harmonics. This can be explained by the fact that in the forced response test the entire frequency range has been excited, whereas for the free response, effectively only the natural frequency has been excited. In other words, the harmonic peaks in the FRF have been swamped by the tube response to direct excitation at those frequencies. However, the coherence between the tube response and

excitation force clearly exhibits a reduction from unity at the second and third harmonics (fig. 6.5). As the flow velocity increases, the coherence in the region of the harmonic frequencies decreases (fig. 6.6), suggesting an increase in non-linear activity. The effect of the acoustic resonance can again be seen above 8.5 *m/s*.

These observations indicate that the fluid force must have a non-linear dependence on the tube motion. Although there must be non-linearities in both stiffness and damping, it is likely that the total stiffness is probably only weakly non-linear, since substantial non-linearity in the stiffness would lead to much clearer harmonic activity. In addition, the predominant functional form of the non-linearities must be odd, so as to account for the comparatively strong odd harmonics.

6.2 An empirical non-linear model

Recall that the equation of motion for the tube subject only to fluidelastic excitation given by equation 5.2 is:

$$m\ddot{y} + c_s\dot{y} + k_s y = E(y, \dot{y}, U) \tag{6.1}$$

This equation assumes that the response due to turbulence can be averaged to zero. The overbar, indicating ensemble averaging has been omitted for convenience. The left hand side describes the structure, while the fluid is modelled by the right hand side term. This fluidelastic force can be decomposed into three functions, one in tube displacement y, the second containing only coupled terms and the third in tube velocity $\dot{y}$:

$$E(y, \dot{y}, U) = -N_1(y, U) - N_2(y, \dot{y}, U) - N_3(\dot{y}, U) \tag{6.2}$$

The minus signs are included for consistency with the linear structural stiffness and damping. In the absence of any additional excitation force, the instantaneous force acting on the tube is simply the product of the mass and the acceleration. Hence the force surface is defined by substituting eq 6.2 into eq 6.1:

$$m\ddot{y} = F(y, \dot{y}, U) = -(N_1(y, U) + k_s y) - N_2(y, \dot{y}, U) - (N_3(\dot{y}, U) + c_s\dot{y}) \tag{6.3}$$

It has been previously assumed that $N_2 = 0$ and that N_1,N_3 are linear and estimates for the linearized parameters have been obtained (see section 5.4). The same free response data, specifying the tube motion, will be used in this section to investigate the functional forms of N_1 N_2 and N_3 using the FSM technique previously described. The resulting empirically based models have also been quantified.

6.2.1 The fluid stiffness, N_1

The data in fig 6.7 has been obtained by calculating the intersection of the force surface with the zero velocity plane. In this plane, $N_2 = N_3 = 0$. Therefore, the graphs represent the development of N_1 with flow velocity. The relative high data density at lower displacement amplitudes is due to the motion decaying exponentially. As the amplitude approaches zero, the rate of change of amplitude is slower, and so the rate at which the zero velocity displacement changes from one period to the next is much smaller at the end of the decay than at the start.

As can be seen, the displacement-force curve appears to be almost linear for all flow velocities. The main effect of fluid loading seems to be a very slight increment in the slope of this line with increased onset flow, indicating a positive fluid stiffness. However, as was noted in section 6.1, to account for the amplitude dependence of the natural frequency, there must be non-linear components in the fluid stiffness. Once the dominant linear variation is removed, the underlying non-linear components are apparent. Fig 6.8 shows the residual of the force after a linear trend has been subtracted from the raw data of fig 6.7. For low velocities (fig 6.8a-c), the residual force seems to have a symmetric (even) dependence on the tube displacement. This will be modelled as a quadratic function. The type of function alone might explain the amplitude dependence of the apparent natural frequency discussed in section 6.1. However, the presence of this symmetric variation in the data for no flow suggests that it cannot be attributed to the fluid system. The fact that the response of the structure in quiescent air is independent of excitation amplitude (see section 3.2.1) indicates that this behaviour

in the force-displacement curve is not due to non-linearities in the structure. Therefore, it is probable that this even component in the data of fig 6.7 is due to an artefact of the instrumentation. As the velocity increases, the data develops additional antisymmetric (odd) components. The absence of these components in fig 6.8(a) suggest that they can be attributed to the fluid system.

A third order polynomial is the simplest function which can account for these elements of the force-displacement data. So the assumed shape of N_1 is:

$$N_1 = k_f y + \eta_1 y^2 + \eta_2 y^3 \tag{6.4}$$

Since measurement contamination due to electrical noise, turbulent excitation or quantization error is as likely to occur in the acceleration measurements as in the displacement measurements, the total least squares (TLS) curve fitting method described in section 4.4 has been used to fit equation 6.4 to each data set. The fitted curves are superimposed on the data in fig. 6.9. As can be seen the data fit is reasonable.

The variation of the quadratic stiffness coefficient η_1 is shown in fig 6.10. All the estimates lie within $\pm 20\%$ of the mean value which is $6.9 kN/m^2$. This reinforces the observation that the quadratic component is due to an artefact of the instrumentation. The cubic stiffness coefficient η_2, plotted in fig 6.11, shows a strong dependence on the flow velocity, dropping from almost zero at $U = 0 m/s$ to $-1340 kN/m^3$ at $7.5 m/s$. The dramatic drop in magnitude at $9 m/s$, which is consistent with the previously observed influence of the acoustic resonance, would further suggest that the cubic component is indeed associated with the fluid loading. The estimates of η_2 are negative across the entire flow velocity range indicating that the fluid stiffness force acts like a softening spring. As previously noted, this type of behaviour would account for the amplitude dependence of the apparent natural frequency. Since it is likely that the quadratic term is not due to the fluid loading, the stiffness term of the fluid elastic force can be written as:

$$N_1 = k_f y + \eta_2 y^3 \tag{6.5}$$

Fig 6.12 shows the linear fluid stiffness k_f obtained from the curve fits in fig 6.9. The data from the non-linear model agrees well with the curve fitted to the estimates from the linear model (see fig 5.23) which were obtained using both the DHS and FRF methods. The data does not vary with the dynamic head (U^2) indicating that Chen's model (1987) is not valid.

Although the numerical values of the coefficients η_1 and η_2 are very large, the contribution of the components to the total stiffness force is small. For example, with a displacement amplitude of $10mm$, the largest quadratic contribution is $0.8N$ and for the cubic component it is $1.3N$ while the total stiffness force is about $20N$. Since the non-linearities are modelled as high order terms, this contribution will be even less at low amplitudes. If only the linear fluid stiffness is considered and the damping is low, as is the case here, the fluidelastic frequency can be calculated as:

$$w_f = \sqrt{\frac{k_s + k_f}{m}}$$

The variation of this frequency, converted to Hertz, is shown in fig 6.13. Estimates of the same parameter from the linear model identified with the DHS method are shown for comparison. The FSM estimates are systematically higher, although the two data sets follow a similar variation with flow velocity. The discrepancy between the two estimates is about 1.5%. This could be caused by an error of just 3% in the calibration factor of either the accelerometer or the displacement transducer to which the DHS method is insensitive. Since this parameter is necessary to calculate the limit cycle amplitude, a straight line has been fitted to the FSM estimates in the range $U = 2.5 \rightarrow 8.5m/s$.

6.2.2 The fluid damping, N_3

The data in fig 6.14 has been obtained by calculating the intersection of the force surface with the zero displacement plane, in a similar manner to fig 6.7.

In this plane, $N_1 = N_2 = 0$. Therefore the force is given by:

$$F(y = 0, \dot{y}, U) = -(N_3(\dot{y}, U) + c_s\dot{y}) \tag{6.6}$$

The graphs represent the development of this function with flow velocity due to the variation of the fluid force N_3.

There appears to be more scatter in the data of fig 6.14 than was evident for the displacement-force data (figure 6.7). This can be attributed to two mechanisms.

The velocity measurement was monitored using 12 bit ADC, just as the displacement was, so one would expect a comparable signal to noise ratio. The acceleration is a subset of the same measurement as that used in fig 6.9, but the range of acceleration in the zero displacement plane is more than a factor of 30 smaller than the full range of measurement. This will mean that the force data will be more susceptible to noise in the acceleration record. Furthermore, although the raw acceleration data was digitized with 12 bit precision, the force data in fig 6.14 will have only 7 bit precision ($2^{12}/30 \approx 2^7 = 128$ levels) so quantization error may be an issue. The intersection between the force surface and the zero displacement plane is calculated by interpolating between the two points measured as the state space trajectory crosses the plane. This will mask the stratification of data which is characteristic of quantization error, but will not alleviate it.

To illustrate the second mechanism, consider the tube motion to be a fixed amplitude sine wave. When the velocity crosses zero, both the displacement and the acceleration are changing slowly with time (both are at the peak/valley of the sine wave). This means that if the time at which the velocity is zero is miscalculated due to noise in the velocity record, neither the corresponding displacement nor force will be strongly effected. The situation at the displacement zero crossing is not the same. Here, the acceleration is changing rapidly, so noise in the displacement record may produce a

large error in estimating the force at zero displacement. Thus, the displacement-force curves (fig 6.7) are not susceptible to noise in the tube velocity, but the velocity-force curves may be corrupted by errors in the displacement record.

Notwithstanding the scatter in the data, there is a clear trend in the graphs of fig 6.14. At first glance the velocity-force curves seem to be predominantly linear. To illustrate what, if any, non-linear relationship exists between the fluid force and the tube velocity, a straight line has been fitted to each data set in fig 6.14 and then subtracted. The resulting residuals are shown in fig 6.15. It is apparent that these residuals are not random, but are in fact governed by a predominantly antisymmetric function, which becomes more pronounced with increased flow velocity.

Two different model prototypes are proposed to account for this:

Either,

$$\begin{aligned} N_3 &= \beta_1(U)\dot{y}^3 + c_f(U)\dot{y} + D \\ \Rightarrow F_{(y=0)} &= -\left[\beta_1(U)\dot{y}^3 + (c_f(U) + c_s)\dot{y} + D\right] \end{aligned} \tag{6.7}$$

or

$$\begin{aligned} N_3 &= \beta_2(U)\text{sgn}(\dot{y}) + c_f(U)\dot{y} + D \\ \Rightarrow F_{(y=0)} &= -\left[\beta_2(U)\text{sgn}(\dot{y}) + (c_f(U) + c_s)\dot{y} + D\right] \end{aligned} \tag{6.8}$$

In both cases D is a constant to account for DC bias in the instrumentation.

The first model is similar to that developed by Price & Valerio (1990). The main difference is that in their model, the fluid stiffness exhibits very strong non-linearity, which results in relatively large amplitude harmonics in the free response of the tube. As discussed above, neither of these phenomenon have been observed here. Notwithstanding that, the basic mechanism which limits the tube motion is high order (i.e. greater than 1) polynomial terms in the fluid damping. Rzentkowski & Lever (1998) extended the linear model of Lever & Weaver (1986), to a non-linear model for fluidelastic instability.

However, after some manipulation, they reduce the solution of this model to include only linear and cubic terms. An alternative physical interpretation of the cubic model is that it is caused by a fluid drag term which will have a form similar to $\dot{y}|\dot{y}|$ which, when expanded into the sum of polynomials, has a strong cubic component.

The second model is simply a discontinuity at zero tube velocity, in addition to the linear variation. In effect, the non-linear fluid force has been modelled as a Coulomb (dry friction) damping with a coefficient dependent on flow velocity. As will be seen, the coefficient β_2 is positive, implying net energy transfer into the structure, therefore this effect can not be attributed to a genuine dry friction mechanism caused by rubbing in the structure. In terms of the fluid dynamics, this type of force component could be a indication of a jet switching mechanism. Roberts (1966) has proposed a successful theoretical model based on jet switching, but it predicts instability only in the in-flow direction. Price (1995) reported that he has attempted unsuccessfully to develop a similar theoretical model for transverse instability based on the jet switching concept.

Therefore, although neither model was produced from a consideration of the prevailing fluid mechanics there are similarities between both models and theoretical models documented in the literature.

One important difference between the two models effects the prediction of the stability boundary. The cubic model can sensibly be linearized, while the Coulomb model can not. As the displacement amplitude increases, the effect of the non-linearity in the cubic model increases, while for the coulomb model the non-linearity becomes less significant. Conversely, when considering low amplitudes, the cubic model can be approximated well by considering only the linear element, while the Coulomb model is dominated by the non-linearity. Thus, the predicted critical velocity would be effected very strongly by the coulomb parameter (β_2), but not at all by the cubic damping (β_1).

The model described by eq 6.7 has been fitted to the data of fig 6.14 using the TLS and the resulting curves superimposed on the data in figure 6.16. The variation of the identified parameters, c_f and β_1, is shown in figures 6.18 & 6.19. In the velocity range from $2.5m/s$ to $8.5m/s$ the parameters vary smoothly suggesting a definite dependence

on flow velocity, as would be expected. The effect of the acoustic resonance is again very clearly visible at $U = 9m/s$. The cubic damping paramter, β_1, is non zero for the no flow case. This may be due to a real non-linearity in the structural damping, however there is no other evidence to support such a non-linearity (see chapter 3). A more likely explanation is that by fitting a cubic function to noisy, but linear data, the least squares algorithm has attempted to model the scatter as a deterministic cubic term. It is true that this arguement could be posed at all flow velocities, thus invalidating the results of fig 6.19. However, re-examination of fig 6.15(a) indicates that the non-linear residual at zero flow is less organized than when there is flow. This is true even for the case of $U = 2.5m/s$ (fig 6.15(b)) for which the magnitude of β_1 identified was similar to that for no flow. Therefore the non-zero value of β_1 at $U = 0$ is not significant.

It is apparent that neither parameter, c_f or β_1, follow the same trend at low flow velocity as at higher speeds. This can be explained using the quasi-static assumptions proposed by Price and Paidoussis (1986). At low flow velocities, the tube velocity is comparable with that of the fluid. Therefore, the local flow impinging on the moving cylinder will rotate, causing the drag force, which acts in the direction of the local flow, to have a component in the transverse or y direction. This effect diminishes as the flow increases. Furthermore, the linear trend in the fluid damping, c_f, at higher flow velocities is predicted by Price and Paidoussis (1986). Neither of the parameter sets predicted by the cubic damping model varies quadratically with flow velocity, suggesting that, for this array at least, Chen's model is inappropriate, even with a non-linear model.

For the purposes of predicting the stability thresholds and limit cycle amplitudes, the dependence of both sets of parameters (fig 6.18 and 6.19) on flow velocity has been reduced to a low order polynomial for the velocity range $U = 2.5m/s \rightarrow 8.5m/s$. For the linear fluid damping c_f a first order polynomial appears adequate, while for the cubic fluid damping, β_1, a third order relationship was used. A conventional least squares (rather than a total least squares) was used to fit these curves since the measured flow velocity can be regarded as reliable.

Fig 6.17 shows the second model fitted to the data, given by equation 6.8. The

parameter values obtained for the linear fluid damping are shown in fig 6.20, and the Coulomb damping coefficient, β_2, is plotted in fig 6.21. As with the first model the parameters seem to vary smoothly with the flow velocity. However, it is interesting to note that at $U = 9.0m/s$, only the Coulomb damping parameter seems to be affected by the acoustic resonance. The linear fluid damping no longer shows a linear trend. Indeed, it seems that a quadratic variation with flow velocity would seem more appropriate, as proposed by Chen (1987). This is in stark contrast to the cubic model.

Comparing fig 6.16 with fig 6.17 suggests that either model could be used to represent the available data. This is borne out by the mean residual error between the fitted curves and the data for the two models (fig 6.22). Unfortunately, data is sparse at the extremities of the velocity axis and non-existent in the zone around zero velocity. Data in either of these regions would resolve unequivocally which model is most appropriate. In the absence of such data, the identified parameters can be used to predict the onset of instability and the resulting limit cycle amplitudes. These can then be compared to the experimental data obtained in section 5.5.

6.2.3 The cross term, N_2

Once the functional forms of N_1 and N_3 had been identified, the time series of cross term N_2 was calculated for each flow velocity:

$$N_2(t) = m\ddot{y} - [N_1(y(t)) + k_s y(t) + N_3(\dot{y}(t)) + c_s \dot{y}(y)] \tag{6.9}$$

Unfortunately, no functional relationship between N_2 and y,$\dot{y}$ was apparent. The only trend to emerge was that the RMS of N_2 increased with flow velocity from almost zero at no flow to $0.3N$ at $8.5m/s$ and this may be indicative of the increase in turbulent excitation. This does not imply that there is no cross term at work in the fluid structure system, only that it is immersed in noise. However, without an identified model for the functional form, N_2 must be ignored.

6.3 Prediction of stability threshold

The work done by the coupled fluid-structure system during a single period of oscillation is given by:

$$W = \int_0^{\frac{2\pi}{\omega}} F(y, \dot{y}, U)\, \dot{y}\, dt \tag{6.10}$$

where ω is the circular frequency of vibration

F is the total force (structural and fluidelastic) acting on the tube (see eq 6.3). The convention that negative work indicates energy being dissipated form the structure has been adopted. The total force as a function of tube displacement and velocity has been determined in the last section:

$$\begin{aligned} F(y, \dot{y}, U) &= -(N_1(y, U) + k_s y) - N_2(y, \dot{y}, U) - (N_3(\dot{y}, U) + c_s \dot{y}) \\ \Rightarrow F(y, \dot{y}, U) &= -\left[(k_f(U) + k_s)y + \eta_2(U)y^3 + (c_f(U) + c_s)\dot{y} + z\right] \end{aligned} \tag{6.11}$$

where z is the non-linear functional of either equation 6.7 or 6.8 (i.e. either cubic or Coulomb damping). Substituting eq 6.11 into eq 6.10 yields the work done per cycle in terms of the model parameters:

$$W = -\int_0^{\frac{2\pi}{\omega}} \left[(k_f + k_s)y + \eta_2 y^3 + (c_f + c_s)\dot{y} + z\right]\, \dot{y}\, dt$$

Since $(k_f + k_s)y$ and $\eta_2 y^3$ are conservative forces, they will do no work over one period, the expression can be further reduced:

$$W = -\int_0^{\frac{2\pi}{\omega}} \left[(c_f + c_s)\dot{y} + z\right]\, \dot{y}\, dt \tag{6.12}$$

Assume that over one cycle the tube displacement is given by a constant amplitude sinusoid.

$$\begin{aligned} y &= A\sin(\omega t) \\ \Rightarrow \dot{y} &= -A\omega\cos(\omega t) \end{aligned} \tag{6.13}$$

A constant amplitude is admissable since the damping levels (whether positive or negative) are low so that the amplitude of vibration is changing slowly. Considering the motion to have only a single frequency component, rather than a combination of harmonics, is justified by the weakness of the non-linearities. The validity of this interpretation is demonstrated by fig 6.3 (the velocity spectrum of free response under fluidelastic loading) where the strongest harmonic is nearly 5 orders of magnitude smaller than the fundamental.

6.3.1 Behaviour of the cubic model

For the first damping model (cubic damping) the work done per cycle is given by:

$$W_1 = -\int_0^{\frac{2\pi}{\omega}} (c_f + c_s)\dot{y}^2\, dt + \int_0^{\frac{2\pi}{\omega}} \beta_1 \dot{y}^4\, dt$$

Using equation 6.13

$$W_1 = -A^2\omega^2(c_f + c_s)\int_0^{\frac{2\pi}{\omega}} \cos^2(\omega t)\, dt + A^4\omega^4\beta_1 \int_0^{\frac{2\pi}{\omega}} \cos^4(\omega t)\, dt$$

$$\Leftrightarrow W_1 = -A^2\omega\pi\left[(c_f + c_s) + \frac{3}{4}(\beta_1 A^2\omega^2)\right] \tag{6.14}$$

It should be noted that ω, c_f and β_1 are functions of the flow velocity U, which have been determined empirically in the last section.

When the tube motion has established a limit cycle, the total work done during the course of one cycle period must be zero.

$$\Rightarrow W = 0$$

Combining this condition with eqn 6.14 provides an expression for the limit cycle amplitude in terms of the parameters from the cubic damping model. Some manipulation yields:

$$\Leftrightarrow A = \sqrt{-\frac{4}{3}\frac{(c_f(U) + c_s)}{\beta_1(U)\,\omega(U)^2}} \tag{6.15}$$

Since β_1 is positive in the range of interest (fig 6.19), and ω by definition is positive (a negative frequency in this situation implies a static divergence), the limit cycle amplitude predicted by eq 6.15 will be real only if $(c_f + c_s)$ is negative. At first, this appears to be the same criterion as was used to obtain stability threshold predictions from the linearized model. However, since the effect of the non-linear damping (which for the cubic model has a stabilizing influence) is accounted for explicitly rather than by measuring an apparent linear damping, the estimates of c_f from the non-linear model are substantially different from those of the linearized model. This can be seen by comparing fig 6.18 with fig 5.22 in the last chapter.

If the limit cycle is to be stable, any pertubation to the limit cycle must decay. In other words, if the motion is disturbed so that the amplitude of motion is increased, the work done per cycle must be negative to dissipate the added energy. Conversely, a reduction in the vibration amplitude must produce positive net work, so that energy is transferred from the flow into the structure. Therefore, $\frac{\partial W}{\partial A}$ must be negative. Differentiation of equation 6.14 yields:

$$\frac{\partial W_1}{\partial A} = -A\pi\omega \left[2(c_f + c_s) + A^2 3\beta_1\omega^2\right]$$

At the limit cycle amplitude (from eq 6.15):

$$A^2 = -\frac{4}{3}\frac{(c_f(U) + c_s)}{\beta_1(U)\,\omega(U)^2}$$

Substituting this the equation above yields a simplified expression for the derivative at the limit cycle amplitude :

$$\frac{\partial W_1}{\partial A} = 2\pi\omega A(c_f + c_s) \tag{6.16}$$

As the limit cycle amplitude A is non-zero and $2\pi\omega$ is positive, $\frac{\partial W_1}{\partial A}$ will be negative only if $(c_f + c_s)$ is negative. This is the same condition for the cubic model to yield a real valued limit cycle amplitude that was noted above. Therefore, any limit cycle amplitude predicted by the cubic model will be stable. It has been suggested by Rzentkowski & Lever (1992, 1998) that the cause of the hysteretic behaviour of the fluidelastic stability

threshold could be attributed to the possibility of an unstable limit cycle. In this context, the fact that the cubic damping model identified here predicts that any limit cycle which occurs will be stable is supported by the observation made in the last chapter that neither array under investigation exhibited hysteretic behaviour.

It is possible that β_1 is negative at flow velocities less than $2.5m/s$. If this is true, then a limit cycle may exist when $(c_f + c_s)$ is positive. Such a limit cycle would be unstable, since the right hand side of eq 6.16 would then be positive. However, since no measurements were made in this velocity range, this is just conjecture.

6.3.2 Behaviour of the Coulomb model

Applying a similar procedure to that employed in deriving eq 6.15, the work done per cycle by the Coulomb model can be determined:

$$W_2 = 4\beta_2(U)\text{sgn}(A)A + (c_f(U) + c_s)\omega(U)\pi A^2 \tag{6.17}$$

The sgn(A) term allows for the possibility of a negative amplitude. Applying the condition of zero work for a limit cycle amplitude and rearranging, an expression for the limit cycle amplitude based on the coulomb damping model has been obtained.

$$|A| = -\frac{4}{\pi}\frac{\beta_2(U)}{\omega(U)(c_f(U) + c_s)} \tag{6.18}$$

For a non-zero amplitude to exist, this model predicts that either β_2 or $(c_f + c_s)$ must be negative. If both are either negative or positive, no limit cycle will exist since eq 6.18 would be reduced to the absurdity of a positive number equated to a negative number. Examination of the parameter estimates in figures 6.20 & 6.21 indicates that once the structural damping is greater than the magnitude of the linear fluid damping, the Coulomb model predicts a limit cycle even at velocities as low as $2.5m/s$. As the flow velocity increases and the total damping, $(c_s + c_f)$, becomes negative, the tube motion becomes dynamically divergent. This sort of divergence has not been observed in this array, suggesting that the Coulomb model is not applicable.

6.4 Comparison with experiment

The variation of tube response with flow velocity at three different levels of structural damping has been determined directly by experiment (see fig 5.7). In order to assess the validity of the two different damping models, the predicted limit cycle amplitude at the same three levels of structural damping was calculated using both eq 6.15 and eq 6.18. The RMS of displacement predicted by the cubic damping model is shown in fig 6.23, while that obtained from the Coulomb damping model is plotted in fig 6.24. Comparison with the direct experimental results suggest that the cubic model offers far superior predictions. The cubic model displays the same qualitative behaviour as the direct experimental results. As the flow velocity is increased, the amplitude increases sharply at some critical velocity and then continues to drift upwards gradually. In contrast the Coulomb model does not exhibit a corner at the onset of instability and the limit cycle amplitude appears to increase exponentially until dynamic divergence sets in. Hence, the cubic fluid damping would appear to be a better model for predicting the phenomenon of fluidelastic instability in this tube array. Table 6.1 compares the experimental critical velocities with the linear model predictions from the last chapter and the predictions from the cubic damping model.

Pitch ratio	1.32		
Logarithmic decrement, δ	0.093	0.106	0.114
Critical reduced gap velocity, V_r	57.3	77.1	90.8
Linear model	104.9	120.3	127.3
Non-linear model	72.7	83.9	88.1

Table 6.1: Predictions for FEI Thresholds using a non-linear model

Although the limit cycle amplitudes from the cubic model show the correct trends, the predicted values are substantially higher than those measured directly. However, the amplitudes presented in fig 6.23 have been calculated in the absence of turbulence.

Rzentkowski & Lever (1998) and Zhu & Yu (1986) have shown that random excitation applied to a self excited system may decrease the amplitude of oscillation. Although in both cases the effect was a decrease of about 20%. The square root in eq 6.15 implies that the cubic parameter β_2 would have to be under estimated by a factor of 4 to account for the over estimation in the limit cycle amplitude. Even though the data was corrupted with noise and the effects of turbulent buffeting, this level of error in the parameter estimate seems unlikely. A more probable source of error is the cross terms which have been not been accounted for.

6.5 Summary

The coupled fluid-structure system has been shown to be non-linear for both arrays, but this non-linear behaviour is more pronounced for a pitch ratio of 1.32. For this array a non-linear model has been identified using the Force State Mapping technique.

The fluid stiffnes is represented by a combination of a linear component and a cubic term. The quadratic element apparent in the raw data has been attributed to instrumentation error. Two non-linear models have been proposed and identified for the fluid damping. The Coulomb damping has been rejected since it does not offer reasonable predictions of limit cycle behaviour.

Neither the linear fluid stiffness nor the linear fluid damping coefficients vary with the dynamic head. Hence, it would seem that Chen's model is not applicable to this array. It was also noted that the shape of the trends were consistent with the quasi-steady model of Price & Paidoussis (1986).

The predictions of critical velocity from the non-linear model are a great improvement over those from the linear model. However, the prediction of limit cycle amplitude, although showing qualitative agreement with experimental data, are nearly 100% too large. This has been attributed to the cross terms which have not been accounted for.

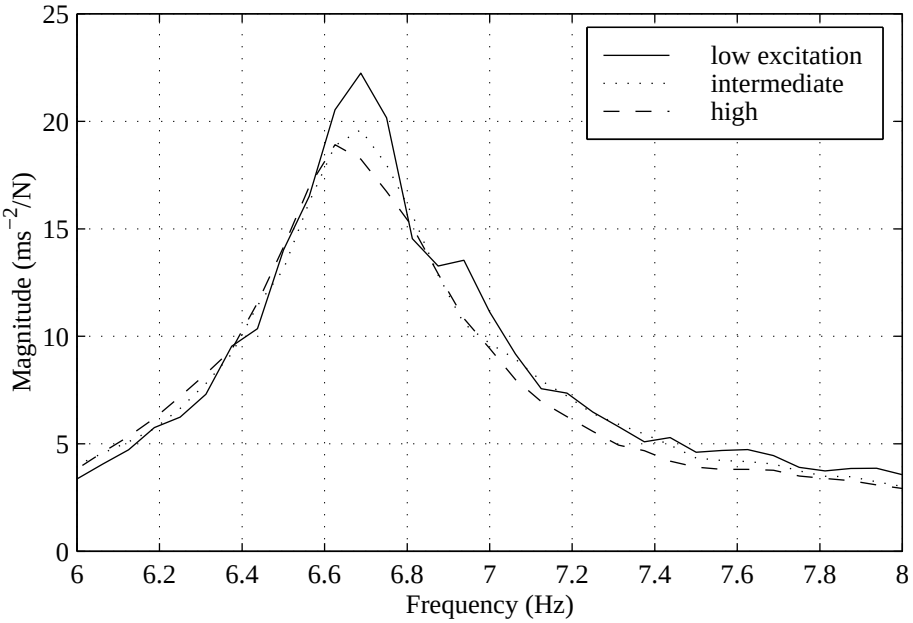

Figure 6.1: FRF with fluid loading at 3 different levels of excitation. P/d=1.58

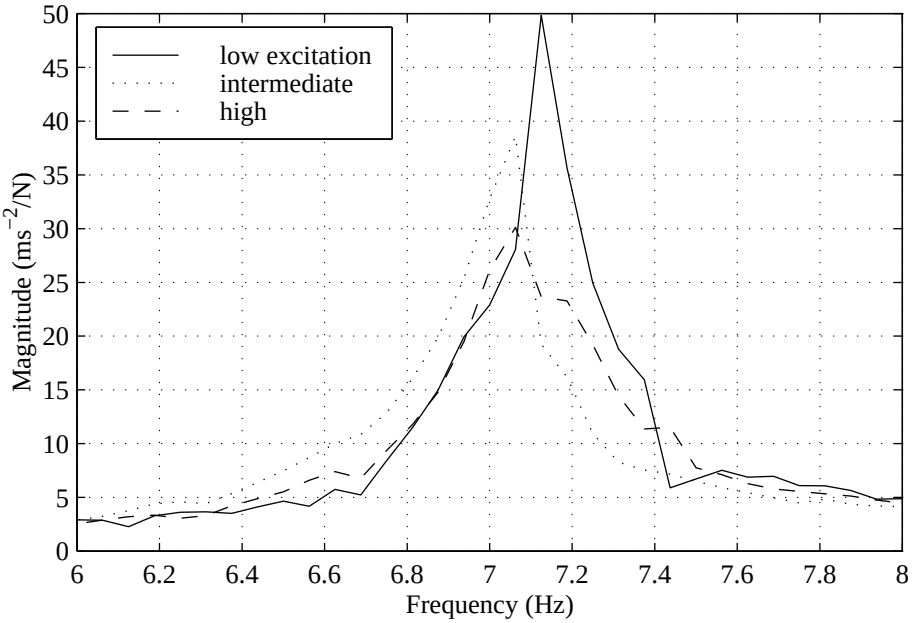

Figure 6.2: FRF with fluid loading at 3 different levels of excitation. P/d=1.32

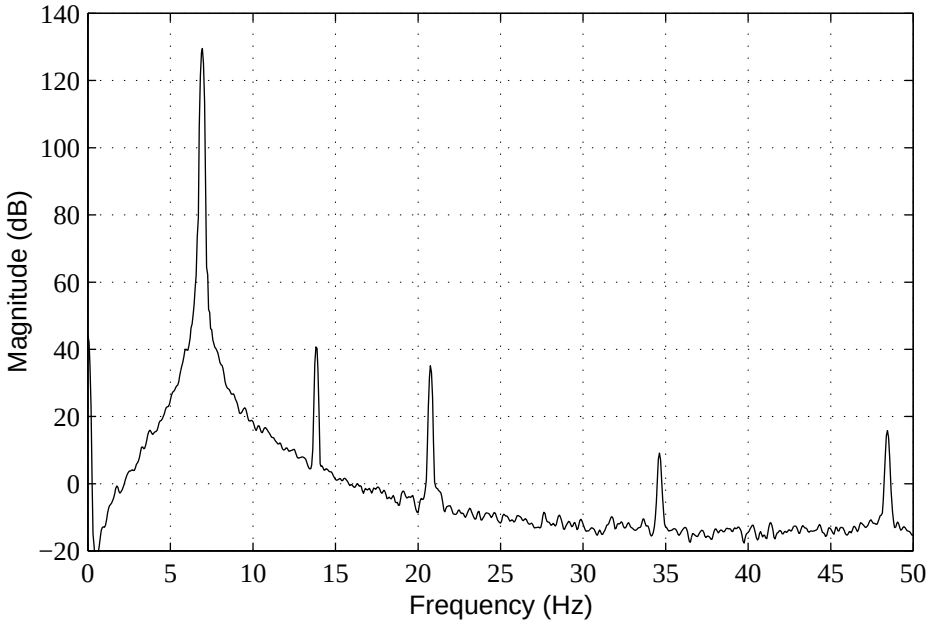

Figure 6.3: Spectrum of tube velocity subject only to fluid excitation. P/d=1.32, $U = 7.5$ *m/s* $\delta = 0.093$

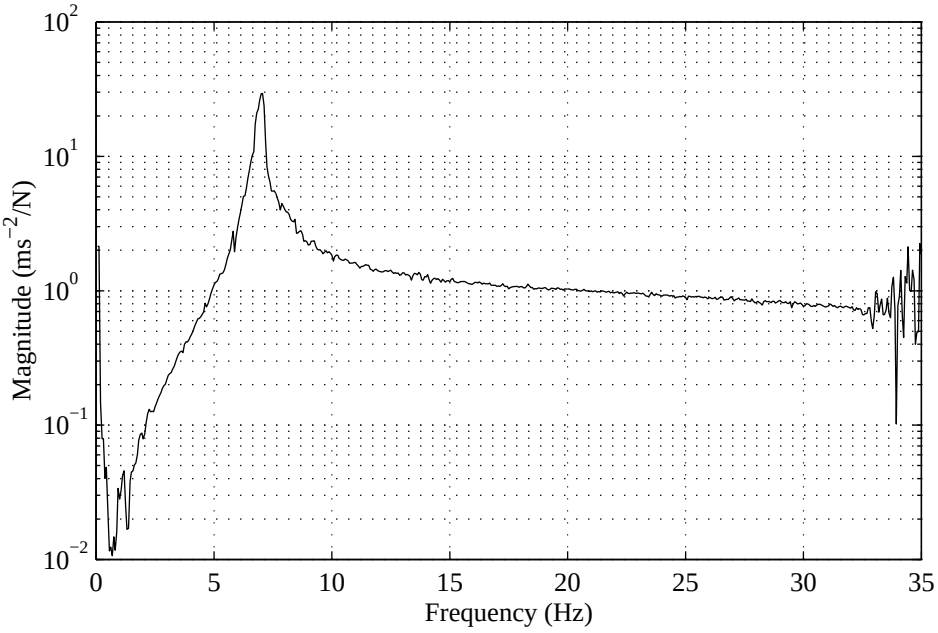

Figure 6.4: Magnitude of a typical FRF with fluid loading. $U = 7.5$ *m/s*

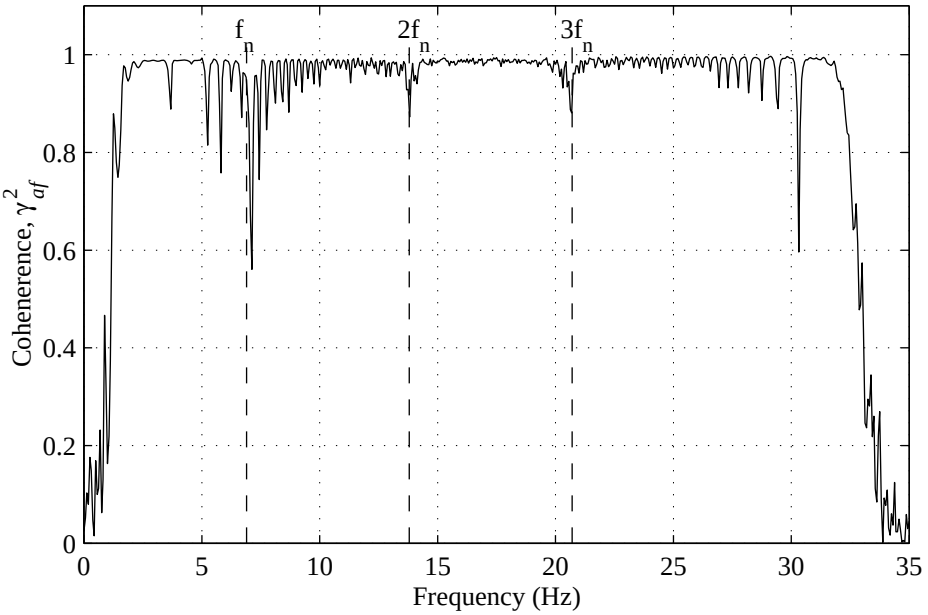

Figure 6.5: Coherence between tube response and excitation force. Same case as fig. 6.3

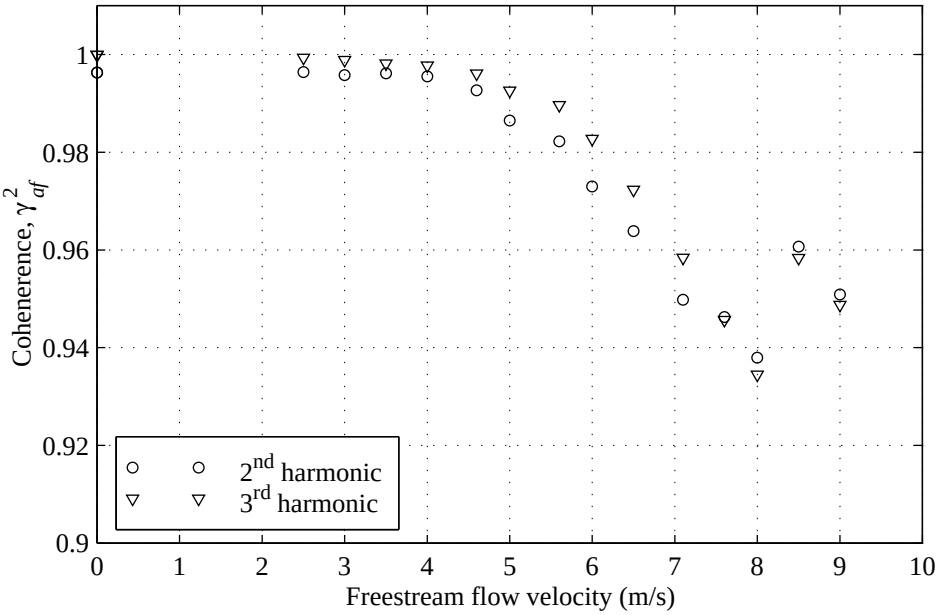

Figure 6.6: Variation of coherence at the second and third harmonics.

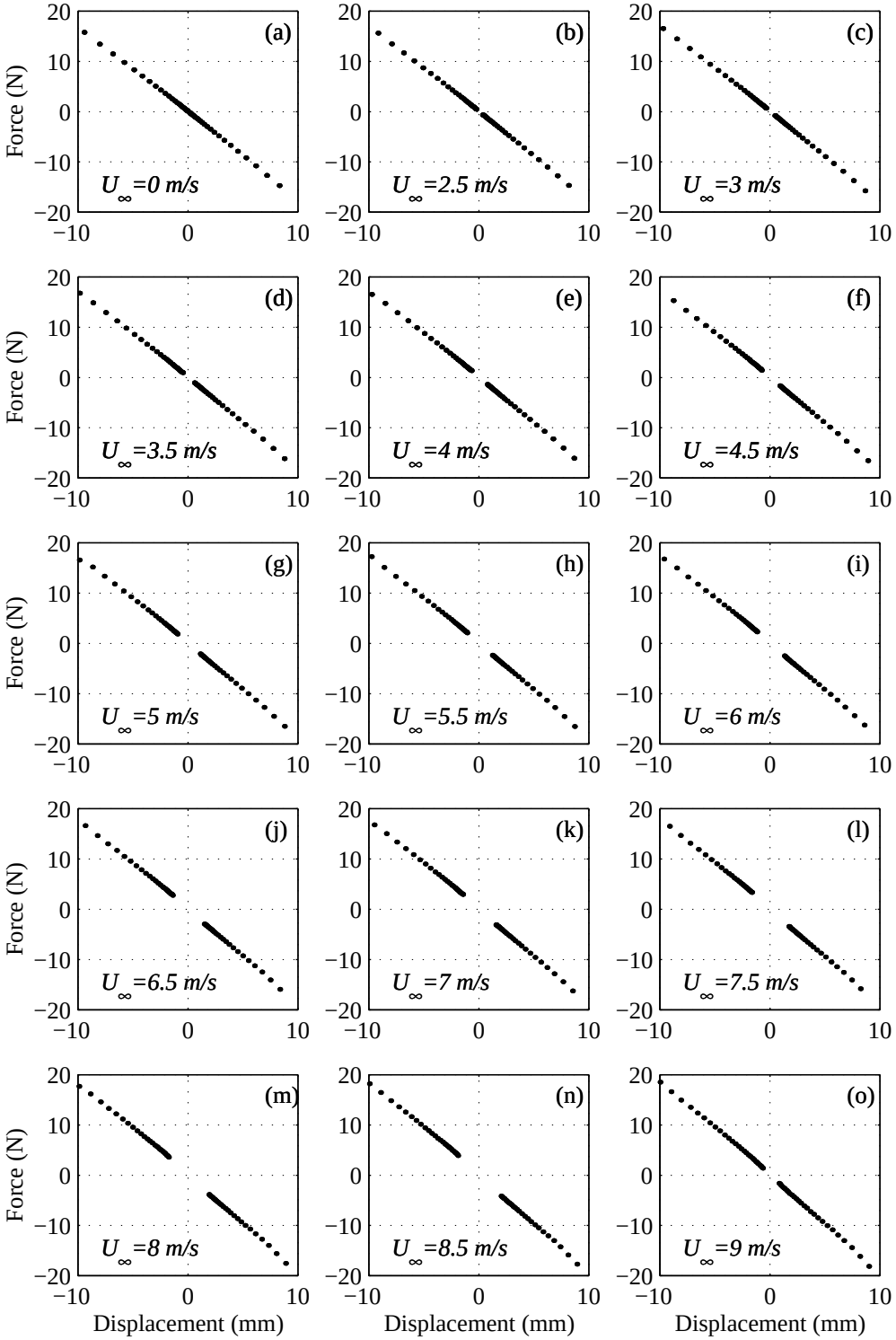

Figure 6.7: Displacement-force data at various flow velocities.

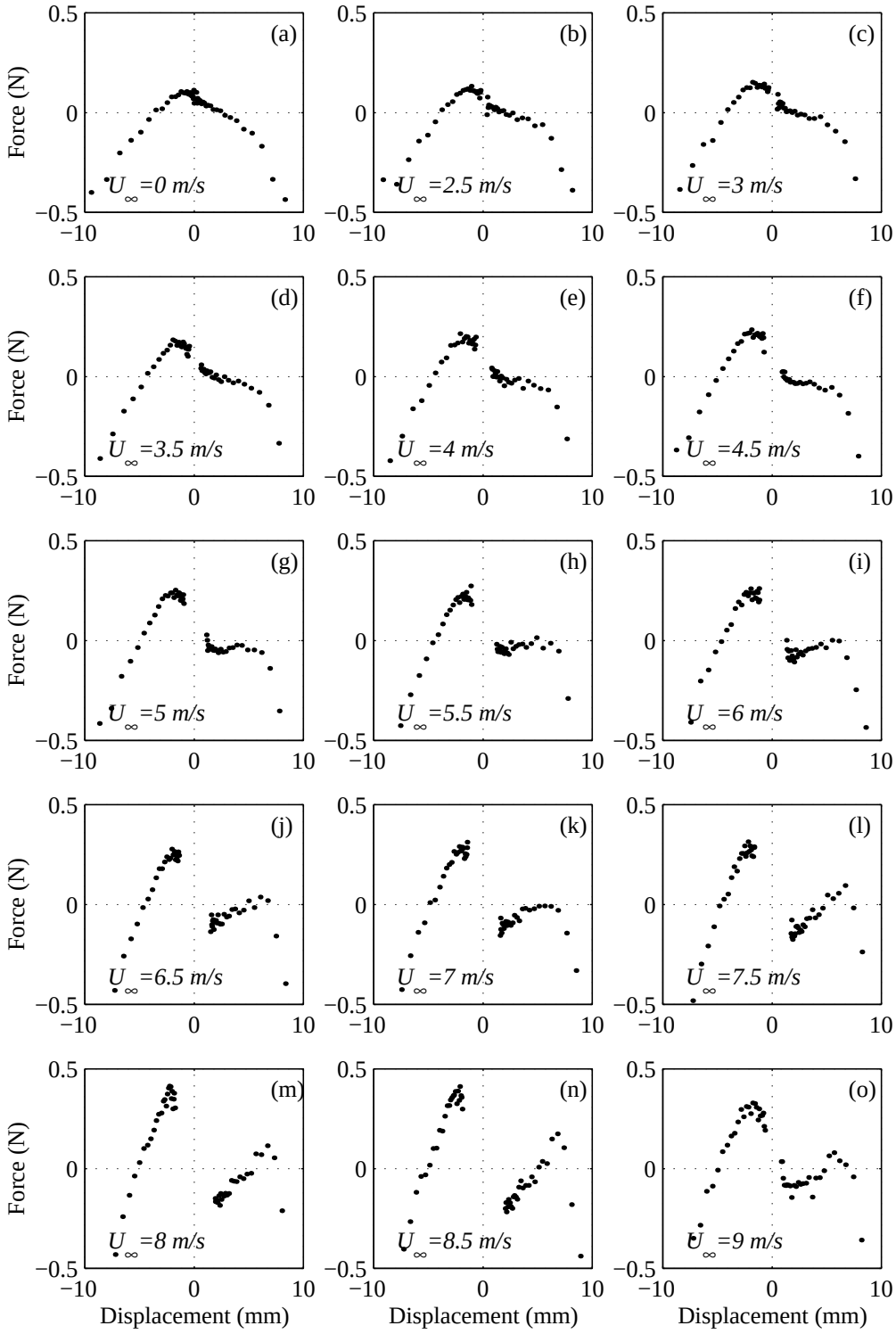

Figure 6.8: Displacement-force data without the linear trend.

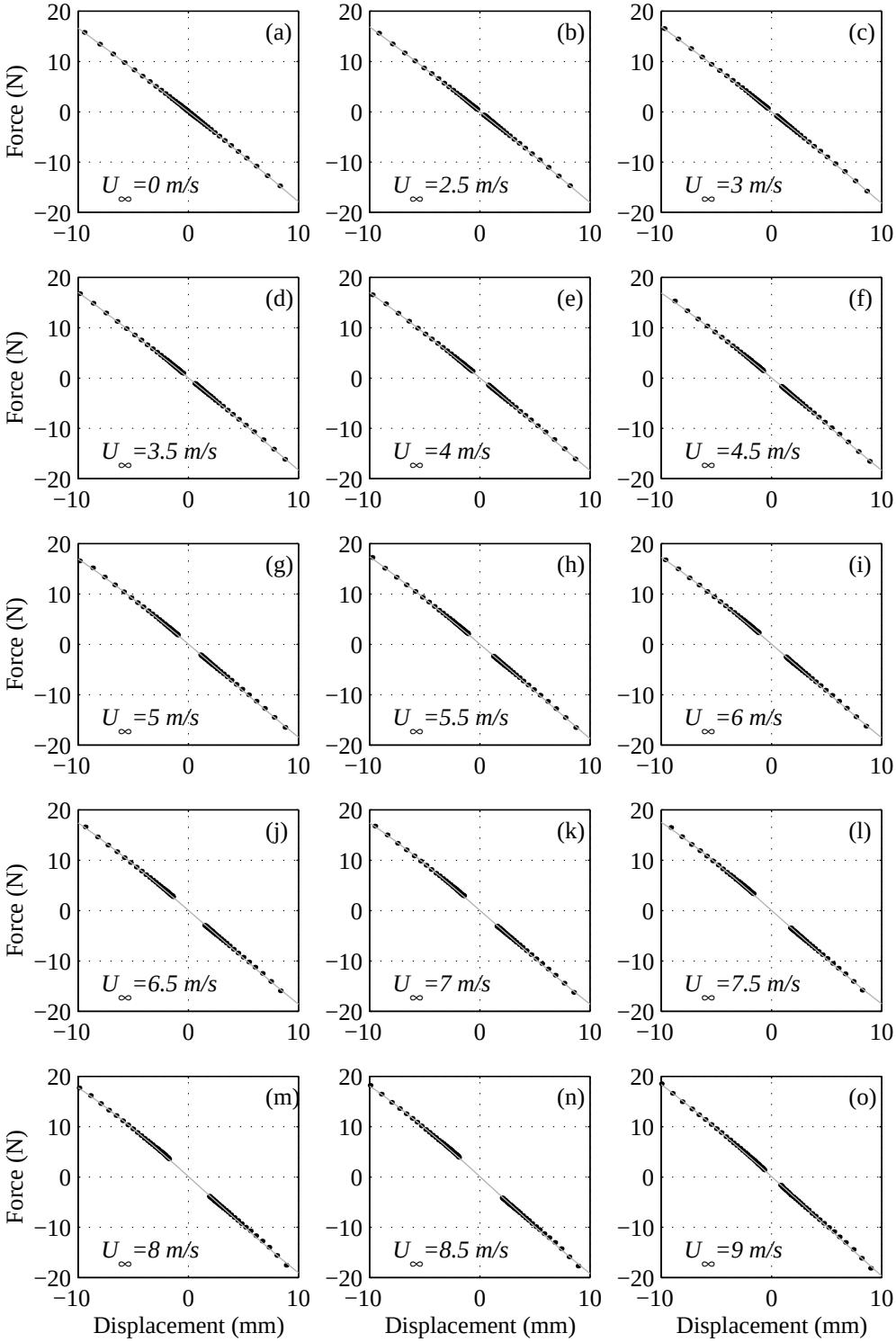

Figure 6.9: 3^{rd} order polynomial fitted to data from fig 6.7.

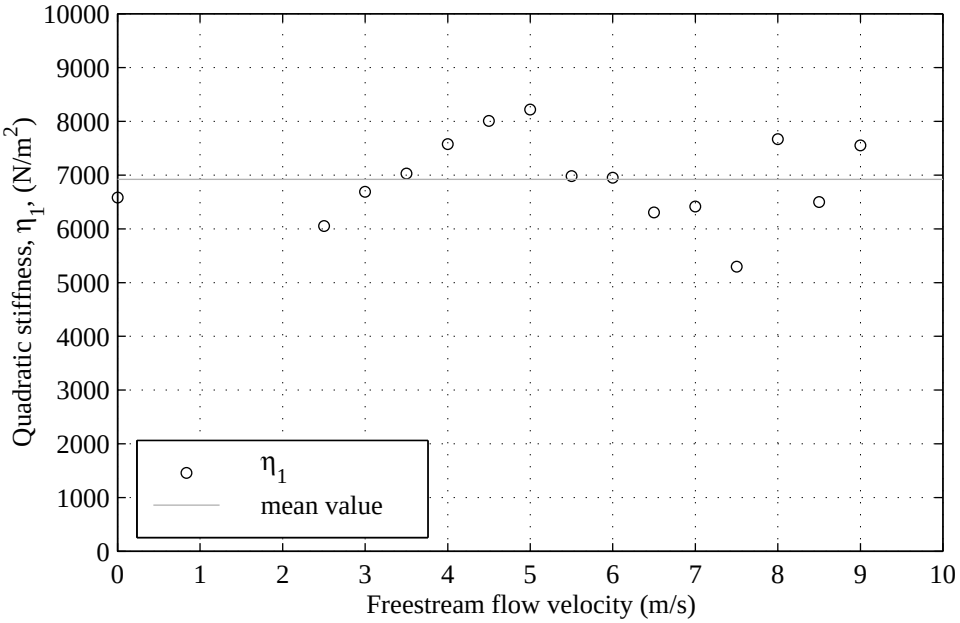

Figure 6.10: Quadratic stiffness coefficient, η_1, identified from fig 6.9.

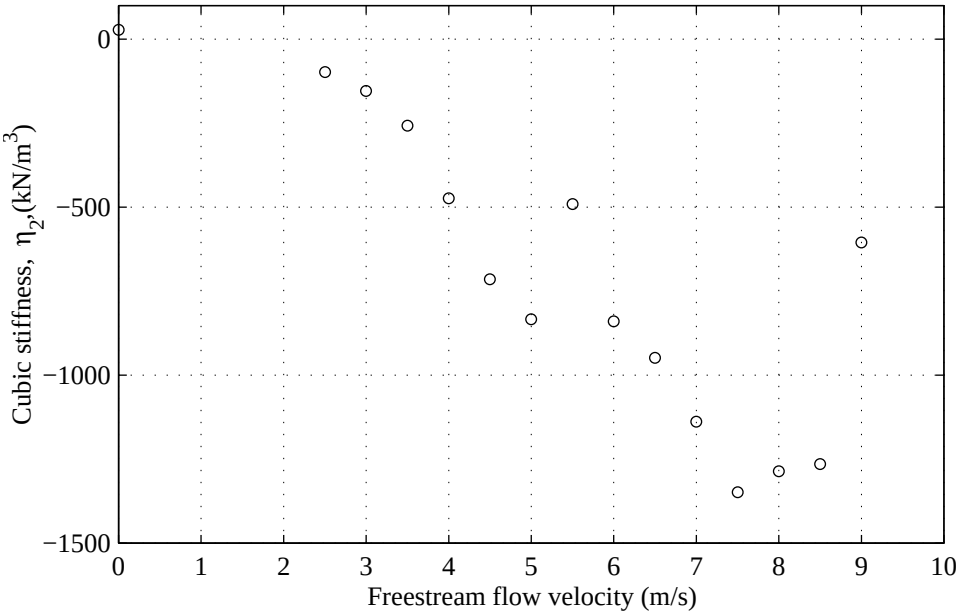

Figure 6.11: Cubic stiffness coefficient, η_2, identified from fig 6.9.

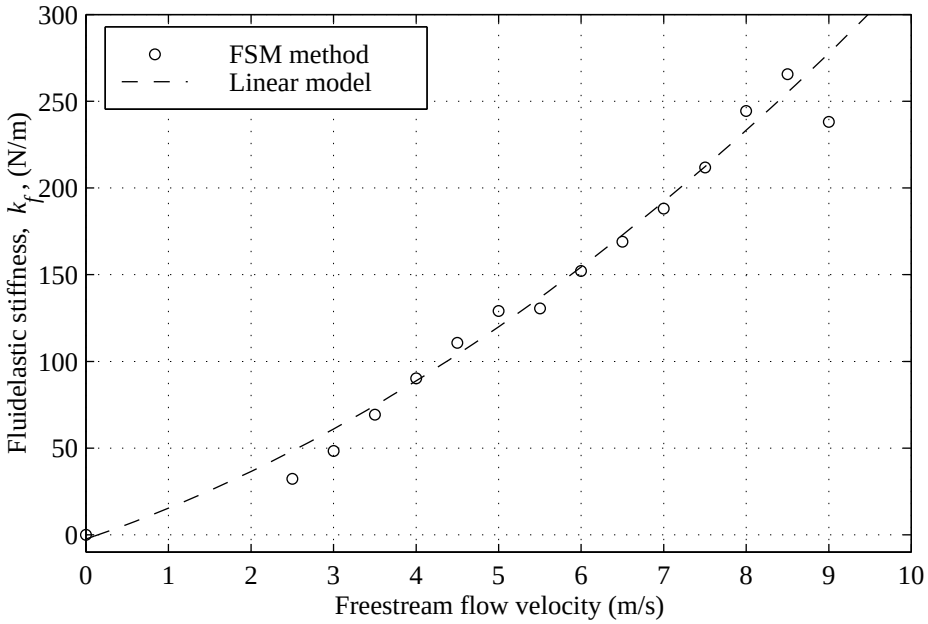

Figure 6.12: Linear fluid stiffness coefficient identified with the Force Surface Mapping (FSM) method and the DownHill Simplex (DHS) method).

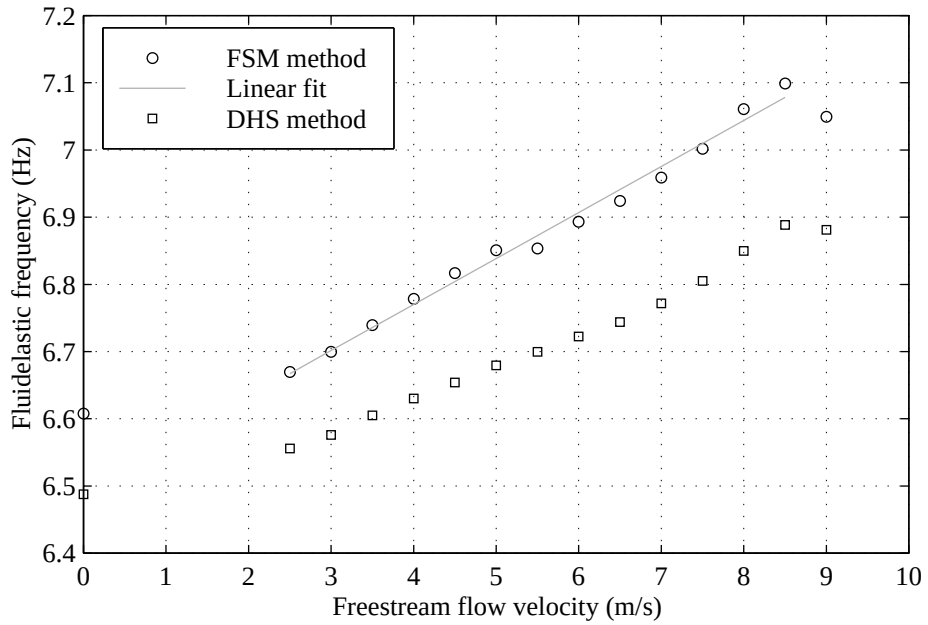

Figure 6.13: Fluidelastic frequency and straight line fit in the range $U = 2.5 \rightarrow 8.5m/s$

.

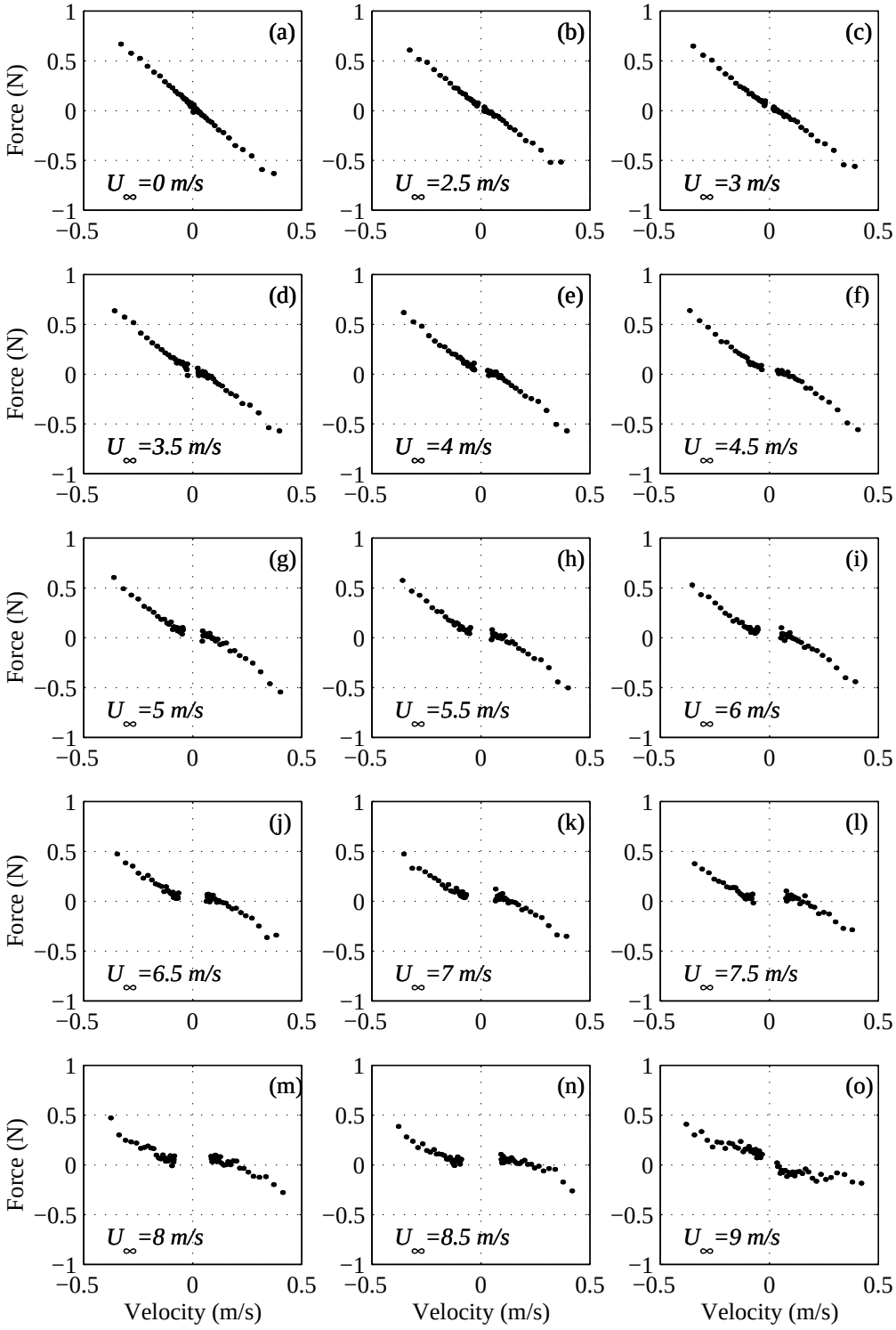

Figure 6.14: Tube velocity-force data at various flow velocities.

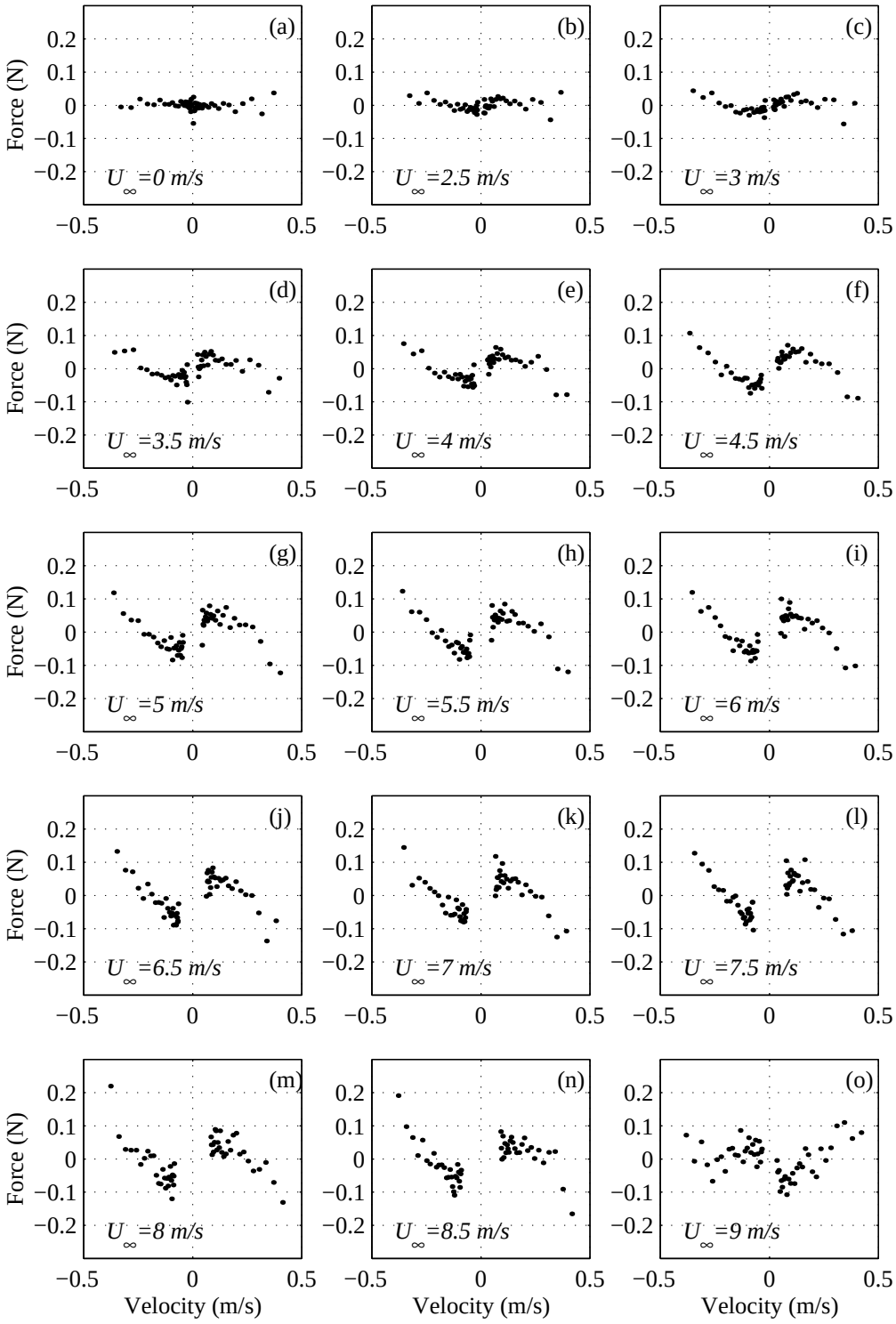

Figure 6.15: Velocity-force data without the linear trend

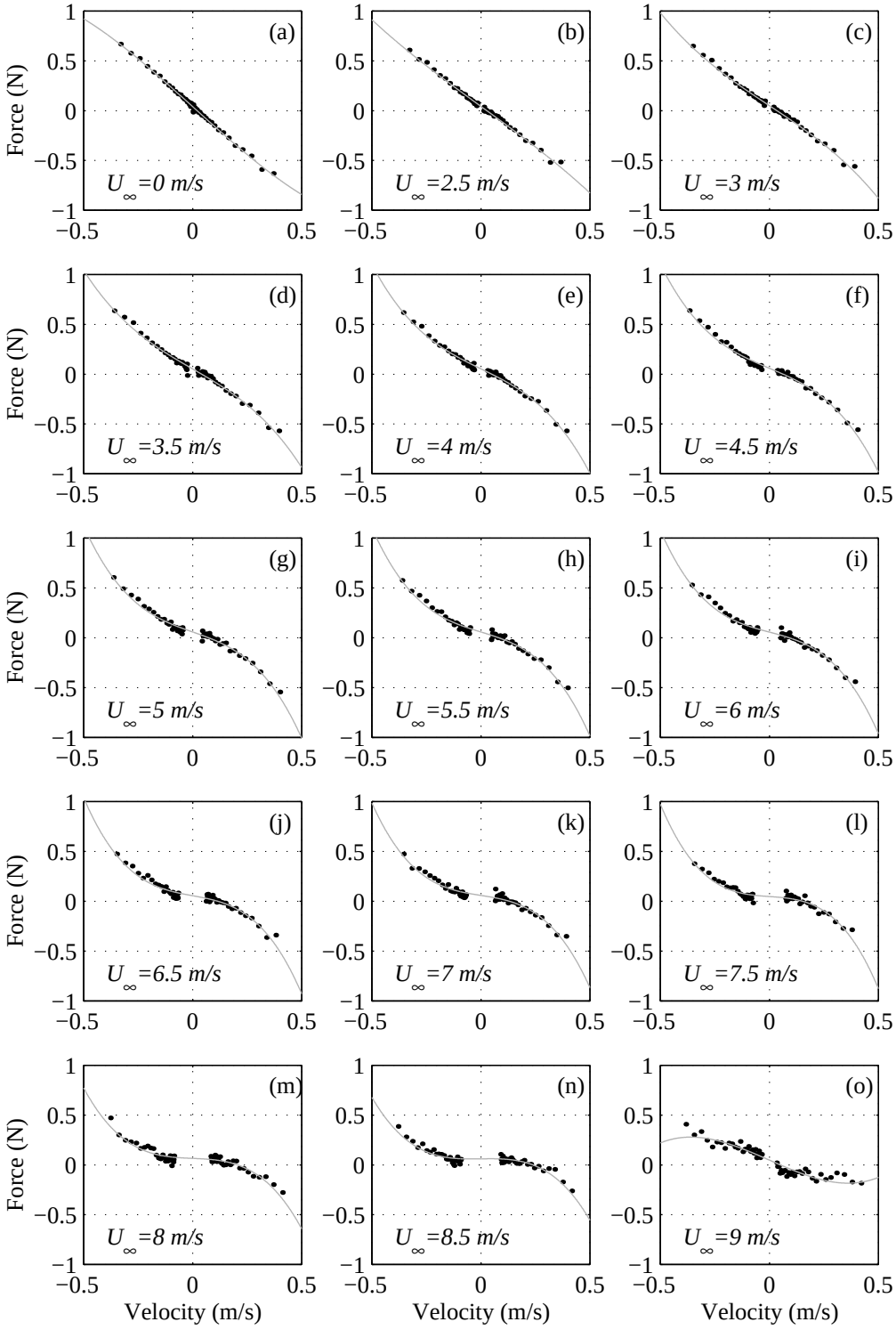

Figure 6.16: Cubic damping model fitted to data from fig 6.14.

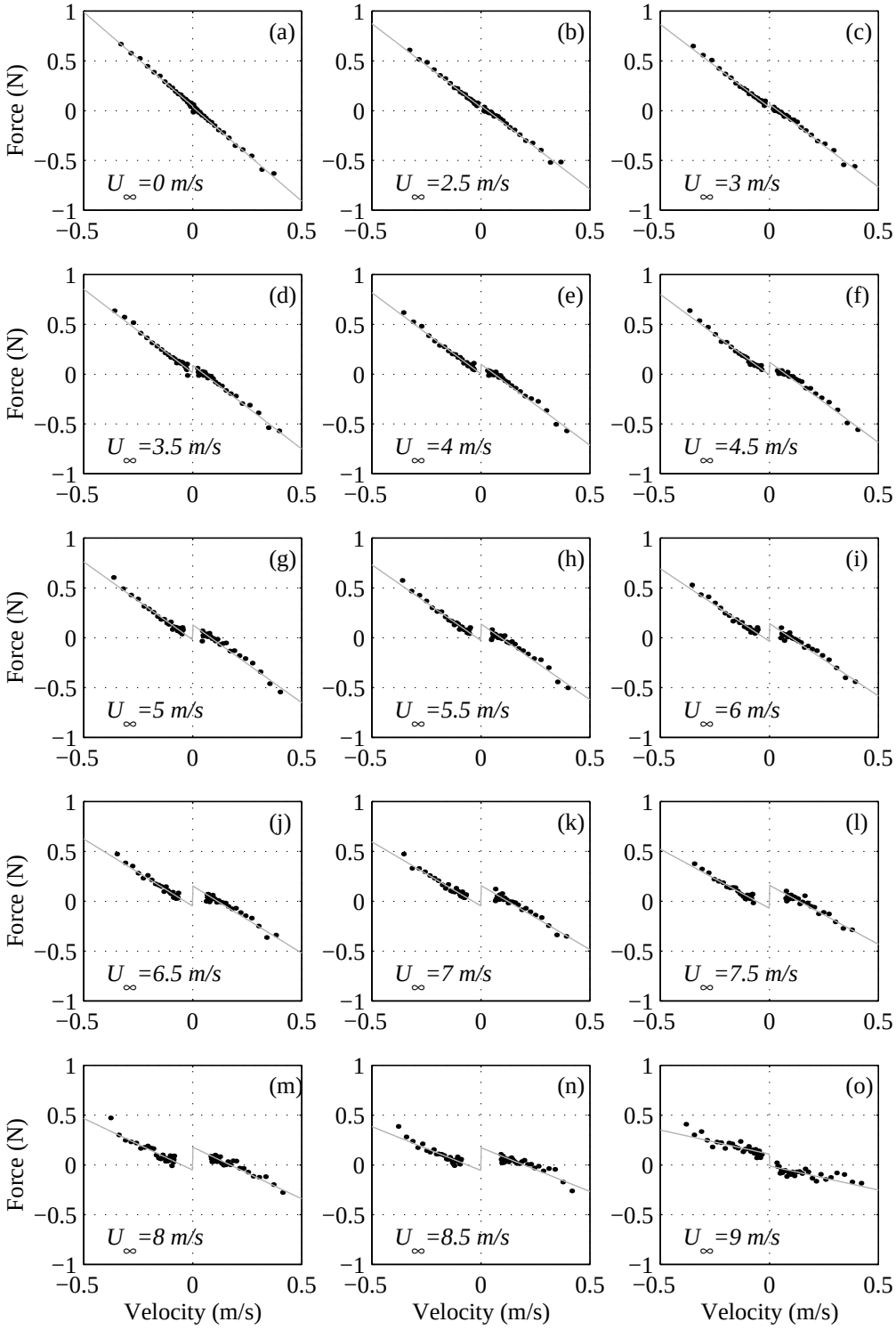

Figure 6.17: Coulomb damping model fitted to data from fig 6.14.

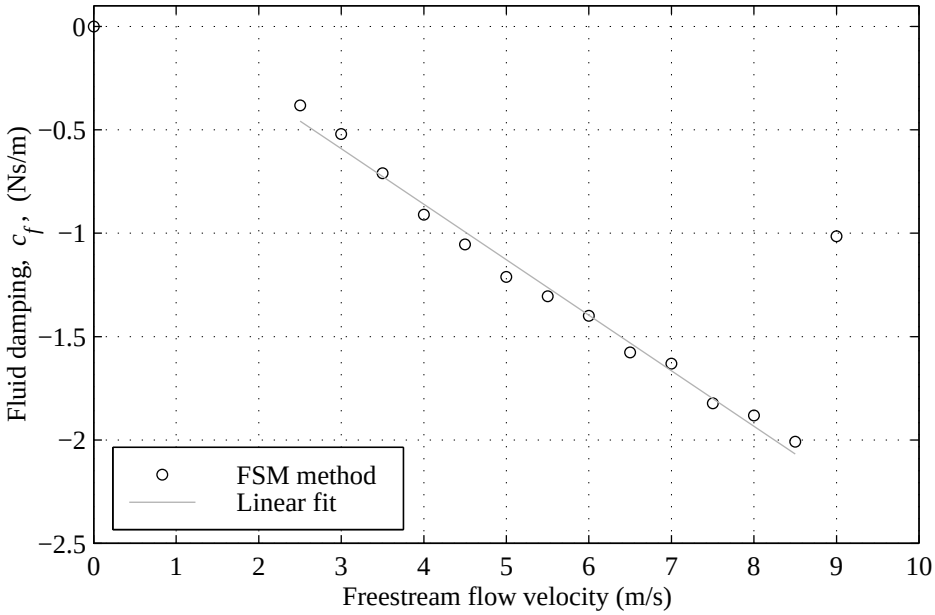

Figure 6.18: Linear fluid damping coefficient associated with the cubic damping model

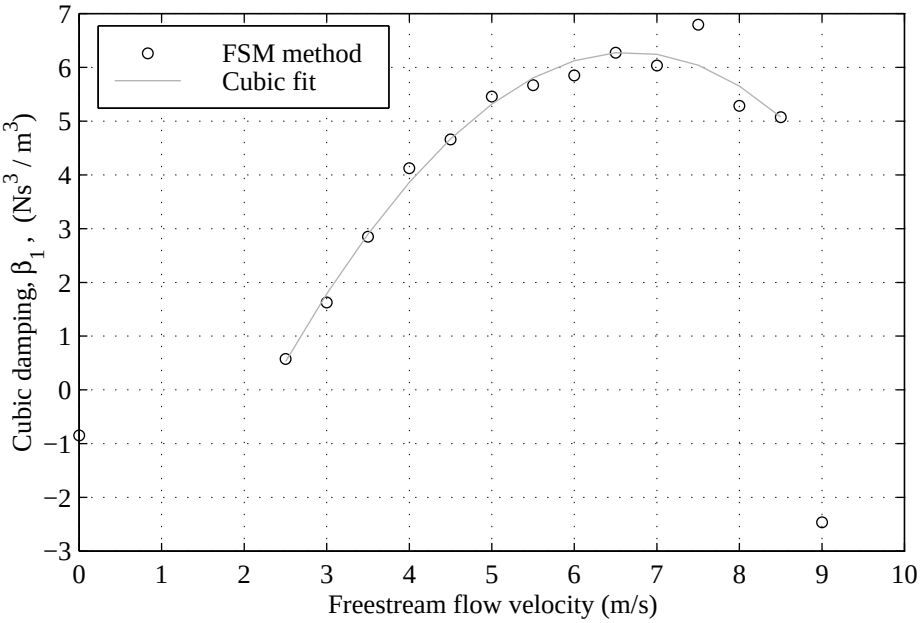

Figure 6.19: Cubic damping coefficient, β_2.

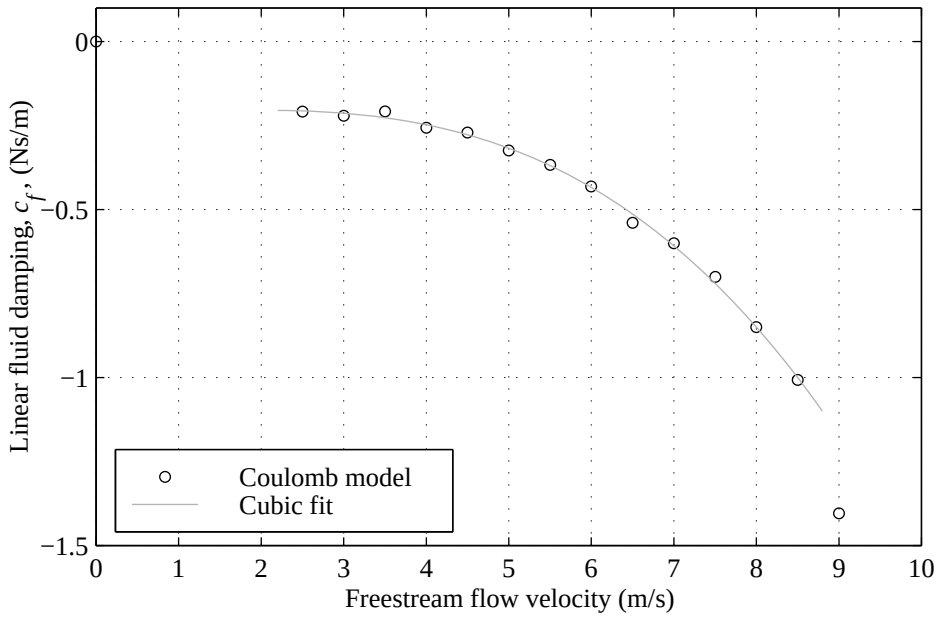

Figure 6.20: Linear fluid damping coefficient associated with the Coulomb damping model.

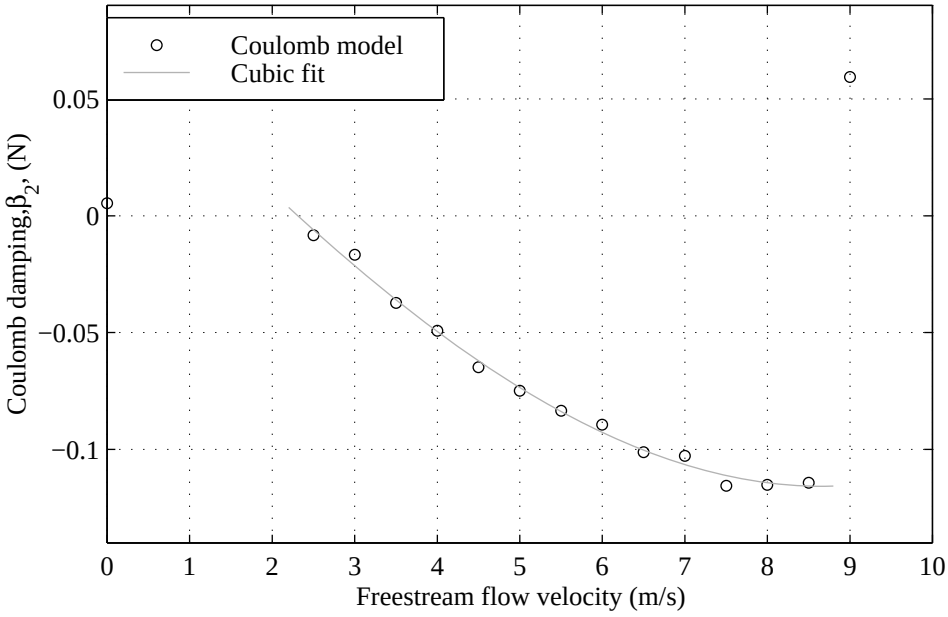

Figure 6.21: Coulomb damping coefficient, β_2.

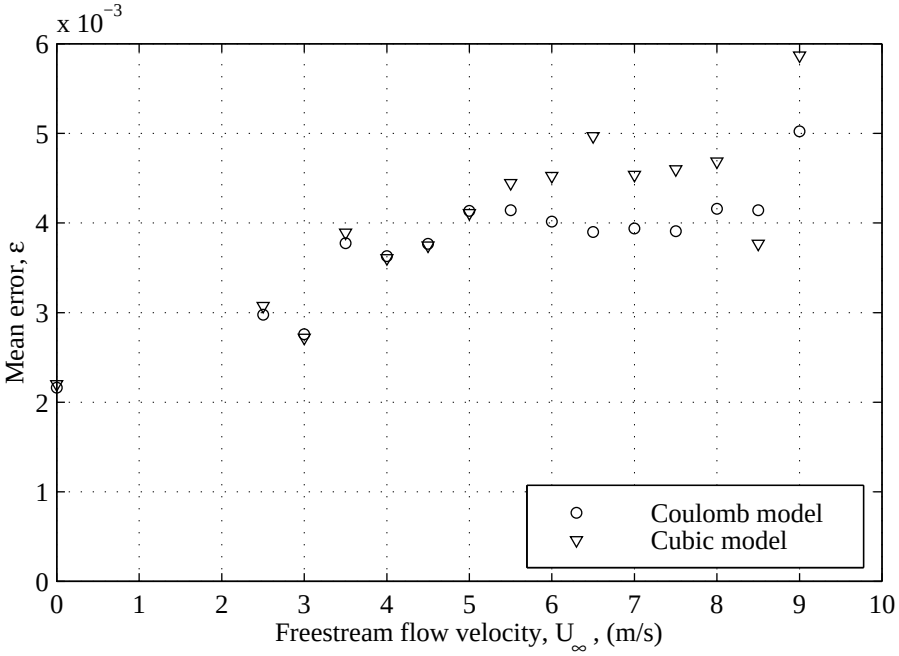

Figure 6.22: Mean error between the TLS fitted curve and the data for both models.

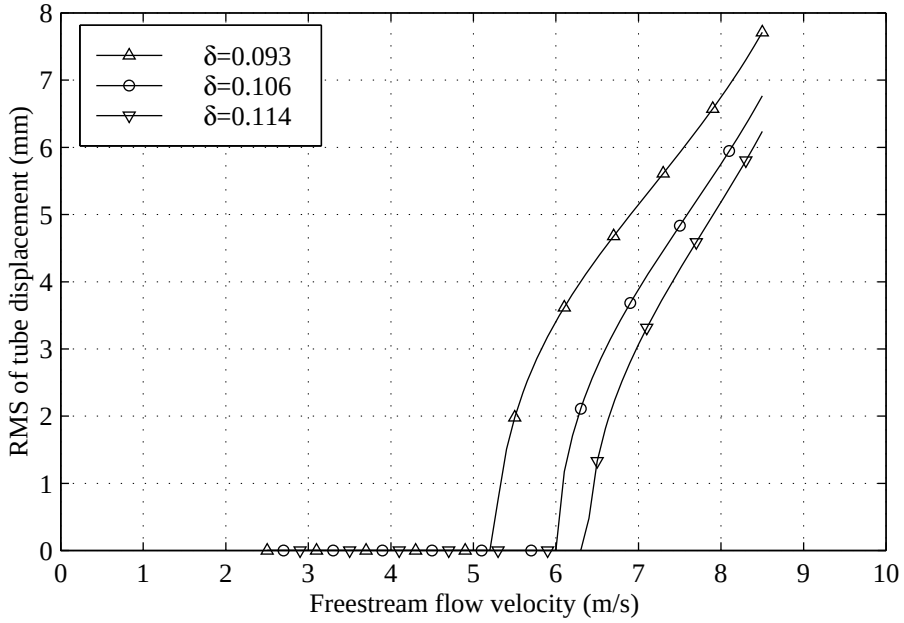

Figure 6.23: Prediction of limit cycle amplitude from cubic damping model.

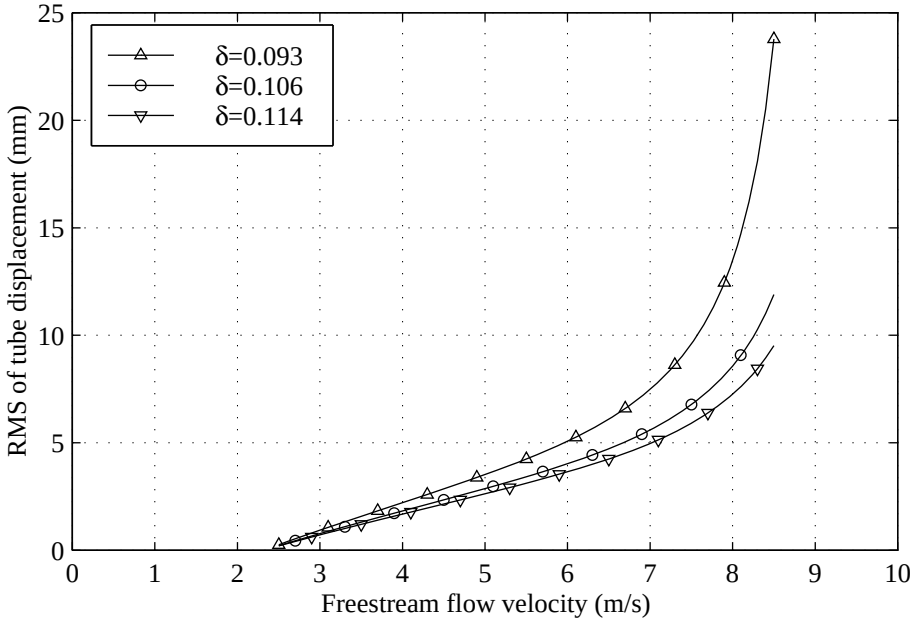

Figure 6.24: Prediction of limit cycle amplitude from Coulomb damping model.

Chapter 7

Discussion

A test facility has been designed and built to investigate the non-linear fluid-structure system responsible for damping controlled fluidelastic instability in normal triangular tube arrays. This rig has two novel features. Firstly, the single flexible tube is mounted on an iso-viscoelastic support which is free to translate only in the cross flow direction. The structure has been shown to be a good approximation to the theoretical ideal of a linear single degree of freedom system. The second novel feature is a non-contact electromagnetic shaker (EMS) which can be used to excite the structure with an arbitrary, measurable force while not limiting tube displacement or modifying the mass or stiffness. This device can also be used as a passive electromagnetic damper. In this mode the total structural damping can be increased by 700%, without effecting the other modal parameters, simply by setting the resistance in the circuit.

The flexible tube has been tested in the 3^{rd} row of a 5 row normal triangular array, with pitch ratio of 1.58 and 1.32. In both cases, the system has exhibited fluidelastic instability. This validates the widely made assumption that only one degree of freedom is necessary for damping controlled FEI. The vortex shedding frequencies have been estimated for both arrays from the spectra of the tube response. Only one Strouhal number has been identified in each array. This is consistent with the observations of Oengören & Ziada (1995) who noted that for normal triangular arrays with low pitch ratios (< 1.6) one shedding frequency dominates. The values of Strouhal number for

each array agree with the data in the literature.

The stability threshold for both arrays has been determined at three levels of damping. When non-dimensionalized, the 6 new critical velocities agree with previously published values for normal triangular tube bundles.

Linear models of the fluid force have been identified for both arrays. The linearized parameter estimates obtained from free and forced response are in reasonable agreement. As would be expected, the parameters are independent of total damping levels. For a pitch ratio of 1.58 both the fluid damping and stiffness coefficients seem to vary with the dynamic head (i.e. the square of flow velocity). This is not the case for a pitch ratio of 1.32, although the behaviour of the fluid damping for this array can be partially explained by the quasi-steady model of Price & Paidoussis (1986). This suggests that the theoretical framework proposed by Chen (1987) is valid for the first array but not for the second.

The linearized parameter estimates have been used to predict the stability boundaries. Since the linearized model develops a dynamic divergence in the post-stable regime, it is not been possible to obtain a prediction for limit cycle amplitudes. The critical velocities obtained from the linear model show reasonable agreement with the experimentally determined values for a pitch ratio of 1.58. However, for $\frac{P}{d} = 1.32$ the predictions overestimate the stability threshold by as much as 100% suggesting that a non-linear model was required for more densely packed arrays.

The non-linear nature of the fluid-structure system in the array with pitch ratio of 1.32 was qualitatively examined by considering the free response of the flexible tube in a post-stable regime and the forced response in a stable regime. The non-linearities have been shown to increase in strength with the flow velocity and the functional form has been shown to be predominantly odd.

The force state mapping (FSM) technique was used to identify a non-linear model of the fluid force. This model consists of a linear and cubic stiffness and a linear and cubic damping. No term involving a cross product of tube velocity and displacement was identified, but this can not be interpreted as evidence of the absence of such a

component. A Coulomb type model, possibly resulting from a Coanda like jet switching mechanism, was also considered for the fluid damping. Although this model fits the force data equally well, it was rejected on the grounds that the predicted behaviour around the stability threshold was not observed in direct experiments.

Both the linear stiffness and damping coefficients from the non-linear model appear to be directly proportional to flow velocity in the range $2.5m/s \leq U \leq 8.5m/s$. This type of variation has some basis in the models of Price & Paidoussis (1986) and Lever & Weaver (1986). The cubic coefficients while still strongly dependent on the flow velocity do not follow either a linear or a quadratic trend. The non-linear model has been used to predict the stability thresholds and limit cycle amplitudes at three levels of damping. When comparing the experimental critical velocities to the predictions, it can be seen that the accuracy of the non-linear model is far superior to that of the linear model. The limit cycle amplitudes while showing the correct trends are substantially overestimated by the model. This has been attributed mainly to the fact that the cross term has not been quantified, but it was noted that the absence of turbulent buffeting in the predictions would also contribute to the discrepancy. The cubic nature of the fluid force has some basis in the non-linear extension of the unsteady theoretical model ofLever & Weaver (1986) which was presented by Rzentkowski & Lever (1998). However, the predictions from this model are very sensitive to the assumed time lag between fluid force and tube motion. Furthermore, the physical mechanisms affecting this lag are unclear. It would seem that the total dynamics of the system might be described by a modified version of this model, but more work is needed to describe the time lag effect accurately. Similar comments could be made about the quasi-steady model of Price & Paidoussis (1986). However, as pointed out by Price (1995), the effect of the quasi-steady assumption must also be clarified.

In the array with a pitch ratio of 1.32, an acoustic resonance with a frequency of $1053Hz$ was observed at a flow velocity of $9m/s$. The resonance, suppressed fluidelastic instability and dramatically modified the parameter estimates in both the linear and non-linear models at this velocity. Price & Zahn (1991) has reported a similar effect for

a pitch ratio of 1.375, but the mechanism of interaction between tube motion at $7Hz$ and acoustic resonance at $1050Hz$ remains unclear.

Chapter 8

Conclusions

A test facility has been designed and constructed to investigate damping controlled fluidelastic instability in tube arrays subject to cross flow. Two normal triangular arrays, each with five rows of tubes, have been investigated when a single flexible tube is placed in the third row. This tube is free to move in only pure translation in the cross flow direction and the damping of the supporting structure can be varied using an electromagnet device.

Dynamic tests on these two configurations have led to three main results:

- A linear model compatible with Chen's theoretical framework (1987) appears to be adequate for a pitch ratio of 1.58. On the other hand a non-linear model is required for $\frac{P}{d} = 1.32$ and this model, although it does not fit with Chen's, has some commonality with the quasi-steady model of Price & Paidoussis (1986) and the unsteady model of Lever & Weaver (1986). This suggests that the underlying mechanism controlling fluidelastic instability in a normal triangular array with one degree of freedom is still not well understood, although any new model must include some of the characteristics of the three cited above. The fact that a single model cannot be used for the two arrays tested implies that the widespread practice of comparing stability thresholds from arrays with different pitch ratio may not be valid.

- Force state mapping has been used to determine an empirical model for the weakly non-linear system governing the fluidelastic behaviour. The model obtained in this way shows quantitative agreement with experimental results for the stability threshold and qualitative agreement for the limit cycle amplitude.

- It has been shown that the non-linear behaviour of the fluid force can be approximated by a cubic stiffness and a cubic damping. Although these terms have not been linked with any particular physical process, possible fluid dynamic mechanisms have been discussed which might give rise to cubic terms. An alternative damping model which resembled Coulomb damping in form has also been considered. Physically this could be attributed to jet switching mechanism, similar to the one proposed by Roberts (1966) for inline motion, however evidence has been presented which suggests that such a mechanism is not responsible for fluidelastic instability in the cross flow direction.

8.1 Future work

It is apparent from the conclusions of this testing programme that more work is needed to understand the fluid dynamics at work in fluidelastic systems of this kind. Several avenues present themselves for future work.

It has not been possible to identify a non-linear model using forced response data. This is because the response of the fluid structure to a broadband excitation with a flat spectrum, as was used here, is dominated by a single frequency. This problem may be alleviated by using a prewhitened excitation signal which will produce a flat repsonse spectrum. Alternatively, using the same strategy for non-linear model identifciation as has been employed in this work, the effect of the natural frequency on the fluid force surface could be investigated by changing either the material or the geometry of the twin beam support. Both these approaches would facilitate an investigation of any phase effects (such as a time lag) in the fluid force.

The presence of a strong acoustic field has been seen to have dramatic effects of the fluidelasic behaviour of the system. This effect might be examined by imposing an acoustic excitation on the flow field using a speaker. The tube response could be used as the input to a closed loop control system with the speaker signal as the output. This type of active control has already been applied to flow induced noise and vibration due to free shear layer instability (Ziada 1995; Huang and Weaver 1994).

Computational power and software codes have reached the stage where a numerical investigation of fluidelastic instability in tube bundles might be viable. Simulations of the flow field around small groups of cylinders with prescribed motion had been reported over ten years ago. The more difficult task of simulating a fully coupled fluid-structure system is now being tackled for simple structural geometries. It may now be possible to use unsteady displacement, velocity and fluid force data from a numerical model rather than experimental data, as input to the techniques described in this work. This would have the advantage of eliminating problems with instrumentation and structural linearity.

Appendix A

Free response of a linear sdof system

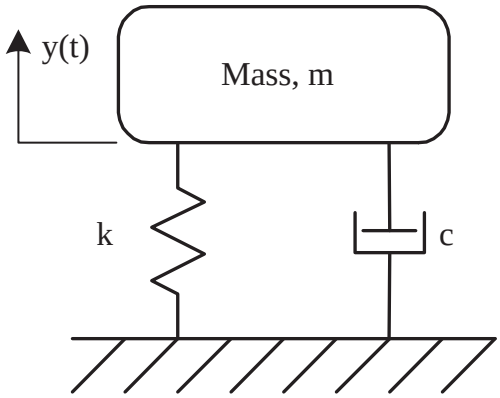

Figure A.1: Schematic of a linear single degree of freedom system.

The equation of motion for a single degree of freedom mass-spring-dashpot system which is not subject to external excitation is:

$$m\ddot{y} + c\dot{y} + ky = 0 \tag{A.1}$$

The time series for displacement, velocity and acceleration for free response is therefore:

$$y(t) = A\mathrm{e}^{-\zeta\omega_n t}\mathrm{e}^{\jmath(\omega t+\phi)} \tag{A.2a}$$

$$\dot{y}(t) = A\mathrm{e}^{-\zeta\omega_n t}(\omega_n \mathrm{e}^{\jmath\theta})\mathrm{e}^{\jmath(\omega t+\phi)} \tag{A.2b}$$

$$\ddot{y}(t) = A\mathrm{e}^{-\zeta\omega_n t}(\omega_n^2 \mathrm{e}^{\jmath 2\theta})\mathrm{e}^{\jmath(\omega t+\phi)} \tag{A.2c}$$

where

$$\zeta = \frac{c}{2\sqrt{km}} \qquad \sin(\theta) = \left(\sqrt{1-\zeta^2}\right)$$

$$\omega_n = \sqrt{\frac{k}{m}} \qquad \cos(\theta) = -\zeta$$

$$\omega = \omega_n\sqrt{1-\zeta^2}$$

$\phi, A =$ constants depending on $y(0)$ & $\dot{y}(0)$

Taking the real part of eq (A.2a) yields:

$$y(t) = A\mathrm{e}^{-\zeta\omega_n t}\cos(\omega t + \phi) \tag{A.3a}$$

$$\dot{y}(t) = A\omega_n\mathrm{e}^{-\zeta\omega_n t}\cos(\omega t + \phi + \theta) \tag{A.3b}$$

$$\ddot{y}(t) = A\omega_n^2\mathrm{e}^{-\zeta\omega_n t}\cos(\omega t + \phi + 2\theta) \tag{A.3c}$$

Bibliography

Al-Hadid, M. A. & Wright, J. R. (1989). Developments in the force-state mapping technique for non-linear systems and the extension to the location of non-linear elements in a lumped-parameter system. *Mechanical systems and signal processing 3*(3), 269–290.

Andjelic, M. (1988). *Stabilitatsverhalten querangestromter Rohrbundel mit versetzter Dreieckteilung*. Ph. D. thesis, University of Hanover.

Andjelic, M., Austermann, R., & Popp, K. (1990). Multiple stability boundaries of tubes in a normal triangular cylinder array. In *Flow induced vibrations*, pp. 87–98. ASME Pressure vessel and piping conference.

Andjelic, M. & Popp, K. (1988). Stability effects in a normal triangular cylinder array. In *FIV in cylinder arrays*, pp. 57–76. ASME International symposium on flow induced vibrations and noise.

Andjelic, M. & Popp, K. (1989). Stability effects in a normal triangular cylinder array. *Journal of Fluids and Structures 3*, 165–185.

Austermann, R. & Popp, K. (1995). Stability behaviour of a single flexible cylinder in rigid tube arrays of different geometry subject to cross-flow. *Journal of Fluids and Structures 9*, 303–322.

Austermann, R., Popp, K., & Kurnik, W. (1992). Fluidelastic instabilities and bifrucations in a rotated triangular tube array subject to cross flow. part i: Experiemntal results. part ii: Modellin and analysis. In *Cross flow induced vibration of cylinder*

arrays, pp. 31–56. ASME International symposium on flow induced vibration and noise.

Axisa, F., Antunes, J., & Villard, B. (1990). Random excitation of heat exchanger tubes by cross-flow. *Journal of Fluids and Structures 4*, 321–341.

Bendat, J. & Piersol, A. (1980). *Engineering applications of correlations and spectral analysis*. Wiley.

Billings, S. & Tsang, K. (1989). Spectral analysis for nonlinear systems, part i: parametric non-linear spectral analysis. *Mechanical sytems and signal processing 3*(4), 319–339.

Chen, S. (1983). Instability mechanisms and stability criteria of a group of circular cylinders suject to cross-flow. part (i): Theory. part (ii): Numerical results and discussion. *Journal of Vibration, Acoustics, Stress and Reliability in Design 105*, 51–51; 253–260.

Chen, S. (1984). Guidelines for the instability flow velocity of tube arrays in cross-flow. *Journal of Sound and Vibration 93*(3), 439–455.

Chen, S. (1987). A general theory for dynamic instability of tube arrays in crossflow. *Journal of Fluids and Structures 1*, 35–53.

Chen, S., Cai, Y., & Srikantiah, G. (1997). Fluid-damping-controlled instability of tubes in crossflow. In P. et al. (Ed.), *Fluid-structure interactions, aeroeleasticity, flow-induced vibration and noise*, pp. 153–162. ASME.

Chen, S. & Jendrzejzcyk, J. (1987). Fluid excitation forces acting on a square tube array. *Journal of Fluids Engineering 97*, 415–423.

Chen, S., Zhu, S., & Jendrzejczyk, J. (1994). Fluid damping and fluid stiffness of a tube row in crossflow. *Journal of pressure vessel technology 116*, 370–383.

Downie, J., Jordinson, R., & Barnes, F. (1984, August). On the design of three-dimensional wind tunnel contractions. *Aeronautical Jounral* , 287–295.

Fitzpatrick, J., Donaldson, I., & McKnight, W. (1986). The structure of the turbulence spectrum of flows in deep tube array models. In C. et al. (Ed.), *Flow-induced vibration*, Volume PVP Vol 104, pp. 21–30.

Gibbings, J. (1993, August). Incompressible flow in contracting ducts. *Aeronautical Jounral* , 230–246.

Golub, G. H. & van Loan, C. F. (1983). *Matrix computations*. North Oxford Academic.

Goyder, H. & Teh, C. (1984). Measurement of destabilising forces on a vibrating tube in cross flow. In *Vol. 2, Vibration of arrays of cylinders ibn crossflow.*, pp. 151–164. ASME symposium on flow induced vibrations.

Granger, S. (1990a). A global model for flow-induced vibration of tube bundles in cross-flow. In *Flow-Induced Vibration*, pp. 139–151. Pressure Vessels and Piping Division, ASME.

Granger, S. (1990b). A new signal processing method for investigating fluidelastic phenomena. *Journal of Fluids and Structures 4*, 73–97.

Granger, S. & Paidoussis, M. P. (1995). An improvement to the quasi-steady model with application to cross-flow induced vibration of tube arrays. In *Flow-induced vibrations*, pp. 339–350. Sixth international conference on flow-induced vibration.

Grover, L. & Weaver, D. (1978a). Cross-flow induced vibrations in a tube bank - turbulent buffeting and fluid elastic instability. *Journal of Sound and Vibration 59*(2), 277–294.

Grover, L. & Weaver, D. (1978b). Cross-flow induced vibrations in a tube bank - vortex shedding. *Journal of Sound and Vibration 59*(2), 263–276.

Hadj-Sadok, C., de Lange, E., & Granger, S. (1995). Inverse methods dor the measurement of fluidelastic forces in tube bundles. In *Flow-induced vibrations*, pp. 363–371. Sixth international conference on flow-induced vibration.

Huang, X. & Weaver, D. (1994). Control of flow induced finvibration by anti-sound. *Journal of Sound and Vibration 169*, 428–432.

Jezequel, L. & Lamarque, C. (Eds.) (1992). *Proceedings of the international symposium on idenfication of non-linear mechanical systems from dynamic tests.*, Euromech 280. Balkema.

Lever, J. & Rzentkowowski, G. (1988). Determination of the fluidelastic stability threshold in the presence of turbulence: a theoretical study. *Proc. of ASME Winter Meeting 2*, 131–150.

Lever, J. & Rzentkowski, G. (1992). Dependence of post-stable fluidelastic behaviour on degrees of freedom of a tube bundle. In *cross-flow induced vibration of cylinder arrays*, pp. 167–188. ASME International symposium on flow induced vibration and noise.

Lever, J. & Weaver, D. (1982). A theoretical model for fluidelastic instability in heat exchanger tube bundles. In C. et al. (Ed.), *Flow-induced vibration of circular cylindrical structures*, Volume PVP Vol 63, pp. 87–108.

Lever, J. & Weaver, D. (1986). On the stability of heat exchanger tube bundles. part 1: modified theoretical model. part 2: numerical results and comparison with experiment. *Journal of Sound and Vibration 107*, 375–410.

Masri, S. F. & Caughey, T. K. (1979). A non-parametric identification technique for nonlinear dynamic problems. *Journal of applied mechanics 46*, 433–447. Original ref to FSM for a sdof problem.

Masri, S. F., Sassi, H., & Caughey, T. K. (1982). Non-parametric identification of nearly arbitrary nonlinear systems. *Journal of applied mechanics 49*, 619–628. Extension of FSM to mdof systems.

Mehta, R. & Bradshaw, P. (1979, November). Design rules for small low speed wind tunnels. *Aeronautical Journal* , 443–449.

Nelder, J. & Mead, R. (1965). A simplex method for function minimization. *The Computer Journal 7*(4), 308–313.

Oengören, A. & Ziada, S. (1995). Vortex shedding, acoustic resonance and turbulent buffeting in normal trianguler tube arrays. In P. Bearman (Ed.), *Flow-Induced Vibration*. Balkema.

Owen, P. (1965). Buffeting excitation of boiler tube vibration. *Journal of Mechanical Engineering Science 7*, 431–439.

Paidoussis, M. (1979). Flow-induced vibrations in nuclear reactors and heat exchangers (practical experiences and state of knowledge). In E. Naudascher and D. Rockwell (Eds.), *Practical experiences with flow-induced vibration*, pp. 1–56.

Paidoussis, M. (1981). Fluidelastic vibration of cylinder arrays in axial and cross flow: state of the art. *Journal of Sound and Vibration 76*(3), 329–360.

Paidoussis, M. & Li, G. (1992). Cross-flow-induced chaotic vibrations of heat-exchanger tubes impacting on loose supports. *Journal of Sound and Vibration 152*(2), 305–326.

Paidoussis, M., Price, S., Nakamura, T., Mark, B., & Njuki, W. (1988). Flow induced vibrations and instabilities in a rotated square cylinder array in cross flow. In *Vol 2, Flow induced vibration and noise in cylinder arrays*, pp. 111–138. ASME symposium of flow induced vibration.

Paidoussis, M. P., Price, S., & Mureithi, W. (1993). Nonlinear and chaotic dynamics of a two-degree-of-freedom analytical model for a rotated triangular array in cross-flow. *Journal of Fluids and Structures 7*, 497–520.

Paidoussis, M. P., Price, S. J., & Murethi, N. (1995). On the practical nonexistence of multiple instability regions for heat-exchanger arrays in cross-flow. In *Flow-induced vibrations*, pp. 283–294. Sixth international conference on flow-induced vibration.

Pettigrew, M. & Gorman, D. (1978). Vibration of heat exchangers components in liq-

uid and two phase cross flow. In *International conference on vibration in nuclear plant*, pp. 2.3. BNES.

Polak, D. R. & Weaver, D. (1995). Vortex shedding in normal triangular tube arrays. *Journal of Fluids and Structures 9*, 1–18.

Press, W., Teukolsky, S., Vetterling, W., & Flannery, B. (1992). *Numerical recipes in FORTRAN* (Second ed.). Cambridge University Press.

Price, S. & Kuran, S. (1990). Fluidelastic stability of a rotated square array with multiple flexible cylinders subject to cross-flow. In *Flow-Induced Vibration*, pp. 107–117. Pressure Vessels and Piping Division, ASME.

Price, S., Paidoussis, M., & Giannias, N. (1990). A generalized constrained mode analysis for cylinder arrays in cross-flow. *Journal of Fluids and Structures 4*, 171–202.

Price, S., Paidoussis, M., Macdonald, R., & Mark, B. (1987). The flow-induced vibration of a single flexible cylinder in a rotated square array of rigid cylinders with pitch-to-diameter ration of 2.12. *Journal of Fluids and Structures 1*, 359–378.

Price, S., Paidoussis, M., & Mark, B. (1992). Flow visualization in a 1.375 pitch-to-diameter parallel triangular arry subject to cross flow. In *Vol. 1, FSI/FIV in cylinder arrays in cross-flow*, pp. 29–38. ASME international symposium on flow induced vibrations.

Price, S. J. (1995). A review of theoretical models for fluidelastic instability of cylinder arrays in cross-flow. *Journal of Fluids and Structures 9*, 463–518.

Price, S. J. & Paidoussis, M. P. (1986). A single-flexible-cylinder analysis for the fluidelastic instability of an array of flexible cylinder s in cross-flow. *Journal of Fluids Engineering 108*, 193–199.

Price, S. J. & Valerio, N. (1990). A non-linear investigation of single degree of freedom instability in cylinder arrays subject to cross flows. *Journal of Sound and*

Vibration 137, 419–432.

Price, S. J. & Zahn, M. L. (1991). Fluidelastic behaviour of a normal triangular array of subject to cross-flow. *Journal of Fluids and Structures 5*, 259–278.

Rae, W. & Pope, A. (1984). *Low-speed wind tunnel testing* (2nd ed.). Wiley.

Rice, H. & Fitzpatrick, J. (1991). The measurement of nonlinear damping in single-degree-of-freedom systems. *Transactions of the ASME 113*, 132–140.

Rice, H. J. & Fitzpatrick, J. A. (1988). A generalized technique for spectral analysis of non-linear systems. *Mechanical Systems & Signal Processing 2*, 195–207.

Rice, H. J., Torrance, A. A., & Eikelman, G. (1998). A model of stiffness non-linearity in fibrous material dynamics. *Journal of Sound and Vibration 212*, 375–381.

Roberts, W. (1966). *Low frequency aeroelastic vibrations in a cascade of circular cylinders.* Mechanical engineering science monographs. Institute of Mechanical Engineers.

Rzentkowski, G. & Lever, J. (1992). Modeling the nonlinear fluidelastic behaviour of a tube bundle. In *Cross flow induced vibration of cylinder arrays*, pp. 89–106. ASME International symposium on flow induced vibration and noise.

Rzentkowski, G. & Lever, J. (1995). The effect of turbulence on fluidelastic instability in tube bundles: a nonlinear analysis. In P. Bearman (Ed.), *Flow-induced vibrations*. Balkema.

Rzentkowski, G. & Lever, J. (1998). An effect of turbulence on fluidelastic instability in tube bundles: a nonlinear analysis. *Journal of Fluids and Structures 12*, 561–590.

Savkar, S. (1984). Buffeting of cylindrical arrays in cross flow. In *Vol. 2, Vibration of arrays of cylinders ibn crossflow.*, pp. 195–210. ASME symposium on flow induced vibrations.

Schoukens, J. & Pintelon, R. (1991). *Identification of linear systems.* Pergamon.

Simpson, A. & Flower, J. W. (1977). An improved mathematical model for the aerodynamic forces on tandem cylinders in motion with aeroelastic applications. *Journal of Sound and Vibration 51*(2), 183–217.

Tanaka, H. & Takahara, S. (1981). Fluidelastic vibration of tube arrays in cross flow. *Journal of Sound and Vibration 77*, 19–37.

Tanaka, H., Takahara, S., & Ohta, K. (1982). Flow-induced vibration of tube arrays with various pitch-to-diameter ratios. In C. et al. (Ed.), *Flow-induced vibration of circular cylindrical structures*, Volume PVP Vol 63, pp. 45–56.

Weaver, D. (1987). *An introduction to Flow-induced vibrations*. Course notes. BHRA.

Weaver, D. & Abd-Rabbo, A. (1985). A flow visualization study of a square array of tubes in water crossflow. *Journal of Fluids Engineering 107*, 354–363.

Weaver, D. & El-Kashlan, M. (1981). On the number of tube rows required to study cross-flow induced vibrations in tube banks. *Journal of Sound and Vibration 75*(2), 265–273.

Weaver, D. & Fitzpatrick, J. (1988). A review of cross-flow induced vibrations in heat exchanger tube arrays. *Journal of Fluids and Structures 2*, 73–93.

Weaver, D. & Koroyannakis, D. (1982). The cross-flow response of a tube array in water - a comparison with the same array in air. *Journal of pressure vessel technology 104*, 139–146.

Weaver, D., Lian, H., & Huang, X. (1992). Vortex shedding in rotated square arrays. In *Vol. 1, FSI/FIV in cylinder arrays in cross-flow*, pp. 39–54. ASME international symposium on flow induced vibrations.

Weaver, D. & Yeung, H. (1984). The effect of tube mass on the flow induced response of various tube arrays in water. *Journal of Sound and Vibration 93*(3), 409–425.

Worden, K. (1990). Data processing and experiment design for the restoring force surface method. part (i): Integration and differentiation of measured time data.

part (ii): Choice of excitation signal. *Mechanical systems and signal processing 4*(4), 295–344.

Xu, K. Q. & Rice, H. J. (1998). On an innovative method of modeling general non-linear mechanical systems. part 1: Theory and numerical simulations. part 2: Experiments. *Journal of Vibration and Acoustics 120*, 125–137.

Yu, X. (1986). An analysis of tube failure in a u-shaped tube bundle. In S. C. et al. (Ed.), *Flow-Induced Vibrations*, Volume PVP 104, pp. 187–192. ASME.

Zhu, W. & Yu, J. (1986). On the response of the van der pol oscillator to white noise excitation. *Journal of Sound and Vibration 117*, 421–431.

Ziada, S. (1995). Feedback control of globally unstable flows: impinging flows. In P. Bearman (Ed.), *Flow-Induced Vibration*. Balkema.

Zukauskas, A. & Katinas, V. (1980). Flow induced vibration in heat exchanger tube banks. In E. N. . D. Rockwell (Ed.), *Practical experiences with flow-induced vibration*, pp. 188–196.

Zukauskas, A. & Katinas, V. (1991). Fluid dynamic forces on vibrating tubes of heat exchangers in cross-flow. *Journal of Fluids and Structures 5*, 279–298.